Modeling and Control of Magnetostrictive-actuated Dynamic Systems

Zhi Li

A Thesis

In the Department

of

Mechanical & Industrial Engineering

Presented in Partial Fulfilment of Requirements

For the Degree of

Doctor of Philosophy (Mechanical Engineering) at

Concordia University

Montreal, Quebec, Canada

February 2015

CONCORDIA UNIVERSITY
SCHOOL OF GRADUATE STUDIES

This is to certify that the thesis prepared

By: Zhi Li

Entitled: Modeling and Control of Magnetostrictive-actuated Dynamic Systems

and submitted in partial fulfillment of the requirements for the degree of

DOCTOR OF PHILOSOPHY (Mechanical Engineering)

complies with the regulations of the University and meets the accepted standards with respect to originality and quality.

Signed by the final examining committee:

Dr. Rabin Raut	Chair
Dr. Xiang Chen	External Examiner
Dr. Amir G. Aghdam	External to Program
Dr. Subhash Rakheja	Examiner
Dr. Wen-Fang Xie	Examiner
Dr. Chun-Yi Su	Thesis Supervisor

Approved by

_____
Chair of Department or Graduate Program Director

February 20,2015

_____
Dean of Faculty

Abstract

Modeling and Control of Magnetostrictive-actuated Dynamic Systems

Zhi Li, Ph.D.

Concordia University, 2015

Magnetostrictive actuators featuring high energy densities, large strokes and fast responses appear poised to play an increasingly important role in the field of nano/micro positioning applications. However, the performance of the actuator, in terms of precision, is mainly limited by 1) inherent hysteretic behaviors resulting from the irreversible rotation of magnetic domains within the magnetostrictive material; and 2) dynamic responses caused by the inertia and flexibility of the magnetostrictive actuator and the applied external mechanical loads. Due to the presence of the above limitations, it will prevent the magnetostrictive actuator from providing the desired performance and cause the system inaccuracy.

This dissertation aims to develop a modeling and control methodology to improve the control performance of the magnetostrictive-actuated dynamic systems. Through thorough experimental investigations, a dynamic model based on the physical principle of the magnetostrictive actuator is proposed, in which the nonlinear hysteresis effect and the dynamic behaviors can both be represented. Furthermore, the hysteresis effect of the magnetostrictive actuator presents asymmetric characteristics. To capture these characteristics, an asymmetric shifted Prandtl-Ishlinskii (ASPI) model is proposed, being composed by three components: a Prandtl-Ishlinskii (PI) operator, a shift operator and an auxiliary function. The advantages of the proposed model are: 1) it is able to represent the asymmetric hysteresis behavior; 2) it facilitates the construction of the analytical inverse; 3) the analytical expression of the inverse compensation error can also be derived. The validity of the proposed ASPI model and the entire dynamic model was demonstrated through experimental tests on the magnetostrictive-actuated dynamic system.

According to the proposed hysteresis model, the inverse compensation approach is applied for the purpose of mitigating the hysteresis effect. However, in real systems, there always exists a modeling error between the hysteresis model and the true hysteresis. The use of an estimated hysteresis model in deriving the inverse compensator will yield some degree of hysteresis compensation error. This error will cause tracking error in the closed-loop control system. To accommodate such a compensation error, an analytical expression of the inverse compensation error is derived first. Then, a prescribed adaptive control method is developed to suppress the compensation error and simultaneously guaranteeing global stability of the closed loop system with a prescribed transient and steady-state performance of the tracking error. The effectiveness of the proposed control scheme is validated on the magnetostrictive-actuated experimental platform. The experimental results illustrate an excellent tracking performance by using the developed control scheme.

Acknowledgement

I would like to express my gratitude to everyone who supported me throughout the course of my Ph.D. study. I am thankful for their inspiring guidance, invaluably constructive criticism and friendly advice during my research. First and foremost, I would like to especially thank my supervisor, Dr. Chun-Yi Su, for his insightful guidance, encouragement and support throughout my program and the thesis writing. I would also like to thank Dr. Subhash Rakheja for his valuable advice and guidance in the experimental verification in my research.

I would also like to thank my wife Ji Qin and my son Jeremy Li. It would not have been possible to accomplish my PhD study without their love, encouragement and support.

Last but not least, I would like to thank my colleagues and friends: Dr. Ying Feng, Dr. Sining Liu, Mr. Hou-Pin Yoong, and Mr. Bin Yu for their kindly help.

Contents

List of Figures

List of Tables

Nomenclature and Abbreviations

Nomenclature

$v(t)$	system input
$u(t)$	system output
r	threshold of the hysteresis operator
$\mu(\cdot, \cdot)$	density function of Preisach model
$\hat{\gamma}[v](t)$	relay operator
$F_r[v](t)$	play operator
$E_r[v](t)$	stop operator
Λ	upper limit of integration in the PI model
$p(r)$	density function of the PI model
$k_p[v, \xi_p](t)$	denotes the KP kernel
H	magnetic field
B	flux density
$f(H)$	continuous function in Duhem model
$g(H)$	continuous function in Duhem model
A_{bw}	a parameter in Bouc-Wen model
B_{bw}	a parameter in Bouc-Wen model
Γ_{bw}	a parameter in Bouc-Wen model
u_p	output of the rate-dependent PI model
$P[v](t)$	Prandtl-Ishlinskii model
$\Psi[v](t)$	shift model
$\Psi_c[v](t)$	shift operator
$C_{pm}[0, T]$	space of monotone, continuous functions on $[0, T]$
$g(v)(t)$	auxiliary function
$e_m(t)$	modeling error of the ASPI model
$\Gamma_{asc}[\cdot, \zeta.]$	ascending branch of the hysteresis loop

$\Gamma_{des}[\cdot, \zeta.]$	descending branch of the hysteresis loop
$\zeta.$	internal state of the hysteresis operator
N	total turns of the solenoid
i	current
i_H	hysteresis loss current
i_a	actual current flowing through the inductance
i_R	eddy current loss
F_a	magnetostrictive force
A	area of the magnetostrictive rod
N	the number of coil turns
R_0	equivalent resistor of the eddy current effect
E^H	Young's modulus at constant value of magnetic field H
d_{33}	slope of the strain versus magnetic field
T_{em}	electromechanical transduction coefficient
T_{Mm}	magneto-mechanical transduction coefficient
m	mass of the moving part of the magnetostrictive actuator
b_s	damping coefficient
k_s	stiffness
i_m	armature current
$\theta(t)$	angular position
L_m	inductance
R_m	resistance
K_{emf}	back-emf constant
K_t	torque constant of the motor
J	inertia of the rotor
B	damping coefficient
Θ^n	contraction in $C[0, T]$
Π^{-1}	inverse of the ASPI model

$\varphi(r)$	initial loading curve
$\bar{p}(r)$	density function of inverse PI model
$(\varphi^{-1})(r)$	initial loading curve of the inverse PI model
$C(s)$	controller
$G(s)$	transfer function of the dynamic component of the system
$G_1(s)$	normalized transfer function of $G(s)$
ξ	damping ratio
ω_n	undamped natural frequency
P^{-1}	inverse of the PI model
$\bar{r}_i$	thresholds of the inverse PI model
$\bar{p}_i$	weights of the inverse PI model
T	isosceles right triangle
$S^+(t)$	area where $\hat{\gamma}_{s-r,s+r}[v](t) = +1$
$S^-(t)$	area where $\hat{\gamma}_{s-r,s+r}[v](t) = -1$
$\Gamma[v](t)$	Preisach model
$\Gamma_\kappa[v](t)$	discrete Preisach model
$\mu_1(s)$	reduced density function of the Preisach model
$\hat{\Pi}[v]$	estimated ASPI model
$\hat{\Pi}^{-1}[u](t)$	inverse of the estimated ASPI model
$e(t)$	compensation error
$\hat{P}[\cdot](t)$	estimated PI model
$\hat{P}^{-1}[\cdot](t)$	inverse of estimated PI model
$e_{pi}(t)$	compensation error of the combination of the PI model and its inverse
$\rho(t)$	performance function
$S(\cdot)$	smooth and strictly increasing function
z_1	transformed error
$V(t)$	Lyapunov function
$\hat{q}_j$	weight of the elementary shift operator

Abbreviations

PI	Prandtl-Ishlinskii
KP	Krasnosel'skii-Pokrovkii
ASPI	Asymmetric Shifted Prandtl-Ishlinskii
J-A	Jiles-Atherton
SMA	Shape memory alloy
IPMC	Ionic polymer metal composites
ppm	parts per million

Chapter 1

Introduction

This dissertation aims to present a systematic study on modeling and control of the magnetostrictive-actuated dynamic system. The core component in the system is the magnetostrictive actuator. Therefore, in this chapter a brief introduction on the magnetostrictive actuator including magnetostrictive materials and the principal of the magnetostrictive actuator is given first. According to the literature, the input and output responses of the magnetostrictive actuator present complex dynamic behaviors. However, the reported experimental results are different from one to the other and thus can not be directly used for our research. Therefore, we established our own experimental platform, the magnetostrictive-actuated dynamic system, and conducted the tests on the platform in order to thoroughly investigate and fully understand the input-output behaviors of the magnetostrictive actuator with different input amplitudes, frequencies as well as mechanical loads. Based on the collected experimental data, the modeling and control approaches are proposed for the purpose of increasing the control precision of the magnetostrictive actuator, which constitutes the main objective of this dissertation.

1.1 Magnetostriction and Magnetostrictive Materials

Magnetostrictive materials are a class of materials that change their shape when exposed to an external magnetic field. This property of the magnetostrictive materials is called magnetostriction [4] which was first discovered by James Joule in the 1842. Magnetostriction appears in most of ferromagnetic materials. It causes the expansion, positive magnetostriction or the contraction, negative magnetostriction, of a magnetostrictive rod in relation to a longitudinal static magnetic field [6]. From the atomic level speaking, magnetostriction occurs as magnetic domains within magnetostrictive materials rotate or realign in response to variation in either magnetic or mechanical energy, causing a change in a material's shape.

Among the available magnetostrictive materials, the giant magnetostrictive material Ter -fenol-D, which was discovered by A.E. Clark in the 1970s at Naval Ordnance Laboratory, is considered the most ideal material for fabricating magnetostrictive actuators. Terfenol-D ($Tb_{0.3}D_{0.7}Fe_{1.9}$) is a rare earth alloy [4]. It is named after Terbium (where "Ter" is from), iron (where "Fe" is from), Naval Ordnance Laboratory (NOL), and the D comes from Dysprosium (Ter + Fe + Nol-D). Terfenol-D has the largest room temperature magnetostriction of any known magnetostrictive material which presents a good trade-off between high strain and high Curie temperature [4]. Because magnetostriction only appears in a material at temperatures below the Curie temperature. However, in general the temperature of the environment is above the Curie temperature of the common used magnetostrictive materials, which severely limits their applications. Table 1.1 shows the saturation strain and Curie temperature in different magnetostrictive materials. In addition, Terfenol-D is capable of providing a positive magnetostrain of 1000-2000 ppm (parts per million) at 50 - 200 kA/m in bulk materials, while nickel contracts by 50 ppm and iron elongates by about 14 ppm subjected to the same magnetic field.

Terfenol-D has been commercially available since 1987 and opens the possibility of developing high power transducers and low voltage high force density actuators. So far, Terfenol-D actuators have been successfully utilized in applications of micro/nano-positioning [7], high

accuracy milling and vibration attenuation [8], high dynamic servo valves [9], high-frequency micro-pumps [10], etc.

Table 1.1: Comparison of strain capability and Curie temperature [4] [5]

Material	Saturation strain in (ppm)	Curie temperature in (K)
Ni	-50	630
Fe	14	1040
Fe_3O_4	60	860
$Terfenol-D$	2000	650
$Tb_{0.5}Zn_{0.5}$	5500	180
$Tb_{0.5}Dy_xZn$	5000	200

1.2 Principle of the Magnetostrictive Actuators

The magnetostrictive actuators are solid state magnetic actuators and they convert electrical current inputs into corresponding mechanical outputs. The magnetostrictive actuators provide an efficient way to harness the power of Terfenol-D technology and respond quickly to input current with repeatable, forceful mechanical motion. Figure 1.1 shows the inside structure of magnetostrictive actuator. The actuator consists of a Terfenol-D drive rod surrounded by the winding coil, bias permanent magnets that produce the bidirectional movement of the rod, a pair of preloaded springs and an output rod attached to the end of one Terfenol-D rod. Since the Terfenol-D rod can produce a large stroke and output force, no additional mechanism is designed to amplify the output motion.

The magnetostrictive actuator works on the principle that when a supplied current flows through the winding coils, a magnetic field H is created, see the schematic illustration of the actuator in Figure 1.2. In the presence of the magnetic field, small magnetic domains rotate

or re-orient themselves along the magnetic lines, see Figure 1.3, to cause internal strains in the Terfenol-D rod. As a result, a magnetostrictive force is produced and exerts on the output rod of the actuator, which causes an output displacement of the output rod. The above process including the transformation among electrical domains, magnetic domains, and mechanical domains thus causes a very complex dynamic input and output responses.
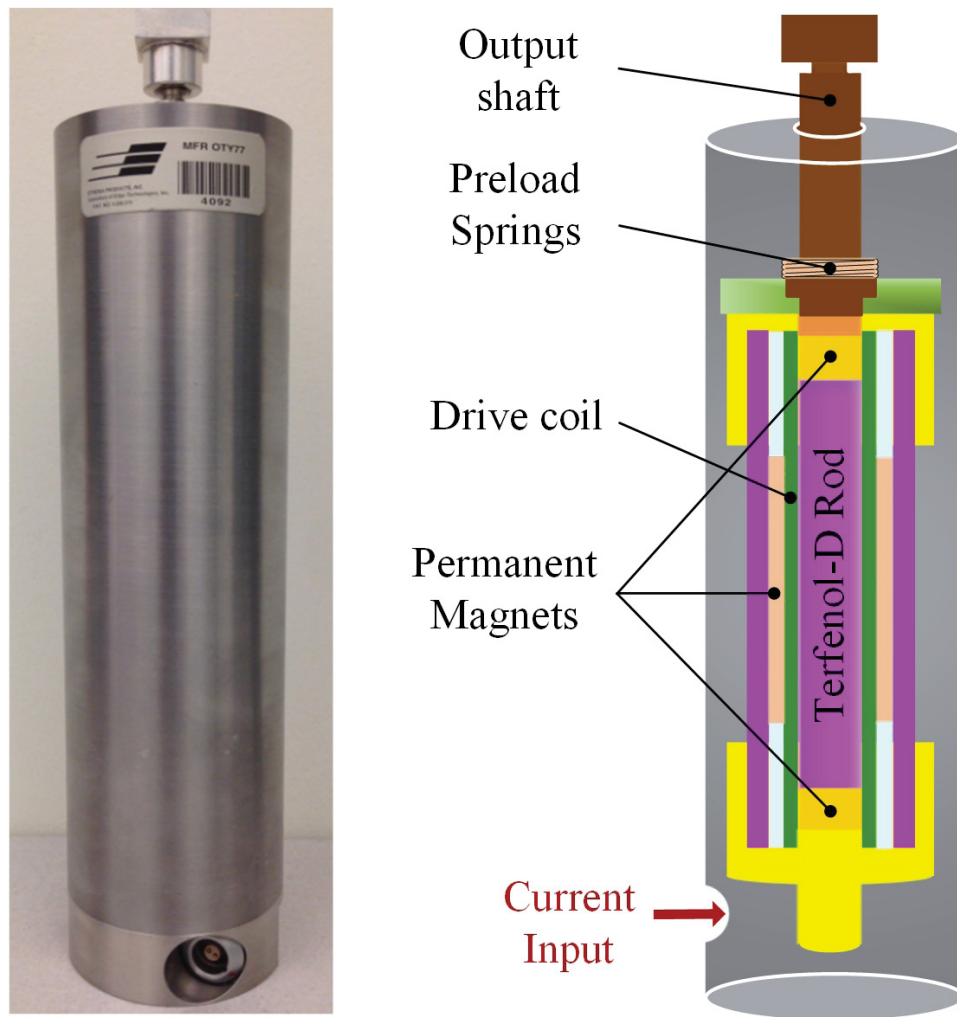
Figure 1.1: The schematic illustration of the magnetostrictive actuator
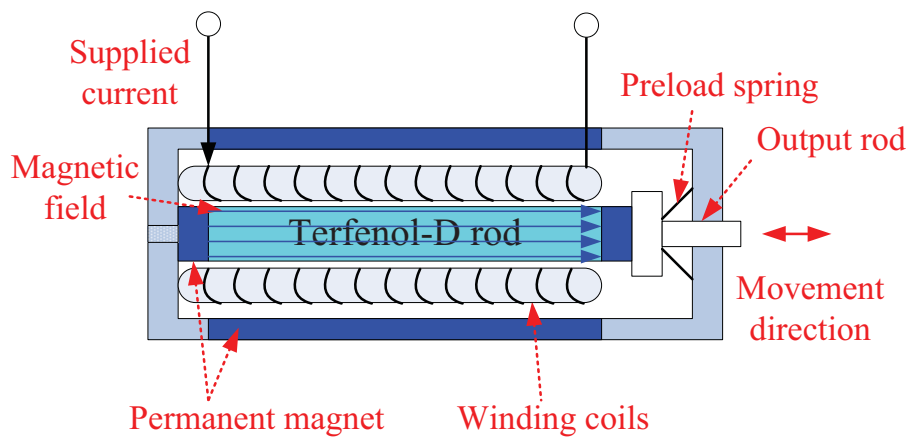
Figure 1.2: Schematic illustration of the Terfenol-D based magnetostrictive actuator
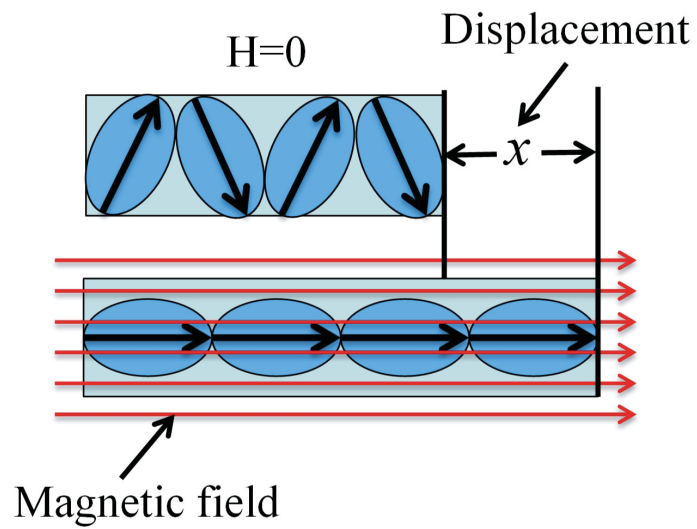
Figure 1.3: Magnetostriction effect

1.3 Input and Output Responses of the Magnetostrictive Actuator

The input and output responses of the magnetostrictive actuator are very important index to evaluate the performance of the actuator. In the literature, the input-output responses of the actuator have been thoroughly studied. However, most of them only investigate the input-output responses with different input frequencies but without considering the loading effect [11] [12] [13] [14] [15]. In [16] [17], although the loading effect (load range 30N-700N) is studied, the experimental tests are conducted under very low input frequency (lower than 0.5Hz), which only show the performance in very limited frequency range. To our best knowledge, there is no comprehensive study on the input-output responses of the actuator both with wide range of input frequencies and mechanical loads. This motivates us to conduct experimental tests on the input-output responses by ourselves. To this end, a magnetostrictive-actuated experimental platform is established first (designed by Prof. Subhash Rakheja, Concordia University and implemented by Dr. Omar Aljanaideh, Concordia University), then a series of experimental tests with different input frequencies, input amplitudes as well as mechanical loads are conducted on the experimental platform. The collected experimental data are utilized for the further study of the modeling and control of the input-output responses of the actuator in the dissertation.

1.3.1 Description of the Experimental Platform

The input and output responses are tested on the designed magnetostrictive-actuated experimental system. The system concludes a magnetostrictive actuator, a capacitive sensor with a sensor driver, a power amplifier, and a dSPACE control board, and the following provides the detailed information.

- The magnetostrictive actuator (Model: MFR OTY77) is manufactured by Etrema Products, Inc, which provides a peak-to-peak output displacement of 100 μ m under

Table 1.2: Actuator Description

Feature	100-LL
Frequency Range, Hz	0-1250
Maximum Dynamic Force, lb(N)	250(1100)
Maximum Stroke (DC), in (μm)	±0.002 (±50)
Blocked Force, lb(N)	500(2220)
Temp. Range, $°F$ ($°C$)	-4 to 212 (-20 to 100)
Max, AC Current, A_{rms}	5
DC Resistance, Ω	1.9
Inductance, mH	3.6
Weight, lb(kg)	8.4(3.8)

excitations at frequencies up to 1250 Hz. Table 1.2 shows the performance of the actuator.

- The capacitive sensor (Lion Precision, model C23-C) with a capacitive sensor driver (Lion Precision, Elite Series CPL190) is used for measuring the displacement of the actuator with a sensitivity of 80 mV/μm, and bandwidth of 15 kHz.

- The power amplifier LVC2016 produced by AE Techron Inc. amplifies the excitation current from the dSPACE to the actuator.

- The dSPACE control board equipped with 16-bit analog-to-digital converters (ADC) and 16-bit digital-to-analog converters (DAC) is used to collect the data from the integrated capacitive sensor and apply the control signal to the amplifier. The Control Desk software in dSPACE is used for the system implementation and to interface the DS1104 PCI dSPACE board

Figure 1.4 illustrates the entire experimental system without mechanical loads. Figure 1.5 demonstrates the magnetostrictive-actuated dynamic system with a mechanical load. The

magnetostrictive actuator 1) is mounted on an aluminum plate 2) via two pillow blocks 3). The mechanical loads 4) are applied to the actuator via the load support frame 5). The capacitive sensor 6) is fixed by a aluminum block attached to the plate. Based on the developed experimental platform, the experimental tests on input-output responses of magnetostrictive-actuated dynamic system could be done under different input amplitudes, input frequencies as well as mechanical loads.
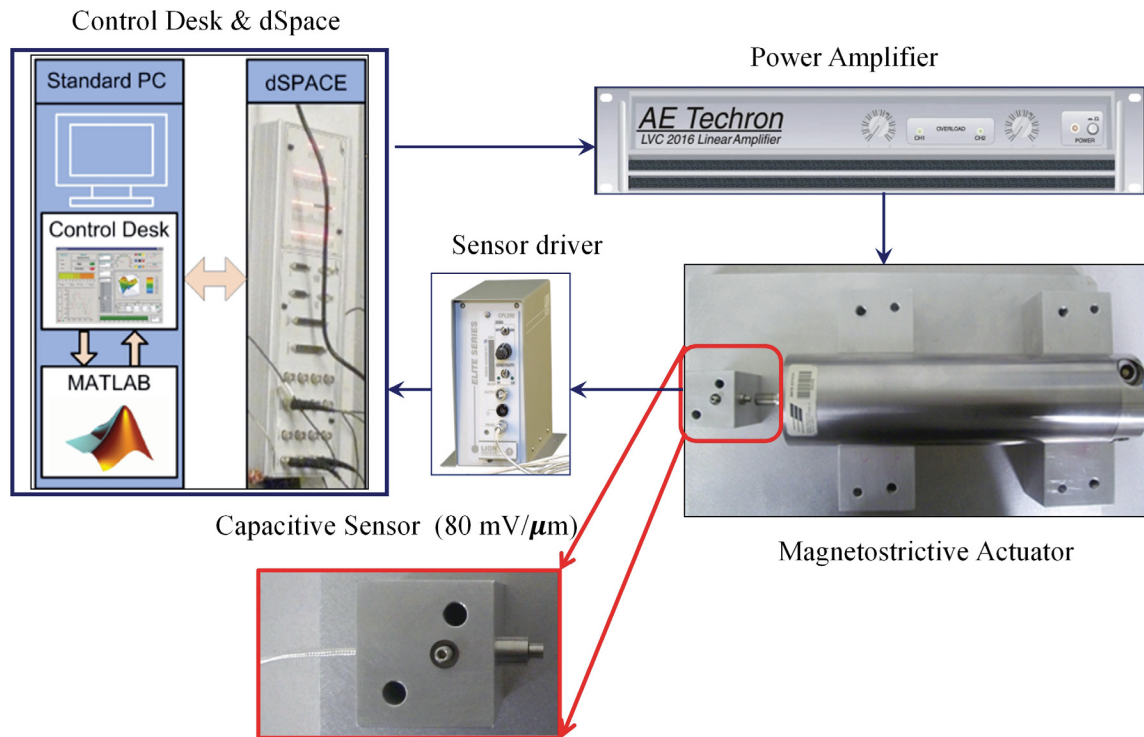
Figure 1.4: The experimental platform
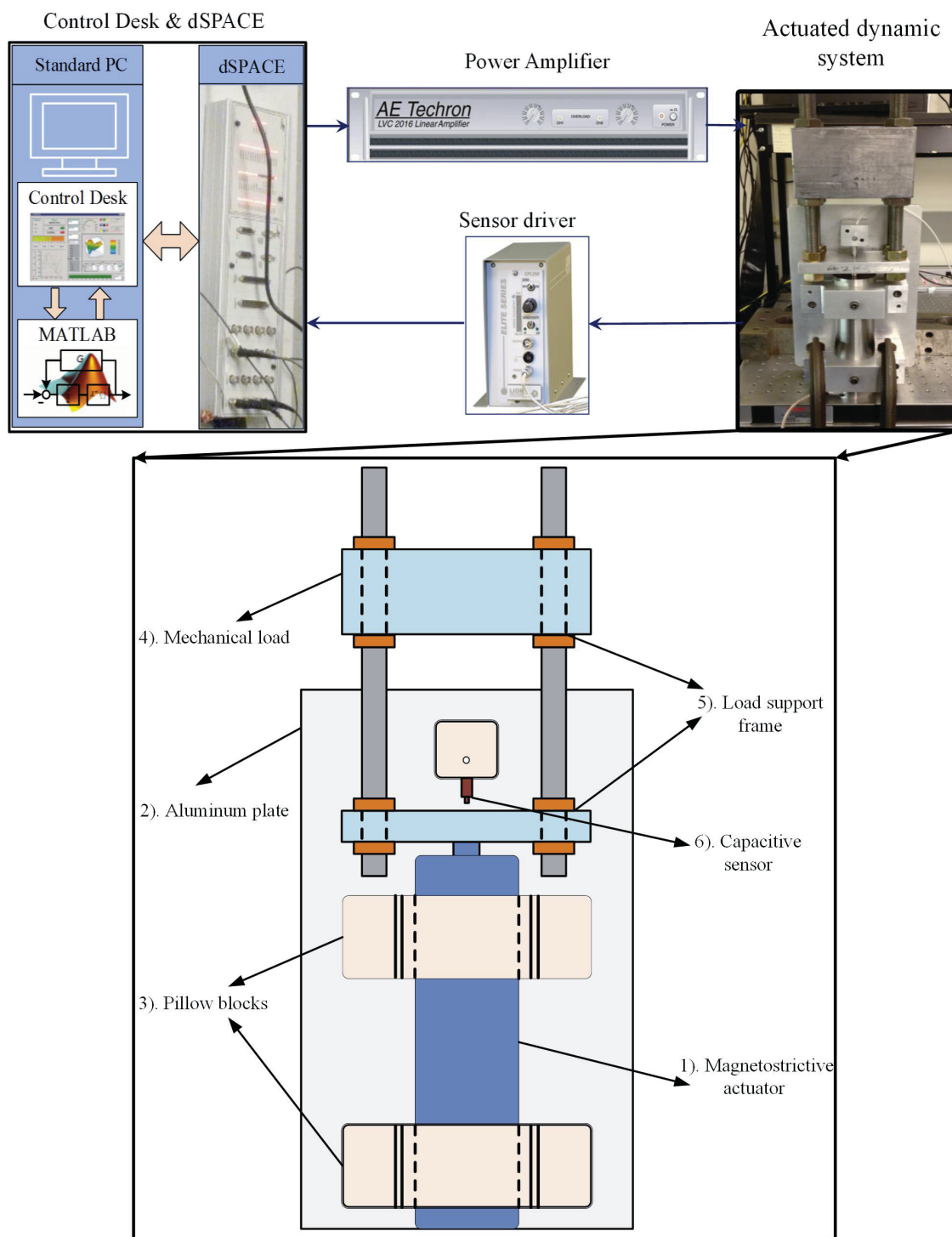
Figure 1.5: The experimental platform with mechanical loads

Control Desk & dSPACE

Standard PC

dSPACE

Control Desk

MATLAB

Power Amplifier

AE Techron
LVC 2016 Linear Amplifier

Sensor driver

Actuated dynamic system

4). Mechanical load

2). Aluminum plate

3). Pillow blocks

5). Load support frame

6). Capacitive sensor

1). Magnetostrictive actuator

1.3.2 The Input and Output Responses with Different Input Frequencies without Mechanical Loads

The input and output responses of the magnetostrictive-actuated dynamic system with different input frequencies (1Hz-200Hz) but without mechanical loads are presented in this section. The input signal to the actuated system is current (A) and the output is displacement (μm) which can be measured via the capacitive sensor. Then we put the input data on the x-axis and the output data on the y-axis, therefore the input-output relationship of the actuated system can be obtained, see Figure 1.6.
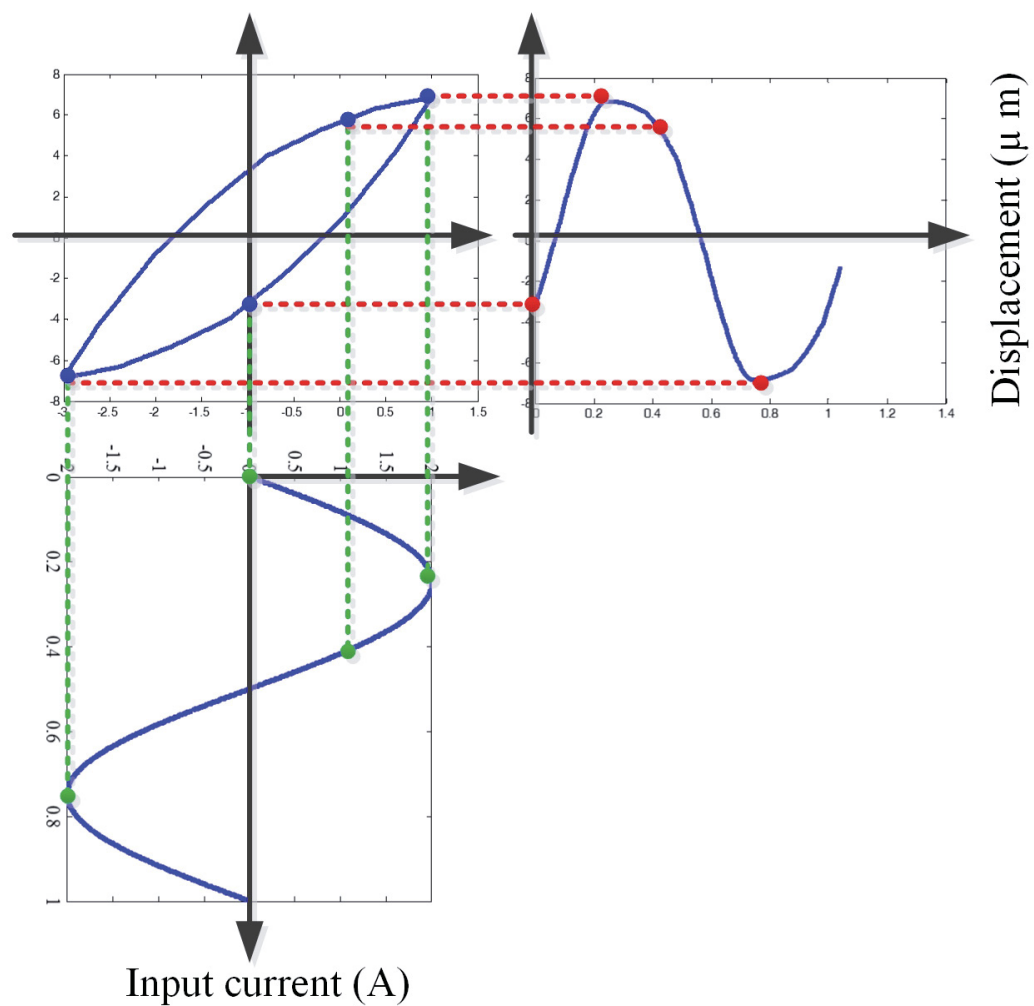
Figure 1.6: The input-output relationship of the magnetostrictive actuator

We first conduct the experimental tests with sinusoidal input signals ($i = A_1 sin(2\pi t)$, $A_1 = 1, 2, 3, 4, 5$). Figure 1.7 illustrates the input and output responses of the actuator. From the figures, it is obviously seen that the input-output responses of the actuator show looped relationship. We call this phenomena hysteresis effect (the definition of the hysteresis will be given in the following development). We also find that the output displacement i.e. peak-to-peak value, is not proportional to the input current, see Figure 1.8. In other words, the magnitude (peak-to-peak value divided by twice the input current) is not constant, see Figure 1.8. From Figures 1.7 and 1.8, we can conclude that the input and output responses present nonlinear hysteresis phenomena. To verify this conclusion in case of the input-output property of the magnetostrictive actuator depending on the specific type of input signal, the triangular signals are also applied to the actuator. Figure 1.9 shows the input and output relationship of the actuator which also demonstrates the nonlinear hysteresis behaviors.

To investigate the input and output responses of the actuator with higher input frequencies, we applied signals ($i = sin(2\pi ft)$, $f = 50Hz, 100Hz, 150Hz$ and $200Hz$). Figure 1.10 shows the input and output relationship of the magnetostrictive actuator with different input frequencies. It can be seen that with the increase of the input frequency the width of the hysteresis loop becomes wider and wider.

In addition, we also studied the input and output responses of the actuator with complex harmonic signal $y = 2.16sin(0.35 \times 2\pi f_0 t) + 2.7sin(0.1 \times 2\pi f_0 t + \frac{\pi}{2} f_0)$ for the purpose of observing the influence of the input frequency on the minor loops (small loops inside of the major loops). Figure 1.11(a) shows the input signal with $f_0 = 1$. The input and output responses of the actuator is shown in Figure 1.11(b) from which we can see that the minor loop AB and CD are congruent under the same two consecutive extrema at point 1, 4, see Figure 1.11(a). Applying the input signals with higher values of f_0 ($f_0 = 101, 401$), the input-output responses are obtained in Figures 1.12-1.13. From Figure 1.13, it can be seen that the minor loops AB and CD are no longer congruent to each other, i.e. the point E on AB is not congruent with the point F on CD. Therefore, the input frequencies also influence the input-output behaviors of the actuator in their minor loops characteristics.

(a) 1 A

(b) 2 A

12

(c) 3 A

(d) 4 A

13
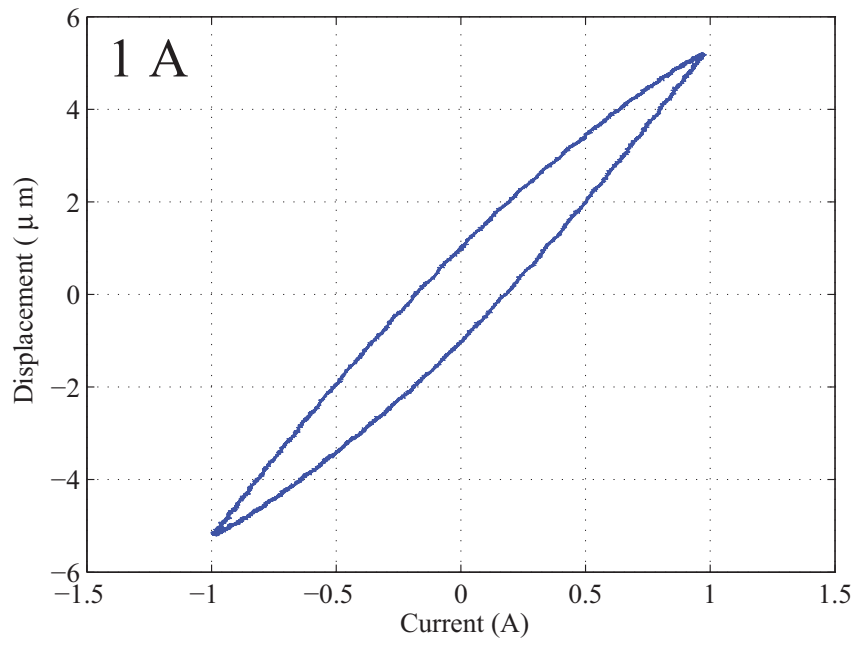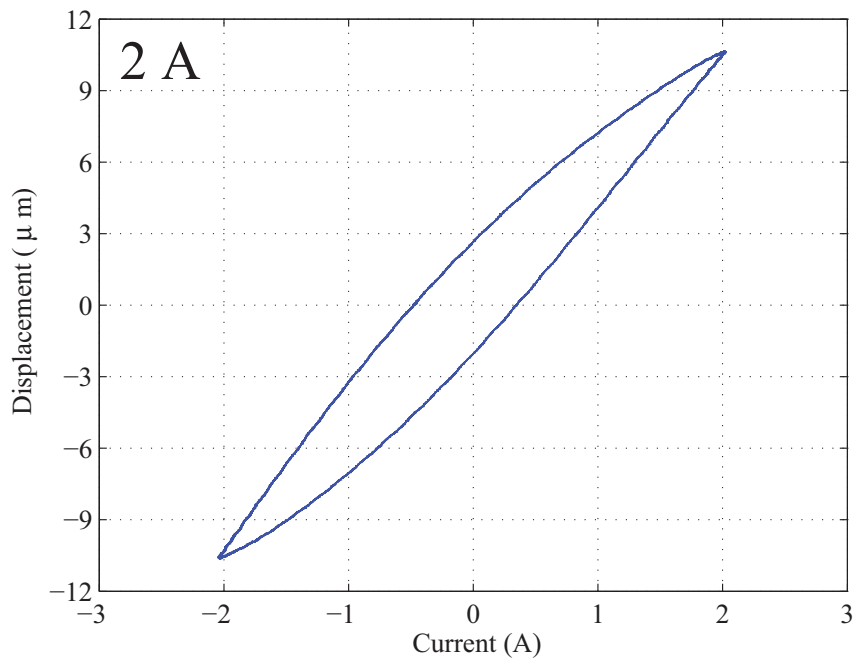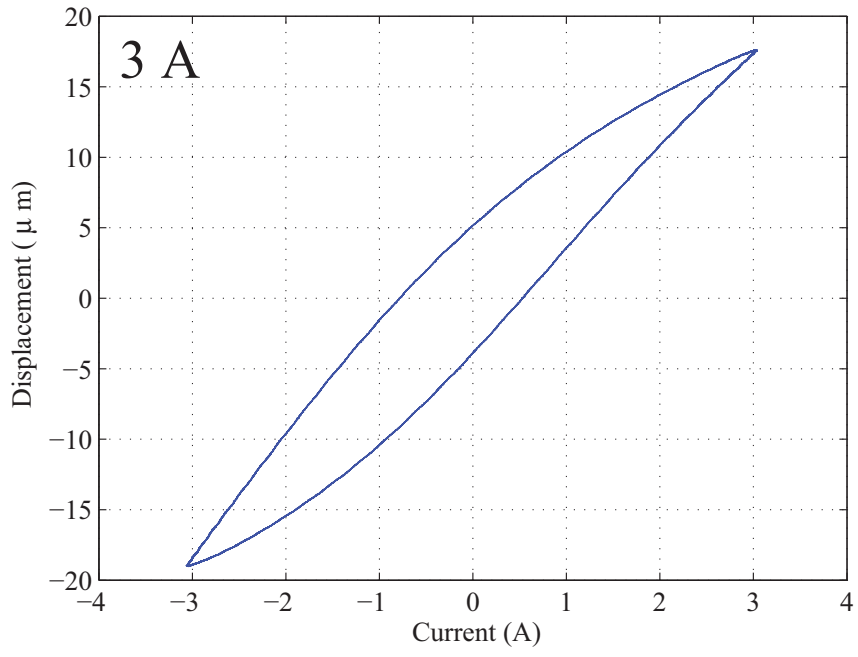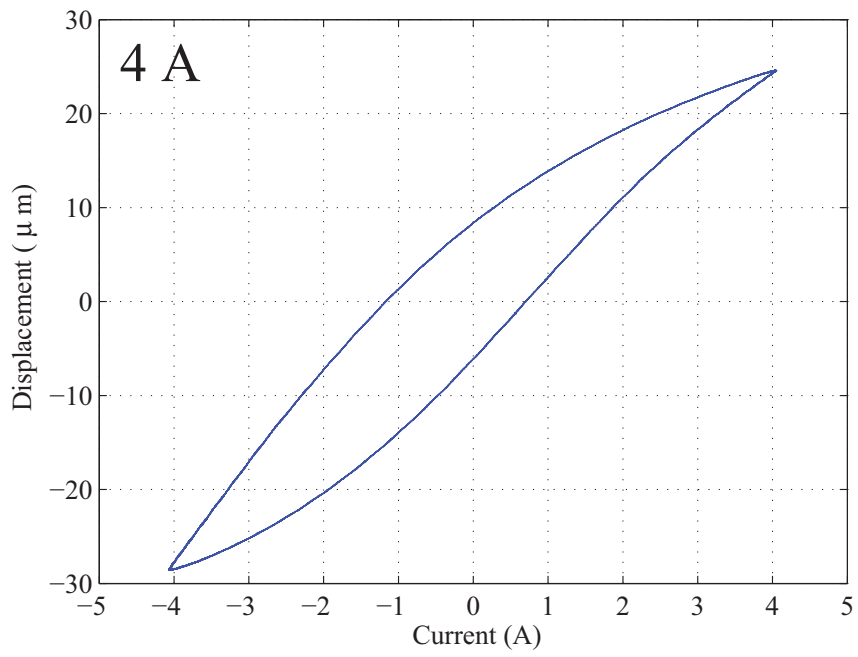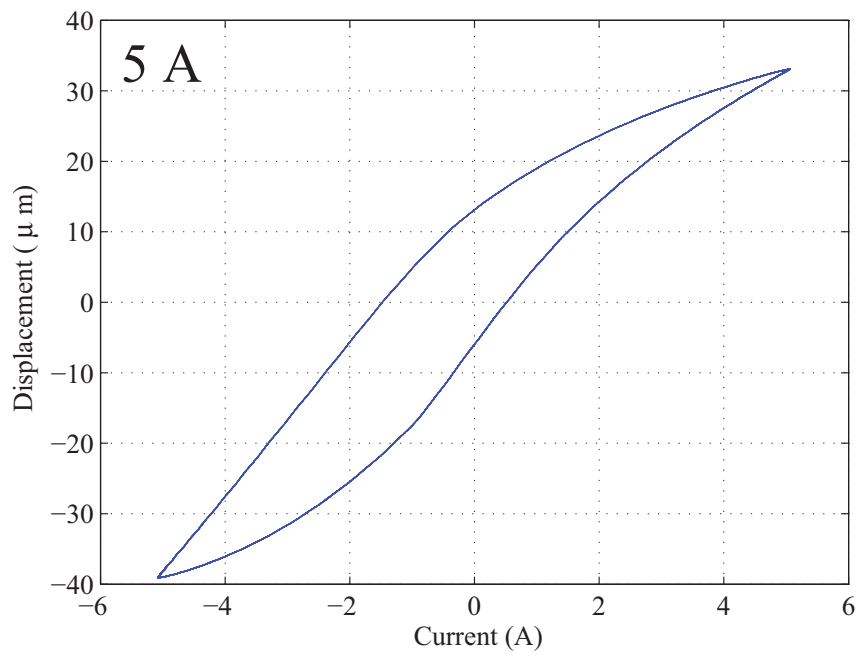
(e) 5 A

Figure 1.7: The input-output relationship of the magnetostrictive actuator with sinusoid input signal
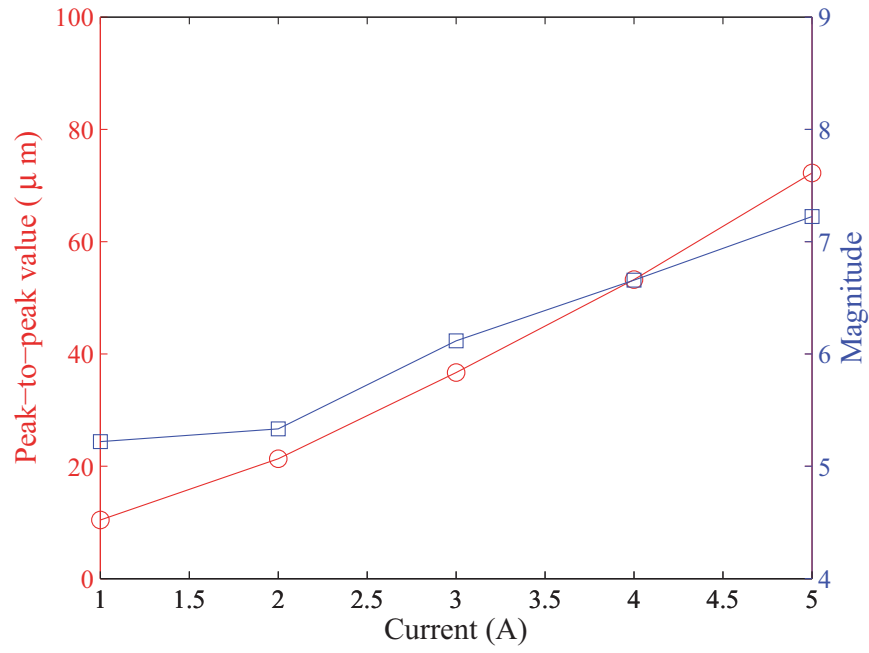
Figure 1.8: The peak-to-peak value versus the input current and their magnitude
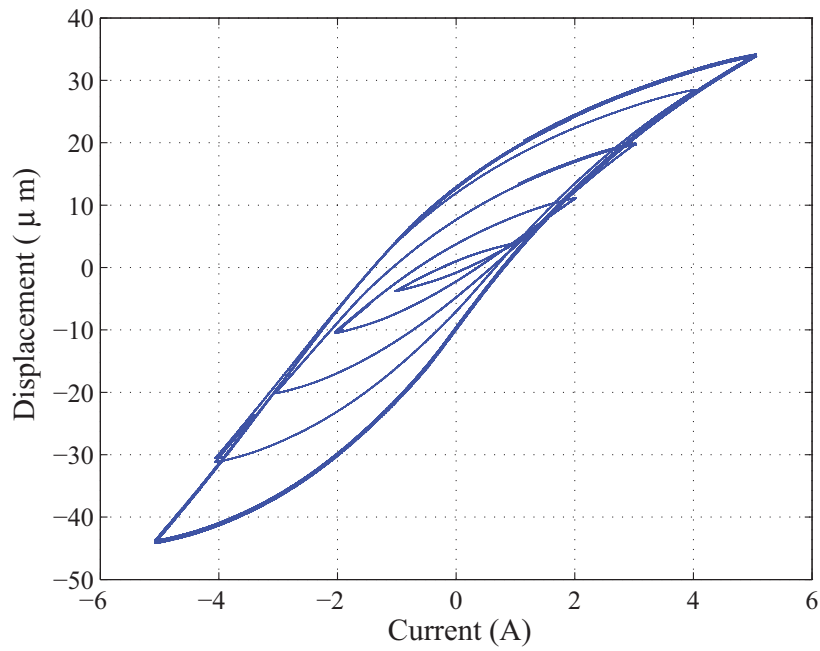
Figure 1.9: The input-output relationship of the magnetostrictive actuator with triangular input signal

(a) 1 A

(b) 2 A

16
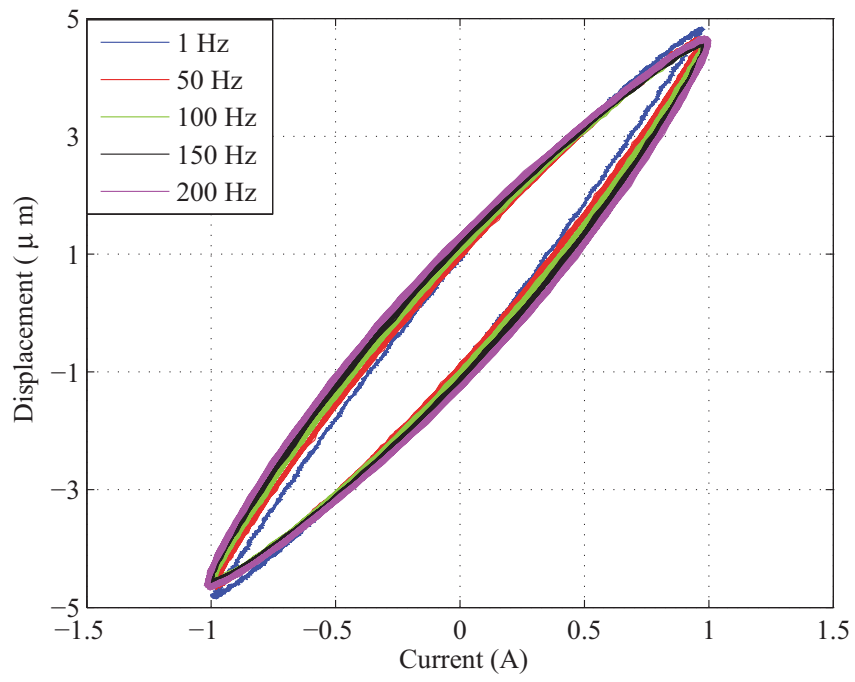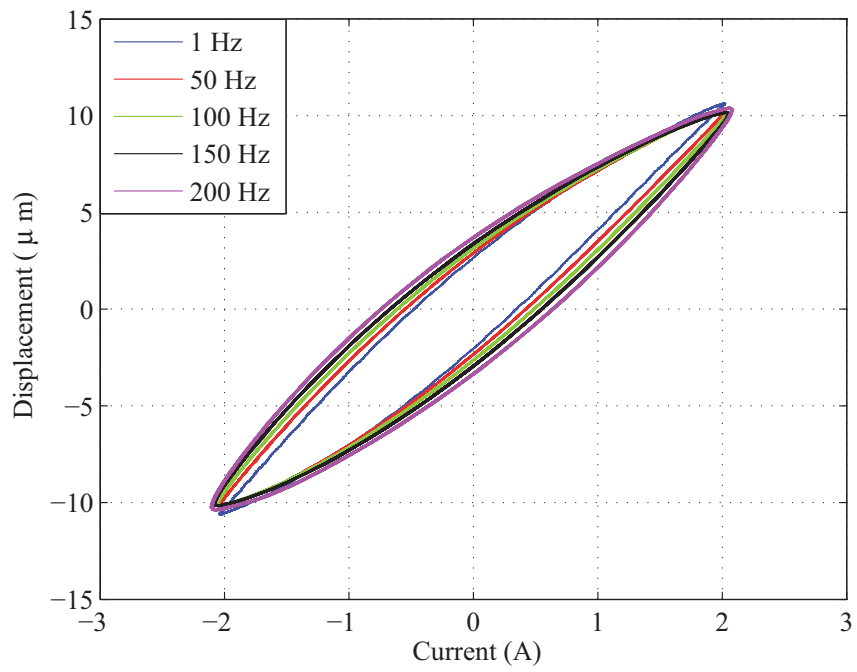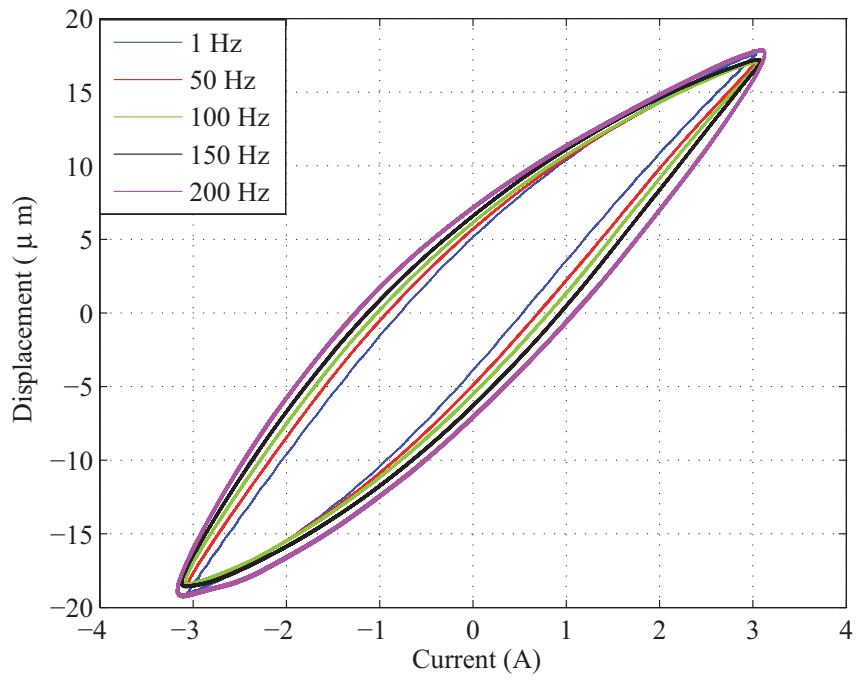
(c) 3 A
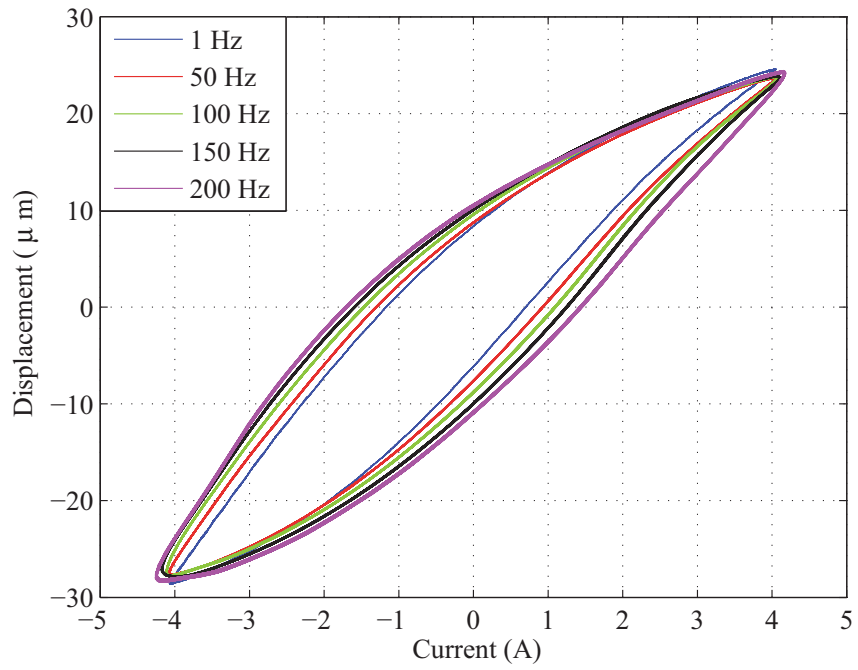
(d) 4 A
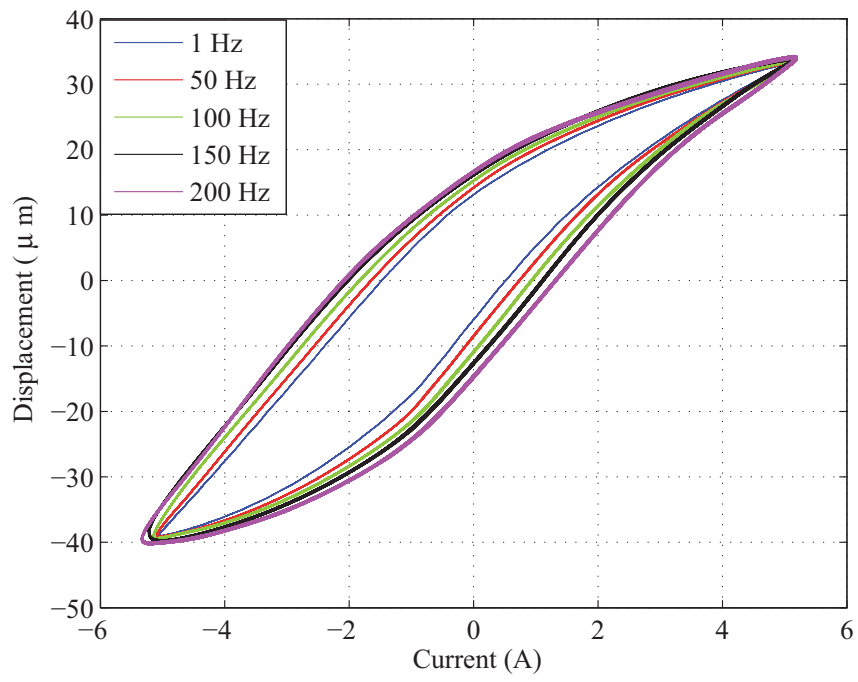
(e) 5 A

Figure 1.10: The input and output relationship under multiple input frequency
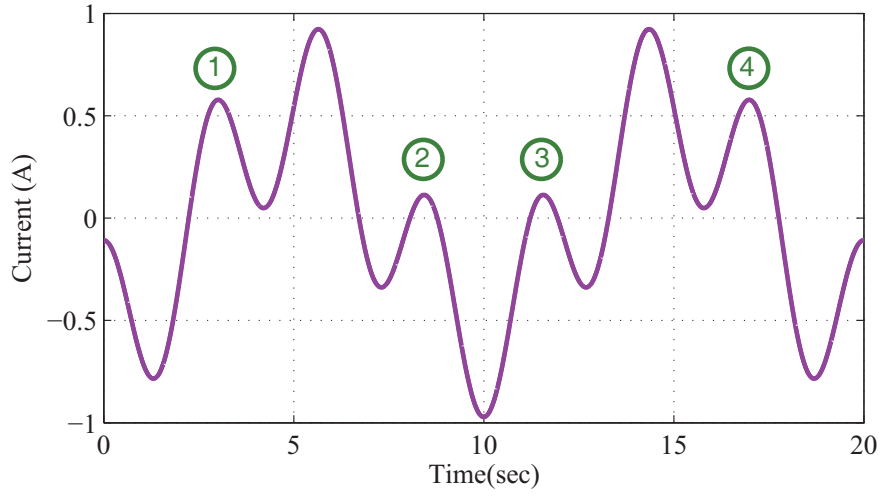
(a) Input signal
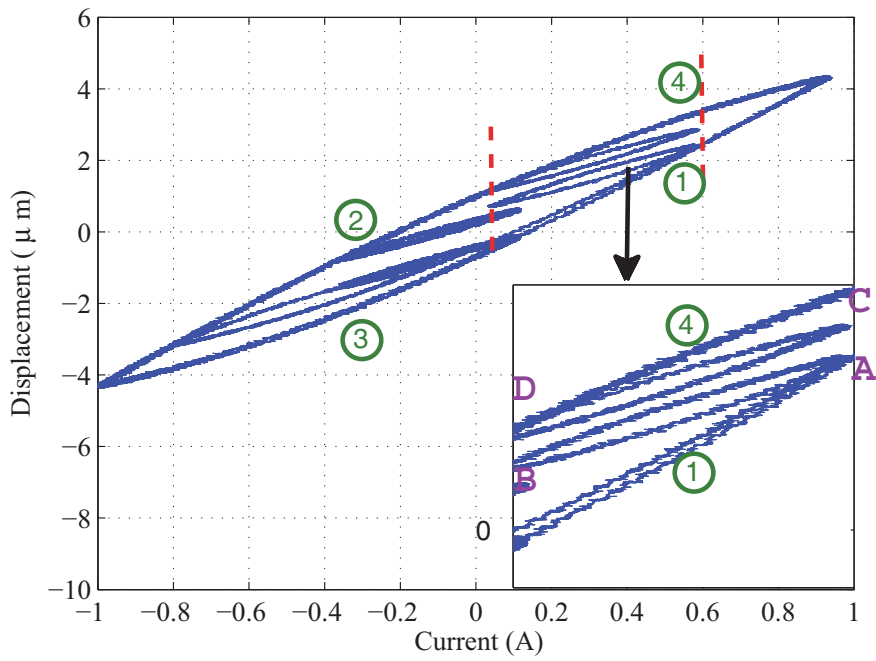
(b) Input and output responses

Figure 1.11: The responses of the actuator under complex harmonic signals with $f_0 = 1$
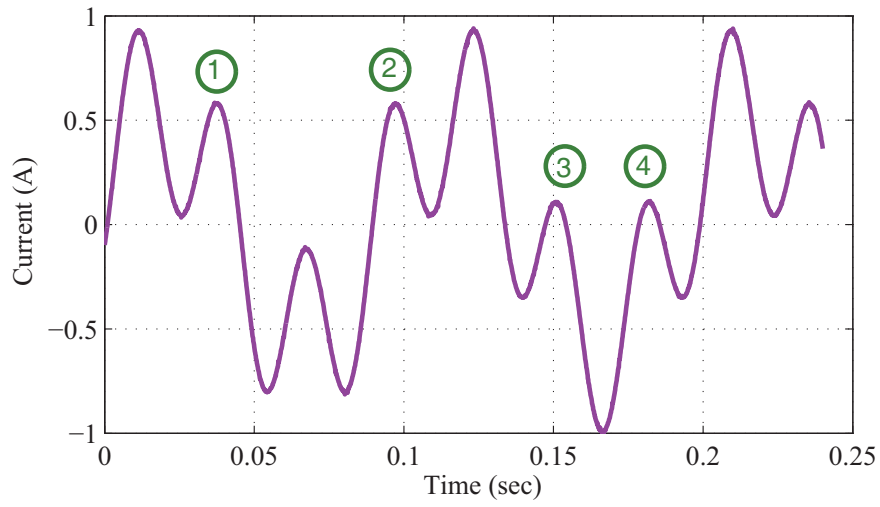
(a) Input signal
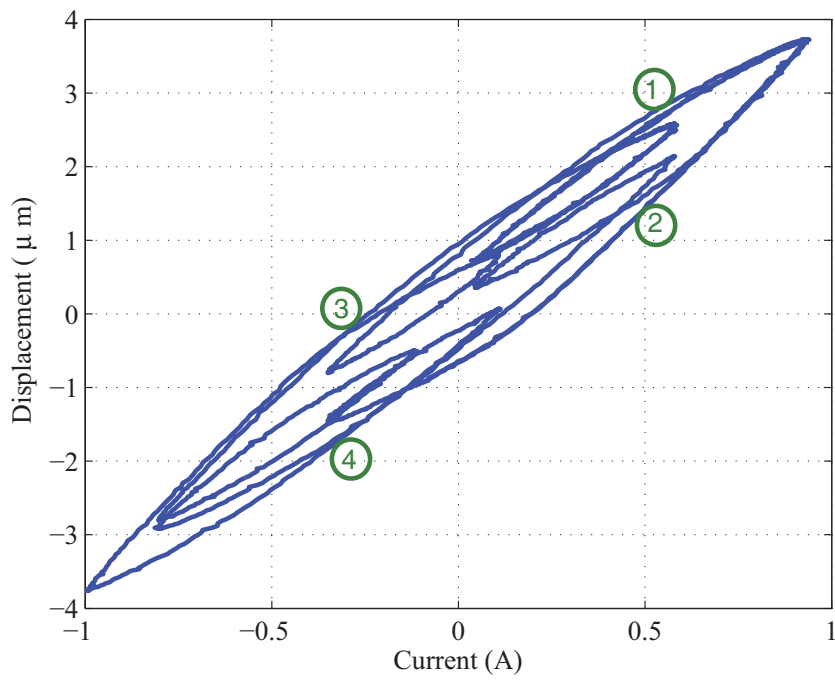
(b) Input and output responses

Figure 1.12: The responses of the actuator under complex harmonic signals with $f_0 = 101$
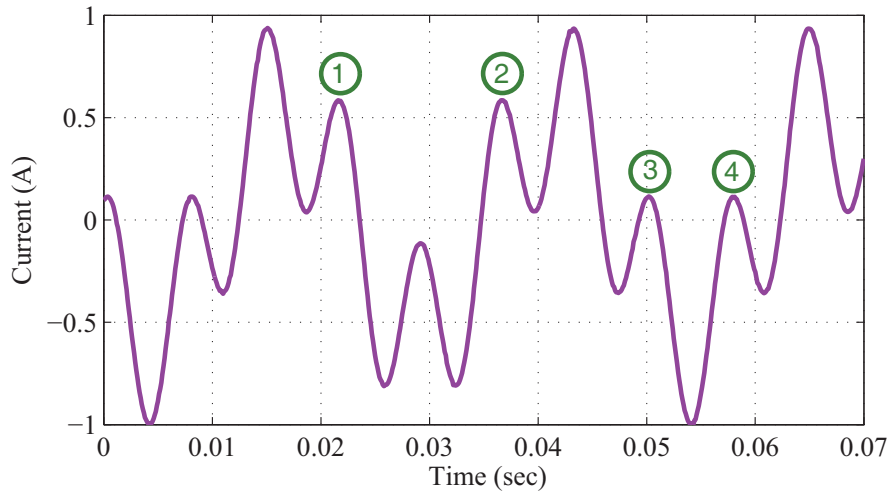
(a) Input signal
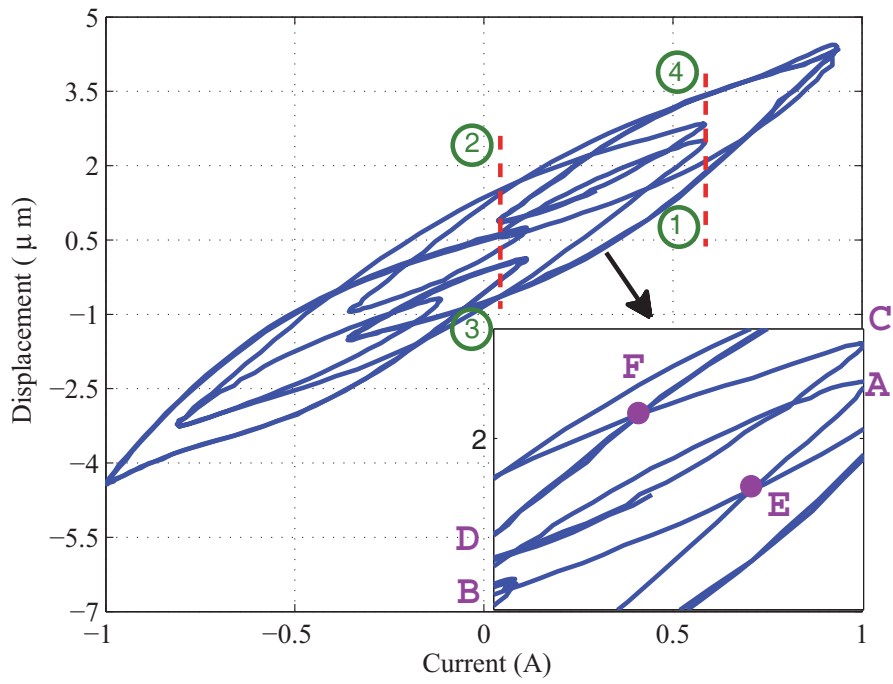
(b) Input and output responses

Figure 1.13: The responses of the actuator under complex harmonic signals with $f_0 = 401$

1.3.3 The Input and Output Responses with Different Input Frequencies and Mechanical Loads

In this section, the input-output responses of the magnetostrictive actuator with mechanical loads ($m = 10.0$ Kg, 21. 5Kg and 33 Kg) and different input frequency ($f = 1Hz, 10Hz, 50Hz, 100Hz, 150Hz, 200Hz$) are investigated, see Figure 1.14. From Figures 1.14(a)-1.14(b), it can be seen that when the actuator operates in the low frequency, i.e. in Figures 1.14(a) and 1.14(b), the mechanical load shows little influence on the performance of the actuator. However, when the actuator works in a high frequency range, i.e. in Figures 1.14(e)- 1.14(f), the mechanical loads impose a great influence on the input-output behaviors of the system.

To clearly show the influence of the mechanical loads and input frequencies on the input-output behaviors, a vertical gap function is adopted as

$$\Phi[u] = |\Gamma_{asc}[u, \zeta_0] - \Gamma_{des}[u, \zeta_1]| \tag{1.1}$$

where $u \in \mathbb{R}$, $\mathbb{R}$ is the set of real numbers; $\Gamma_{asc}[\cdot, \zeta_0]$ is defined as the ascending branch of the input-output curve, $\Gamma_{des}[\cdot, \zeta_1]$ is defined as the descending branch of the input-output curve; ζ_0, ζ_1 denote the internal state of the input and output responses, see Figure 1.15.

Figure 1.16 shows the vertical gap values of the input and output responses of the actuator with different input frequencies and the mechanical loads. In the figure, it can be obviously seen that the value of the vertical gap becomes greater with the increase of the input frequency and mechanical loads. For example, the vertical gap value of the input and output curve at frequency $f = 200Hz$, mechanical load $m = 33kg$ is around 16 times over that at frequency $f = 1Hz$, mechanical load $m = 0kg$. Therefore, from the experimental observations, we can conclude that when the magnetostrictive actuator operates in high frequency, the loading effects dominate the input-output behaviors of the actuator.

(a) 1 Hz

(b) 10 Hz

23

(c) 50 Hz

(d) 100 Hz

24
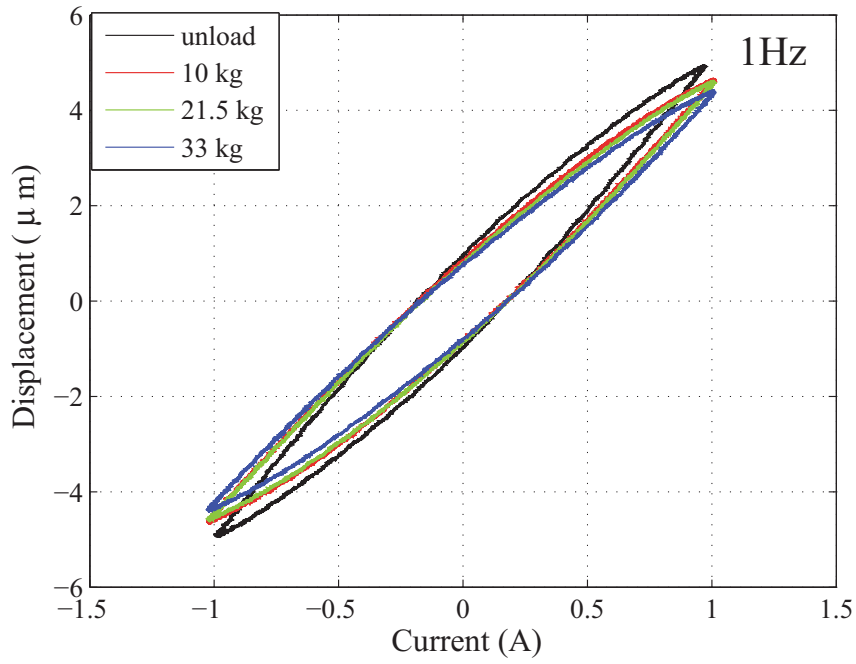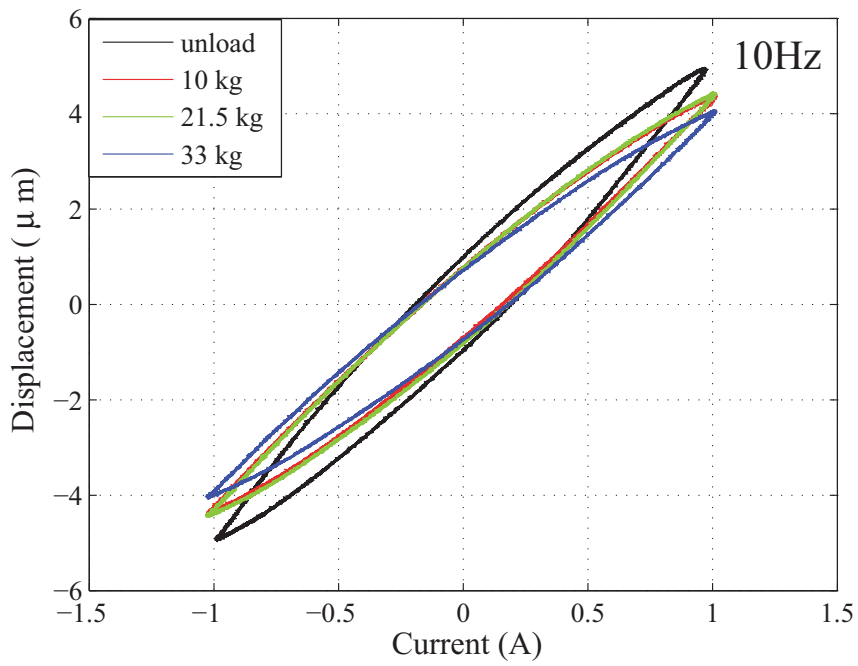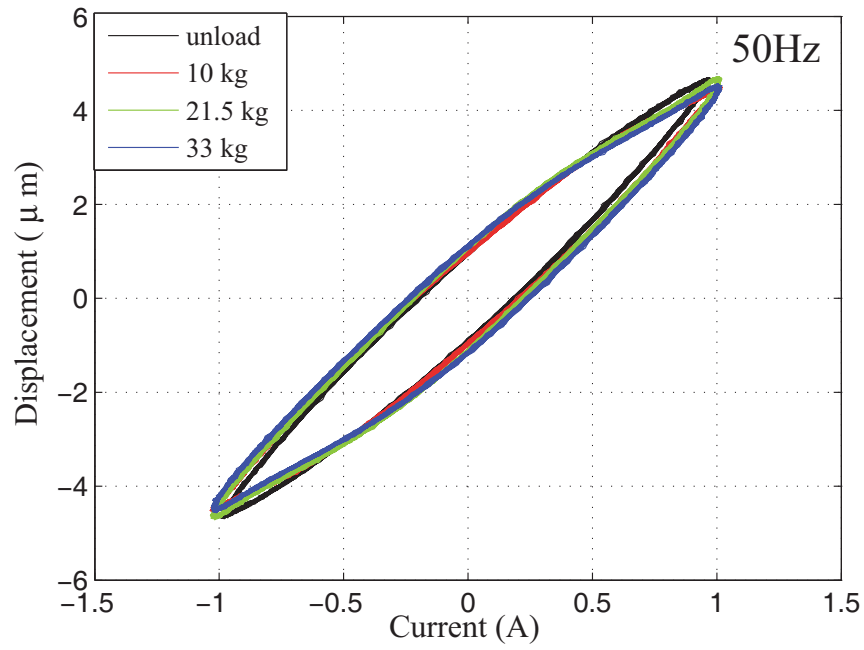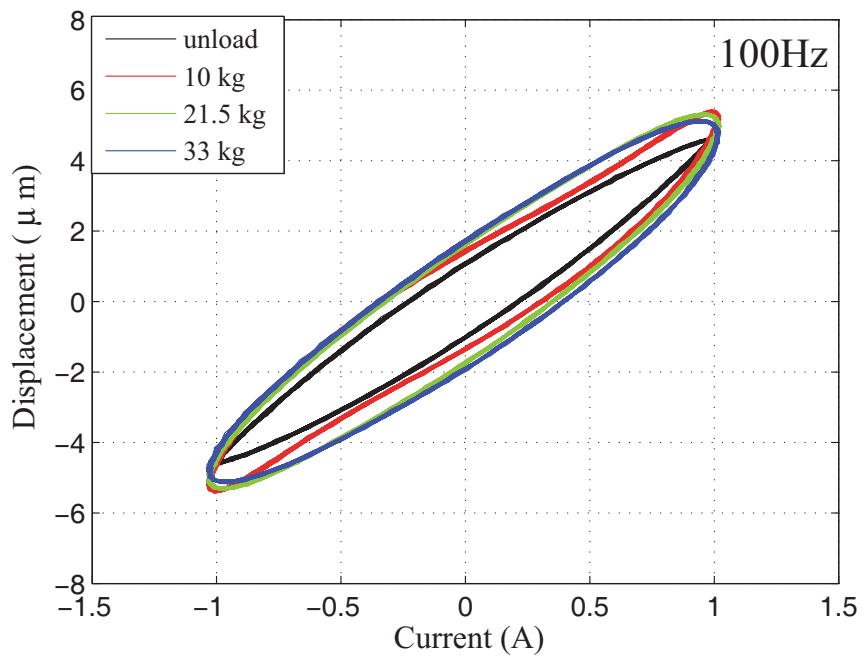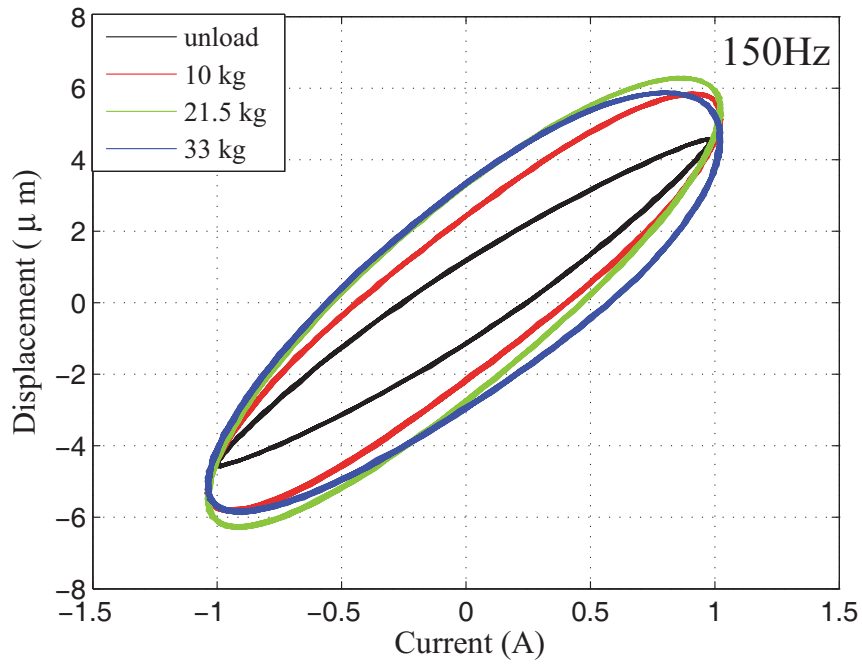
(e) 150 Hz
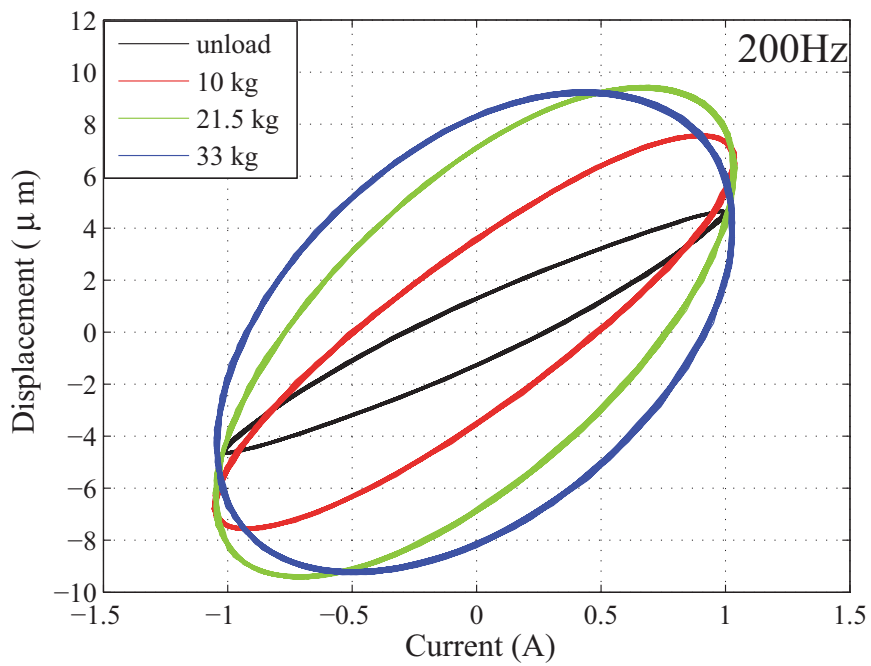
(f) 200 Hz

Figure 1.14: The input and output responses of the magnetostrictive actuator with mechanical loads under different input frequencies

25
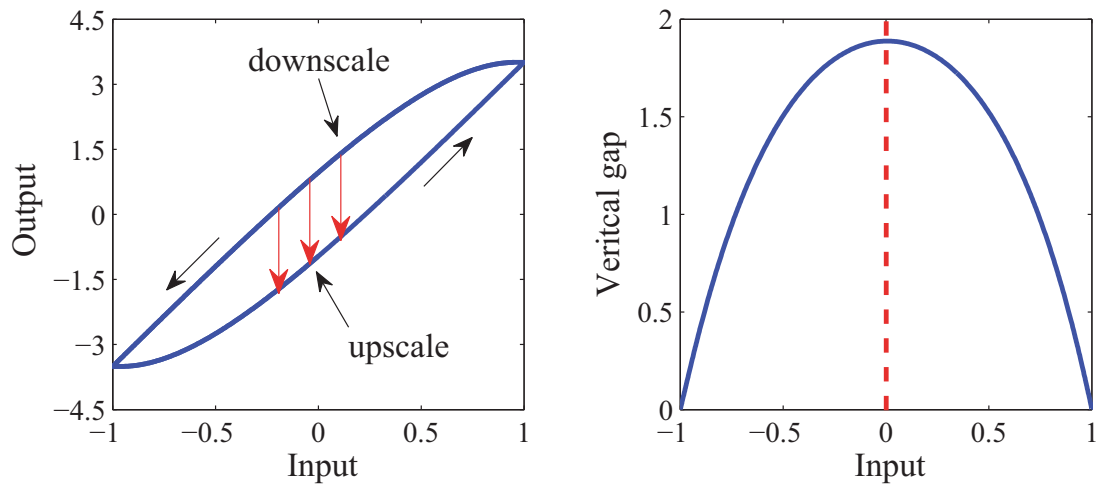
Figure 1.15: The input and output responses and its vertical gap function curve
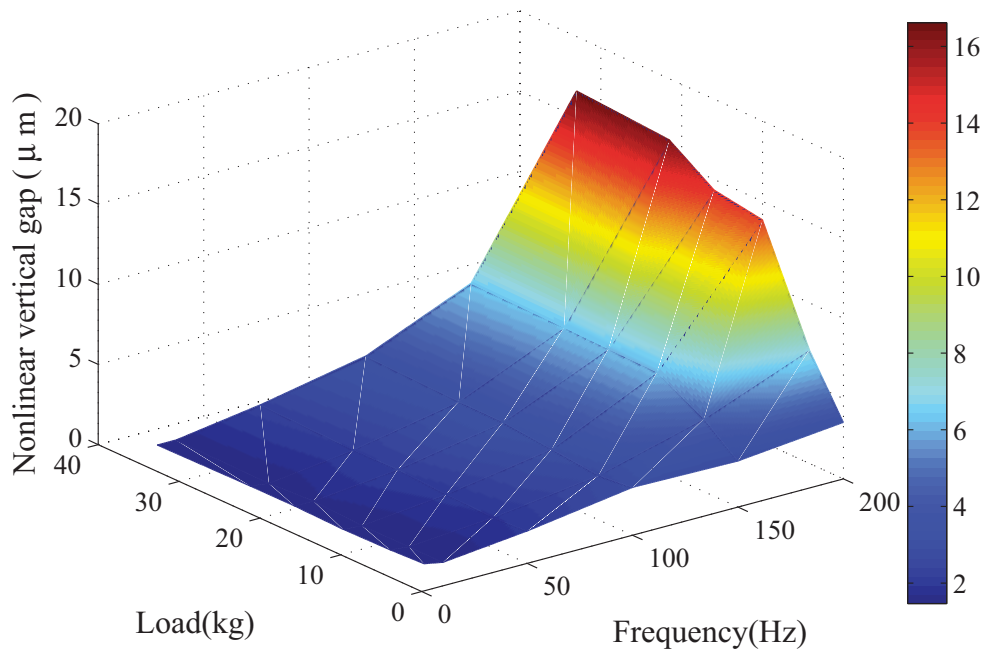
Figure 1.16: The gap values of the input and output responses of the magnetostrictive actuated system with different loads and frequencies

1.3.4 Experimental Results Summary

From the above experimental tests, we can summarize the following experimental phenomena:

- When the magnetostrictive actuator operates with different input frequencies and without mechanical loads, the input and output responses of the magnetostrictive actuator show dynamic hysteretic behaviors. The width of the hysteretic loop increases with increasing with input frequencies.

- When the magnetostrictive actuator operates with different input frequencies and mechanical loads, the input and output responses of the magnetostrictive actuator show strongly frequency-dependence and load-dependence properties, especially for operating in high input frequency and heavy mechanical load.

1.4 Objectives and Contributions

1.4.1 Objectives of the Dissertation Research

From the experimental results reported in Section 1.3, it can be seen that the input and output responses of the magnetostrictive actuated dynamic systems show complex dynamic nonlinear effect. As is well known, control systems with actuators showing such a nonlinearity will generate inaccuracy, oscillations and some other unexpected effects, which poses great challenge on applications of the actuator. Therefore, this dissertation research aims at developing an effective modeling and control methodology to compensate the complex nonlinear effect and improve the tracking performance of the magnetostrictive-actuated dynamic systems.

In order to describe this complex nonlinear phenomenon, a model that can represent the input and output responses needs to be developed first. In the literature, the common approach to describe the input and output behaviors of the magnetostrictive actuator is

to establish a phenomenon model (black box model). This approach only works under certain input frequencies and without mechanical loads or very low input frequencies with mechanical loads. From last section, we have known that the input-output behaviors of the magnetostrictive-actuated dynamic system associated with different input frequencies and mechanical loads present complex nonlinear behaviors. Only treat the actuated system as a black box can not completely predict its behaviors. Therefore, the physical principle that takes place inside of the actuated system should be considered. Towards this target in the dissertation, a physical based dynamic model, comprehensively considering the electric, magnetic and mechanical domain inside of the actuated system as well as the interactions among them, should be developed.

To improve the positioning and tracking performance of the magnetostrictive-actuated dynamic system, a control scheme needs to be developed based on the proposed dynamic model. In the literature, there are many control approaches available, such as sliding mode control, back-stepping control, etc. Among them the back-stepping based prescribed adaptive control, which can both guarantee the global stability of the closed loop system and the transient and steady-state performance of the dynamic system, is a good option. The challenge here lies in how to fuse the available prescribed control approaches with the developed dynamic model. To reach this goal, the feedforward inverse compensation approaches based on the developed dynamic model will be applied and serve as a bridge to connect the model and control approaches.

1.4.2 Contributions of the Dissertation Research

According to the objectives mentioned above, the main contributions of the dissertation are highlighted as follows

- Experimental tests are conducted to study the input-output characteristics of magnetostrictive-actuated dynamic system under different input amplitudes (1A-5A), frequencies (1Hz-200Hz) as well as mechanical loads ($m = 0$ Kg, 10.0 Kg, 21. 5Kg and

33 Kg). The experimental results are thoroughly investigated. It can be observed from the experiments that: 1) when the magnetostrictive actuator operates with different input frequencies and without mechanical loads, the input and output responses of the actuator show dynamic hysteretic behaviors and the width of input and output curves increase with increasing of the input frequencies; 2) when the magnetostrictive actuator operates with different input frequencies and mechanical loads, the input and output responses of the magnetostrictive actuator show strongly frequency-dependence and load-dependence properties, especially operating in high input frequency and heavy mechanical load.

- A dynamic model both considering the nonlinear hysteresis effect and the dynamic behaviors is proposed. The developed model is based on the principle of operation of the magnetostrictive actuator, which comprehensively considers the electric, magnetic and mechanical domain as well as the interactions among them. In order to describe the asymmetric hysteresis effect, an asymmetric shifted Prandtl-Ishlinskii (ASPI) model, which is composed by three components: a Prandtl-Ishlinskii (PI) operator, a shift operator and an auxiliary function, is proposed. The advantages of the proposed AS-PI model are that it can represent the asymmetric hysteresis behavior and facilities the inverse compensation for the purpose of canceling the hysteresis effects in the magnetostrictive actuator. Then, the dynamic model validation is conducted on the magnetostrictive actuated platform. The experimental results illustrate that the proposed dynamic model has an excellent agreement with the dynamic behavior of the system.

- Since the hysteresis effect shown in the magnetostrictive actuator generates undesired and detrimental effects, which will deteriorate the performance of the magnetostrictive actuator and cause inaccuracy and oscillations, the feedforward inverse compensation approaches are applied. At beginning, the Preisach model is selected to represent the hysteresis effect in the proposed dynamic model, and the inverse multiplicative structure compensator is then developed and applied for compensating the hysteresis

effect. However, inverse multiplicative structure needs the exact knowledge of the hysteresis model, which is very restrict for a practical actuator. Based on this point, the proposed ASPI model is utilized to describe the asymmetric hysteresis effect in the dynamic model and the direct inverse compensation approach is applied to find the inverse of the ASPI model. Both inverse compensation approaches have been examined on the magnetostrictive-actuated platform.

- In practical control systems, the use of an estimated hysteresis model in deriving the inverse compensator will yield some degree of hysteresis compensation error. This error will cause tracking error in the closed-loop control system. To accommodate such a compensation error, the analytical expression of the inverse compensation error is derived first. Then, a prescribed adaptive control method is applied to suppress the compensation error and simultaneously guaranteeing global stability of the closed loop system with a prescribed transient and steady-state performance of the tracking error without knowledge of system parameters. The effectiveness of the proposed control scheme is validated on the magnetostrictive-actuated experimental platform. The experimental results show excellent tracking performance by using the proposed control scheme.

1.5 Organization of the Thesis

The dissertation is organized in the following way:

In Chapter 2, based on the experimental tests shown in the introduction, a dynamic model both considering the nonlinear hysteresis effect and the dynamic behaviors is presented.

In order to specially describe the hysteresis effect in the proposed dynamic model in Chapter 2, an asymmetric shifted Prandtl-Ishlinskii (ASPI) model which is constructed by three components: a PI model, a shift model and an auxiliary function, is reported in Chapter 3.

In Chapter 4, the model parameters identification and model validation are conducted to verify the effectiveness of the proposed model in Chapter 2 and Chapter 3.

In Chapter 5, in order to compensate the hysteresis effect in the magnetostrictive actuator, the feedforward inverse compensators are constructed for the Preisach model and the ASPI model separately. The effectiveness of the developed inverse compensation approaches are verified on the magnetostrictive-actuated experimental platform.

In practical control systems, using the inverse for hysteresis compensation generally exhibits notable compensation errors which will yield the tracking error in the closed-loop control system. To accommodate such a compensation error, the analytical expression of the inverse compensation error is obtained first and then a prescribed adaptive control method is adopted in Chapter 6. The effectiveness of the proposed control scheme is verified on the magnetostrictive-actuated platform.

Finally, the Chapter 7 gives a conclusion and recommendations for further work.

Chapter 2

Modeling of Magnetostrictive-actuated Dynamic Systems

From the experimental results reported in Chapter 1, it can be seen that the input and output responses of the magnetostrictive actuator associated with input frequencies and mechanical loads demonstrate complex dynamic nonlinear effect. Such a complex effect poses a great challenge to come up with a proper model that is capable of representing all the relevant behaviors. To face this challenge, comprehensively considering the electric, magnetic and mechanical domain inside of the actuator as well as the interactions among them, a dynamic model is therefore developed for the purpose of describing the complex input-output behaviors of the magnetostrictive actuator in this chapter.

A literature review is presented in Section 2.1 to introduce the available modeling approaches of the magnetostrictive actuator. In Section 2.2, the proposed dynamic model of the magnetostrictive-actuated dynamic system is provided in details.

2.1 Literature Review

In Chapter 1, we have shown that the input and output responses of the magnetostrictive-actuated dynamic system associated with different input frequencies and mechanical loads present complex dynamic behaviors. For example, when the magnetostrictive actuator operates in low input frequency and no mechanical loads, the input and output responses only show hysteretic behaviors, however when it operates in high input frequency and heavy mechanical loads, the input and output responses not only present hysteretic behaviors but become highly depending on the input frequency and the mechanical loads. The reason for this phenomenon can be explained as with the increase of the input frequency and the mechanical loads, the inertia force and flexibility of the magnetostrictive actuator greatly hinder the rapid change of the actuator, which leads to larger phase lag and wider hysteresis curves, thus the dynamic responses start to dominate the input-output relations of the system. In order to reflect these complex behaviors, in the literature, several models are established, which can be classified into two categories: the phenomenon-based modeling approach and the physical-based modeling approach.

The main idea of the phenomenon-based modeling approach is to use the input (current) and output (displacement) experimental data of the magnetostrictive actuator to do the curve fitting. For the operation of the magnetostrictive actuator in low input frequency and no mechanical loads, the input and output responses can be predicted only using the hysteresis models [11], [12], [18], [19], [20] (the detailed information of the hysteresis models will be introduced in the following chapter). However, these models are only focusing on describing the hysteresis effect in the working condition with low input frequency and without mechanical load, and thus they fail to describe the dynamic behaviors of the actuator when the magnetostrictive actuator operates in high input frequencies and heavy mechanical loads.

To reflect the influence of the input frequency, the rate-dependent dynamic model can be therefore adopted. In [21] [22] [23], the time derivative of the model output or the time derivative of the input signal is introduced into the model to characterize the variation of

the input frequency as

$$u(t) = \iint_{T_0} \mu_0(\alpha, \beta)\hat{\gamma}_{\alpha,\beta}[v](t)d\alpha d\beta + \frac{du}{dt}\iint_{T_0}\mu_0(\alpha,\beta)\hat{\gamma}_{\alpha,\beta}[v](t)d\alpha d\beta \qquad (2.1)$$

The term $\frac{du}{dt}$ is utilized to reflect the change of the input frequency in (2.1). In [24], the rate-dependent model is proposed as

$$u_p = w(v, \dot{v})v + \int_0^R g(v, \dot{v})p(r)F_r[v]dr \qquad (2.2)$$

where $w(v, \dot{v})$ and $g(v, \dot{v})$ are both functions of $\dot{v}$, and the variable r

$$r = \alpha \sum_{l=1}^{z} ln(\beta_l + \lambda_l|\dot{v}(t)|^{\varepsilon l}) \qquad (2.3)$$

is also function of $\dot{v}$. By introducing $\dot{v}$ into the function $w(\cdot, \cdot)$ and the variable $r(\cdot)$, the proposed rate-dependent model is capable of describing the dynamic behavior with different input frequencies. However, the rate-dependent dynamic model can only reflect the change of the input frequencies but fail to describe the loading effect, since no load variable appears in the model (2.1) and (2.2).

To characterize the loading effect, similar with the modeling strategy on frequency dependence, the load term should be introduced into the model as [16]

$$\epsilon(t) = \Gamma[f(i, T)](t) \qquad (2.4)$$

where $\epsilon(t)$ is the output, i is the input current, T denotes the applied load. Similarly, the load term m can also be introduced into the weight function $\mu(\alpha, \beta, m)$ of the model as [25],

$$y(t) = \Xi[u, \zeta_0, m](t) = \iint_{T_0}\mu(\alpha, \beta, m)\hat{\gamma}_{\alpha,\beta}[u](t)d\alpha d\beta \qquad (2.5)$$

Although the proposed model in [16] and [25] can describe the loading effect, the working conditions of the magnetostrictive actuator in different input frequencies are not considered.

Besides the phenomenon based model mentioned above, there are also some physics based models, which are built according to physical principles such as electromagnetic theory, magnetism theory and continuum mechanics equations [26]. Among the physical-based models,

the Jiles-Atherton model [27] is the most popular one. The Jiles-Atherton model developed based on the energy balance theory presents the capability of depicting the input and output responses with different input frequencies and mechanical loads. Unfortunately, the input of the model is magnetic filed and the output is magnetization, which are not our research interests. Moreover, this kind of physical-based model normally has complex structure and the parameters are difficult to determine. Therefore, the physical-based model can not directly applied for our research purpose.

2.2 Development of the Dynamic Model for the Magnetostrictive Actuators

Based on analysis reported in Section 2.1, we can conclude that in the literature, there is no such a comprehensive model that can describe the input (current) and output (displacement) responses of the actuator both with a wide range of input frequencies and mechanical loads. In order to capture the complex input and output behaviors, current-magnetic flux hysteresis, frequency responses of the actuator, nonlinear magnetic behaviors, as well as the mechanical loads should be comprehensively considered in the modeling strategy. To this end, a dynamic model based on the principle of operation of the magnetostrictive actuator, which comprehensively considers the electric, magnetic and mechanical domain as well as the interactions among them is proposed in this dissertation.

Figure 1.1 clearly shows the inside structure of the magnetostrictive actuator, which consists of current-carrying winding coils, a movable Terfenol-D drive rod surrounded by the winding coils, bias permanent magnets that produce the bidirectional movement of the rod, a pair of preloaded springs and an output rod attached to the Terfenol-D rod. The drive rod produces a stroke and output force by the moving magnetic field generated by the current-carrying winding coils on the physical principles of Terfenol-D. The preloaded springs and the bias permanent magnets are utilized to produce bidirectional movement of

35

the Terfenol-D rod. Since the Terfenol-D rod can produce a large stroke and output force, no additional mechanism is designed to amplify the output motion.

The magnetostrictive actuator works on the principle that when a supplied current i flows through the solenoid, a magnetic field H is created, according to Ampere's Law

$$H = Ni \tag{2.6}$$

where N denotes the total turns of the solenoid. In the presence of the magnetic field H, small magnetic domains rotate themselves to cause internal strains in the Terfenol-D rod, leading to a magnetostrictive force F_a as

$$F_a = AE^H d_{33} H \tag{2.7}$$

where A denotes the area of the magnetostrictive rod, E^H denotes the Young's modulus at constant value of magnetic field H, d_{33} is the slope of the strain versus magnetic field. Submitting (2.6) into (2.7), we have

$$F_a = AE^H d_{33} Ni = T_{em} i \tag{2.8}$$

where $T_{em} = AE^H d_{33} N$ denotes the electromechanical transduction coefficient. Since we only interest in the displacement of the endpoint of the actuator, the mechanical dynamic (force-displacement) responses of magnetostrictive actuator can be equivalent as a simple mass-spring-damper system, which is defined as

$$m\ddot{x} + b_s \dot{x} + k_s x = F_a \tag{2.9}$$

where x denotes the displacement of the endpoint of the actuator, m is the mass of the moving part with the mechanical loads, b_s is the damping coefficient, and k_s is the stiffness. Thus, the dynamic responses of magnetostrictive actuator can be expressed by (2.8) and (2.9), which indicate a linear relationship between the supplied current i and the displacement x.

However, due to the existence of electrical-magnetic losses: hysteresis loss and eddy current loss (the definition will be given in the following development), the responses of the
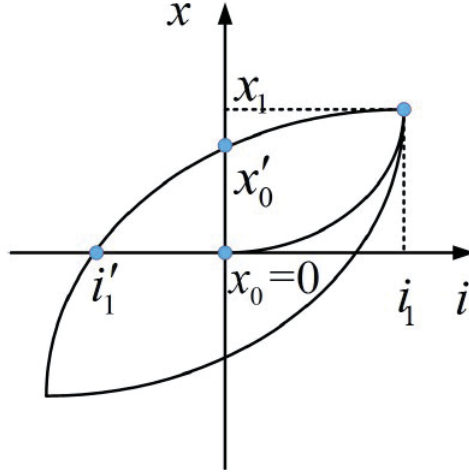
Figure 2.1: The hysteresis nonlinear behavior

supplied current i and the displacement x actually exhibit nonlinear characteristics. Figure 2.1 shows the hysteresis effect of the magnetostrictive rod and its physical meaning is briefly explained as follows. When a current is applied to the winding coils, a magnetic field is produced along the magnetostrictive rod and the rod elongates at point (i_1, x_1). Then remove the supplied current, the produced magnetic field disappears immediately, while the magnetostrictive rod, point $(0, x_0')$, will not relax back exactly to zero magnetization, point $(0, 0)$, before the current was applied. It must be driven to zero by imposing a current in the opposite direction to force the magnetic domain to rotate back, point $(i_1', 0)$. Therefore, the current-displacement curve of the actuator shows a looped relationship, namely hysteresis loop. For every loop, due to this domain reversal there will be extra work done. For this reason, there will be a consumption of electrical energy which is known as hysteresis loss of the transducer. Due to the presence of the hysteresis loss, the actual current i_a flowing through the inductance is no longer equal to the supplied current i, and one has

$$i_a = i - i_H \tag{2.10}$$

where i_H denotes the hysteresis loss current, which shows a nonlinear relationship with the displacement x as

$$i_H = \Pi[x] \tag{2.11}$$

37

Π represents the hysteresis operator, which can be described by the ASPI model reported in Chapter 3.

In addition to the hysteresis loss, the actuator also has the eddy current effect. In presence of a supplied current i, a magnetic field is created, which leads to a magnetic flux Φ'. Meanwhile, according to the Faraday's law and Lenz's law, an induced electromotive force upon the rod gives rise to a current (eddy current) whose magnetic field (with a magnetic flux Φ_{eddy}) opposes the original change in magnetic flux Φ'. Then the opposed magnetic flux Φ_{eddy} will react to the winding coils and creates an opposed current (eddy current loss) i_R, see Figure 2.2.
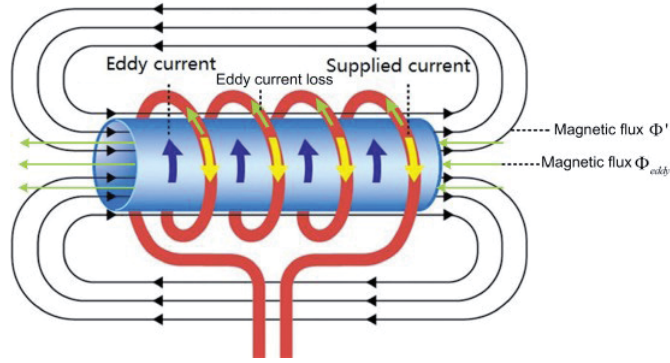
Figure 2.2: The illustration of the eddy current effect

Considering both hysteresis loss and eddy current effect, the actual current i_a flowing through the winding coils is obtained as

$$i_a = i - i_H - i_R \tag{2.12}$$

Based on the Faraday's law, the eddy current loss i_R is obtained as

$$i_R = \frac{\dot{\Phi}}{R_0} \tag{2.13}$$

where R_0 is the equivalent resistor of the eddy current effect. Φ denotes the overall magnetic flux as

$$\Phi = \Phi_L + \Phi_T \tag{2.14}$$

where $\Phi_L = i_a L_a$ is the magnetic flux generated by the actual driven current, L_a denotes the equivalent inductor of the winding coils, $\Phi_T = T_{Mm} x$ is transformed from the mechanical side which is similar to the back-emf in piezoelectric actuator [28] [29], T_{Mm} is magnetomechanical transduction coefficient. Figure 2.3 illustrates the dynamic electro-magneto-mechanical model of the magnetostrictive actuator resulting from the aforementioned analysis.
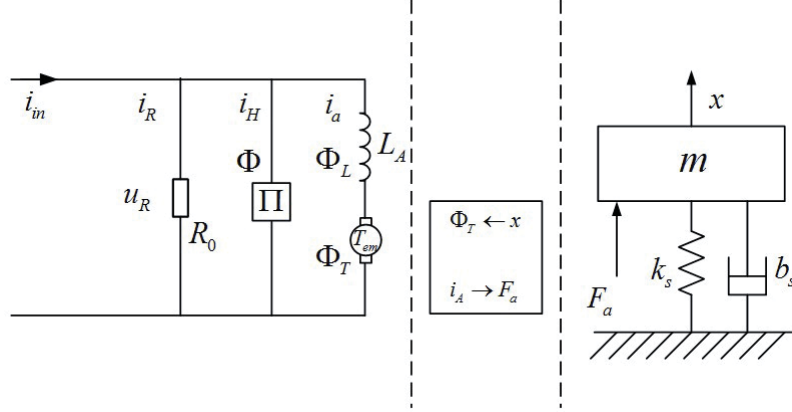
Figure 2.3: Dynamic modeling of the magnetostrictive positioning platform system

According to (2.7)-(2.14), the dynamic model of the magnetostrictive-actuated dynamic system is represented by the following equations:

$$m\ddot{x}(t) + b_s\dot{x}(t) + (k_s + \frac{T_{em}T_{Mm}}{L_a})x(t) = \frac{T_{em}}{L_a}\Phi \tag{2.15}$$

$$L_a\frac{\dot{\Phi}}{R_0} + \Phi - T_{Mm}x = L_a(i - \Pi[x]) \tag{2.16}$$

Remark: It is well known that dynamic model of a permanent magnet dc motor can be described as:

$$L_m\frac{di_m(t)}{dt} + R_m i_m(t) + K_{emf}\frac{d\theta(t)}{dt} = v_{in}(t) \tag{2.17}$$

$$J\ddot{\theta}(t) + B\dot{\theta}(t) = K_t i_m(t) \tag{2.18}$$

where $i_m(t)$ is the armature current, $\theta(t)$ is the angular position, L_m, R_m, K_{emf}, and K_t are the inductance, resistance, back-emf constant, and torque constant of the motor, respectively, J is the inertia of the rotor and the equivalent mechanical load, and B is the damping coefficient. From (2.15) and (2.16), we can find that the dynamic model of the

magnetostrictive-actuated system is similar to the traditional dc motor (2.17) and (2.18) except the hysteresis nonlinearity $\Pi[x]$. Therefore, the challenge for control of the magnetostrictive positioning platform system mainly lies in accommodating the nonsmooth nonlinear hysteresis $\Pi[x]$, which usually deteriorates the system performance in such manners as generating undesirable inaccuracies or oscillations.

2.3 Concluding Remarks

In this chapter, a dynamic model considering both the nonlinear hysteresis effect and the dynamic behaviors has been proposed. The developed model is based on the physical principle of the magnetostrictive actuator, which comprehensively considers the electric, magnetic and mechanical domain as well as the interactions among them. It should be noted that the dynamic model of the magnetostrictive-actuated system is similar to the traditional dc motor. The only difference between the proposed dynamic model and the model of the dc motor is the hysteresis nonlinearity $\Pi[x]$ in (2.16), which brings a great challenge in the modeling work.

Moreover, it should mention that the model validation is not reported in this section since it depends on the selection of the hysteresis model. In the next section, we will address the issue of hysteresis modeling. After the determination of the hysteresis description, we will then demonstrate the validation of the developed model.

Chapter 3

Hysteresis Modeling in Magnetostrictive-actuated Dynamic Systems

In Chapter 2, a dynamic model that can both represent the hysteresis effect and the dynamic behaviors in the magnetostrictive actuator has been proposed. In order to conduct the model validation, a proper hysteresis model needs to be developed first. Therefore, in this chapter, we are going to discuss the hysteresis modeling strategy and the developed modeling approaches for describing the hysteresis nonlinearity $\Pi[x]$ in the model (2.15) and (2.16) in Chapter 2.

In Section 3.1, a literature review is presented to give a general status on the hysteresis modeling. In Section 3.2, the proposed asymmetric shifted Prandtl-Ishlinskii (ASPI) model for describing the hysteresis behaviors of the magnetostrictive actuator is reported.

3.1 Literature Review

The hysteresis effect shown in magnetostrictive actuators is a very common phenomenon which appears in many different fields. Ferromagnetic hysteresis [30] and plastic hysteresis [27] are two typical examples. Hysteresis appears in all the smart materials, such as magnetostrictive materials, piezoceramics, SMA, etc., which all reveal a looped and branched nonlinear relation between the input excitation and the output displacement. Hysteretic behaviors also arise in aerodynamics [31] [32], where the aerodynamic forces and moments show hysteresis when the attack angle of the airplane varies. Others are encountered in mechanical systems [33] [34] [35], economics [36], neuroscience [37] [38] and electronics engineering [39] [40] etc. Therefore, in this section, we starts with the historical overview of the hysteresis. Then, we will review the available modeling approaches for describing the hysteresis effect.

3.1.1 Historical Overview of the Hysteresis

The study of hysteresis has a long history. The term hysteresis was coined by the Scottish physicist James Alfred Ewing in 1881 to describe the effects observed on iron and steel wires when they were magnetized [36]. The specific definition of the hysteresis was given as

When there are two quantities M and N, such that cyclic variations of N cause cyclic variations of M, then if the changes of M lag behind those of N, we may say that there is hysteresis in the relation of M and N.

In 1905, Madelung [30] formalized three practical rules from the experiments to determine a hysteresis behavior in ferromagnetic materials:

- 1) Any curve Γ_1 emanating from a turning point A of the input-output graph, see Figure 3.1, is uniquely determined by the coordinates of A.

- 2) If any point B on the curve Γ_1 becomes a new turning point, then the curve Γ_2 originating at B leads back to the point A.

- 3) If the curve Γ_2 is continued beyond the point A, then it coincides with the continuation of the curve Γ which led to the point A before the $\Gamma_1 - \Gamma_2$ cycle was traversed.
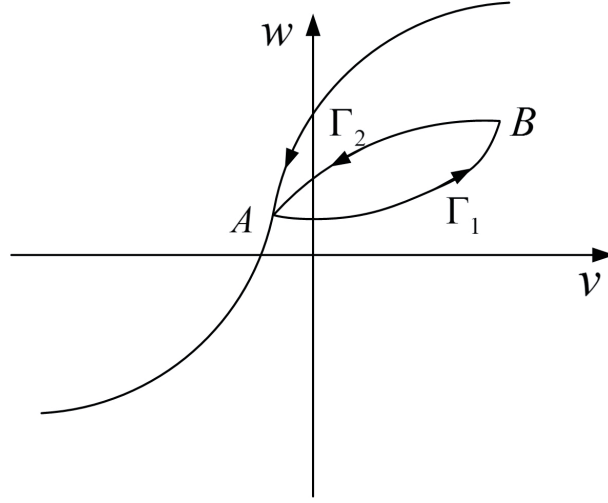
Figure 3.1: Madelung's rules

If a nonlinear relation satisfy the Madelung's rules, this nonlinear relation can be called as hysteresis. Following Madelung's rules, in 1928, L. Prandtl [30] proposed the Prandtl model which was constructed by superposing the stop operators with a designed density function to describe the hysteresis effect in elastic-plastic materials. In 1935, F. Preisach [41] proposed the Preisach model based on some hypotheses concerning the physical mechanisms of magnetization [42]. The model is defined as a superposition of the relay operators, which has a similar structure with Prandtl model. However, the proposed Prandtl model and Preisach model were still associated with specific physical meaning and no mathematical analysis of these models were conducted [43]. It was until 1966, an engineering student R. Bouc [35] firstly demonstrated a mathematical methodology to analyze hysteresis where he treated hysteresis as a map between function spaces.

In 1970s, a group of Russian mathematicians led by Krasnosel'skii [44] conducted a systematic analysis of the mathematical properties of Prandtl-Ishlinskii model. They suggested an investigation of hysteresis phenomenon using the theory of nonlinear operators (or hysterons). Moreover, they separated Preisach model from its physical meaning and represented

it in a purely mathematical form.

In 1980's, a further study on Preisach model was conducted by Mayergoyz [42]. He summarized two conditions for the Preisach model: the wiping-out property and the congruency property, which constitute necessary and sufficient conditions for hysteresis transducer to be represented by the Preisach model. In addition, he also put forward an identification technique for Preisach model by using a set of first-order reversal curves, which was the first time to provide a systematic identification approach for the Preisach model. Meanwhile, Visintin [45], Brokate and Sprekels [46] studied the existence and uniqueness of solutions of ordinary differential equations (ODE) and partial differential equations (PDE) coupled with hysteresis operators [47].

From 1990's to present, the hysteresis phenomenon re-attracts the attention of many researchers due to the development and explosive growth research on smart materials. The hysteresis modeling techniques are therefore well developed. Some novel characteristics of the hysteresis models have been explored and numerous extended and modified hysteresis models have been proposed for describing more complex hysteretic behaviors, such as asymmetric hysteresis phenomenon, rate-dependent hysteresis. The further development of the hysteresis models are summarized as follows.

3.1.2 Hysteresis Models

In the literature, the developed hysteresis models can roughly be classified into two categories: the operator-based hysteresis model and differential equation based hysteresis model, see Figure 3.2. Operator-based hysteresis models including Preisach model [41], Prandtl-Ishlinskii (PI) model [30] and Krasnosel'skii-Pokrovkii (KP) model [48] are constructed by superposing weighted elementary operators, such as relay operator, play operator, KP kernel. Operator-based hysteresis models show excellent hysteresis prediction. However, the modeling accuracy is proportional to the number of the superposed elementary operators. A large number of operators will bring heavy computational cost. The differential equation-
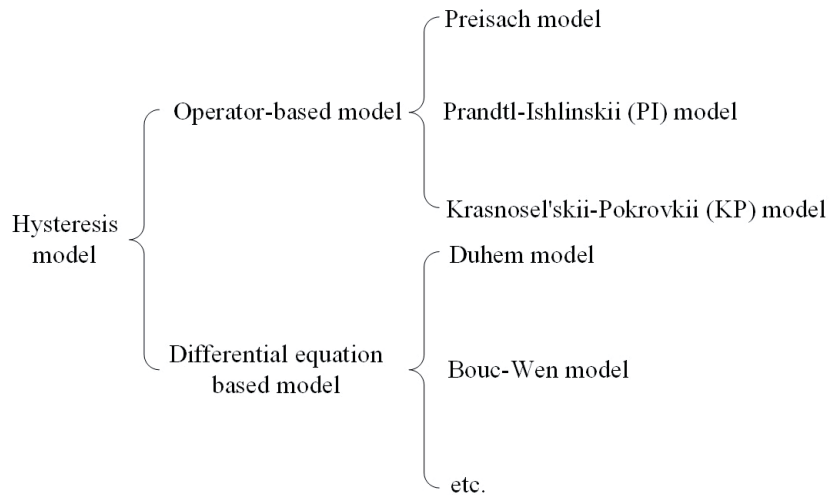
Figure 3.2: Classification of the hysteresis models

based hysteresis models, on the other hand, are finite dimensional, which only need limited parameters to govern the scale and general shape of the hysteresis curves. Thus they can avoid the computation complexity when conducting the model identification. Nevertheless, limited model parameters lead to large model estimation errors. In the following development, a brief summarization of the general operator based hysteresis models and differential equation based hysteresis models are reviewed.

Preisach Model

The Preisach model was first suggested in 1935 by F. Preisach in his paper "Über die magnetische Nachwirkung" [41]. The model was established on some plausible hypotheses concerning the physical mechanisms of magnetization. Therefore, at first the Preisach model was regarded as a physical hysteresis model. In 1970, a group of Russian mathematicians led by Krasnosel'skii separated Preisach model from its physical meaning and represented it in a general mathematical form. As a result, the Preisach model becomes a phenomenological model and can describe different types of physical nature of hysteresis, such as ferromagnetic hysteresis, adsorption hysteresis, ferroelectric hysteresis, etc. The phenomenological treatment of the Preisach model opens a new way in the study of hysteresis as it can be found in

Mayergoyz [42] [21] [49], Visintin [45], Bertotti [50] and Brokate [30].

The Preisach model is defined as

$$u(t) = \Gamma[v](t) = \iint_{T_0} \mu(r,s)\hat{\gamma}_{s-r,s+r}[v](t)drds \qquad (3.1)$$

where $\hat{\gamma}_{s-r,s+r}[v](t)$ denotes the relay operator, see Figure 3.3 as

$$\hat{\gamma}_{s-r,s+r}[v](t) = \begin{cases} +1 & \text{if } v(t) > s+r \\ -1 & \text{if } v(t) < s-r \\ \hat{\gamma}_{s-r,s+r}[v](t^-) & \text{if } s-r \leq v(t) \leq s+r \end{cases}$$

$t^- = \lim_{\varrho>0,\varrho\to0} t - \varrho$, s and r are two parameters that determine switching values $+1$ (the switch is "on") and -1 (the switch is "off"), $v(t)$ denotes the input signal, $\mu(r,s)$ is the density function of the Preisach model, which is selected by designers. Without losing the generality, the density function $\mu(r,s)$ is defined on a compact support [51]: $T = \{(r,s) \in T_0 | r - R \leq s \leq -r + R, R > 0\}$ with a bound $R > 0$, and $\mu(r,s)$ is equal to zero outside the triangle T, T_0 denotes the set $\{(s,r)| -\infty < s < \infty, r \geq 0\}$. The Preisach model is a widely accepted hysteresis model in the literature which has been employed to describe various hysteretic behaviors in smart materials, such as piezoelectric materials [52] [53], magnetostrictive materials [20], ion-exchange polymer-metal composites (IPMCs) [54] and electro-rheological (ER) fluid [55] etc.

Prandtl Ishlinskii(PI) Model

The Prandtl-Ishlinskii (PI) model is defined as a superposition of play operator or stop operator, which is expressed as

$$P[v](t) = p_0 v(t) + \int_0^\Lambda p(r)F_r[v](t)dr \qquad (3.2)$$

where p_0 is a positive constant; $p(r)$ is a given density function, satisfying $p(r) \geq 0$ with $\int_0^\infty rp(r)dr < \infty$. Since the density function $p(r)$ vanishes for large values of r, the choice
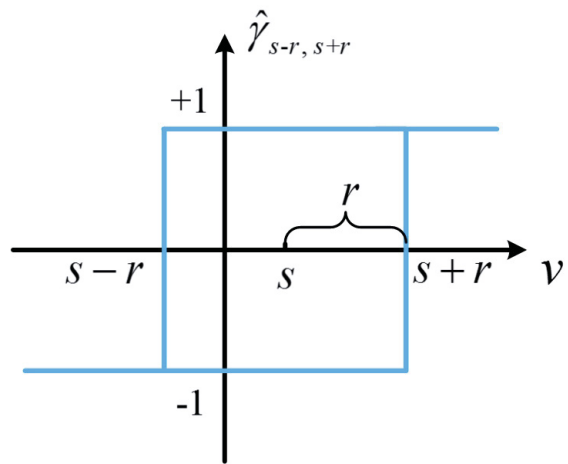
Figure 3.3: Relay operator
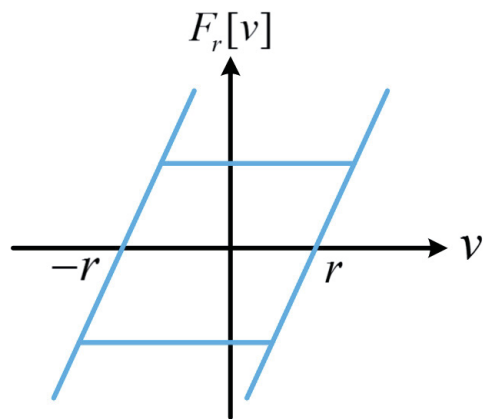
Figure 3.4: Play operator

of Λ as the upper limit of integration in the literature is just a matter of convenience [56]. $F_r[v]$ is the play operator, see Figure 3.4:

$$F_r[v](0) \quad = \quad f_r(v(0), 0) \tag{3.3}$$

$$F_r[v](t) \quad = \quad f_r(v(t), F_r[v](t_i)) \tag{3.4}$$

for $t_i < t \leq t_{i+1}, 0 \leq i \leq N - 1$, with

$$f_r(v, w) = max(v - r, min(v + r, w)) \tag{3.5}$$

where $0 = t_0 < t_1 < \ldots < t_N$ is a partition of $[0, t_N]$, such that the function $v(t)$ is monotone on each of the subintervals $[t_i, t_{i+1}]$.

According to the definition of the play operator, the PI model can only describe the symmetric hysteresis effect. However, there are many cases that the hysteresis exhibits asymmetric behaviors such as hysteresis in magnetostrictive actuators, shape memory alloys (SMA) actuators. To keep the feature of PI model, the extension of the PI model to describe the asymmetric hysteresis behavior has been exploited in the literature, including: 1) cascading a nonlinear operator with the PI model. In [57], a modified PI model, superposition of one-sided dead-zone operators proceeded by the PI model, was proposed. This model can describe certain asymmetric hysteresis behaviors and has analytical solutions of its inversion, but it cannot describe the saturated asymmetric hysteresis behaviors; 2) modifying the elementary play operator. In [58], the elementary play operator was redefined as a right-side play operator and a left-side play operator. In [59], a non-symmetric play operator was considered as the elementary operator. In [60], a generalized play operator with envelope functions was proposed. The disadvantage of this type of modified model is its inverse construction and the selection of the asymmetric function.

Krasnoselskii-Pokrovskii(KP) Model

The Krasnoselskii-Pokrovskii model developed by Banks, Kurdila and Webb [48] [61] represents scalar hysteresis as the cumulative effect of weighted elementary hysteresis operators

$k_p[v, \xi_p](t)$ that are distributed over the domain in R^2. The KP model can be expressed as

$$u(t) = H[v](t) = \int_P k_p[v, \xi_p](t) \, \mu(p) \, dp \qquad (3.6)$$

where $\mu(p)$ is the distribution function, P is the Plane defined by

$$P = \left\{ p(p_1, p_2) \in R^2 : v^+ \geq p_2 \geq p_1 \geq -v^- \right\} \qquad (3.7)$$

where v^- and v^+ denote input values of negative and positive saturation states of hysteresis, respectively. The kernel k_p is defined as

$$k_p[v, \xi_p](t) = \begin{cases} max\{ \xi_p(t), r(v(t) - p_2) \} & \text{for } \dot{v}(t) \geq 0 \\ min\{ \xi_p(t), r(v(t) - p_1) \} & \text{for } \dot{v}(t) \leq 0 \end{cases}$$
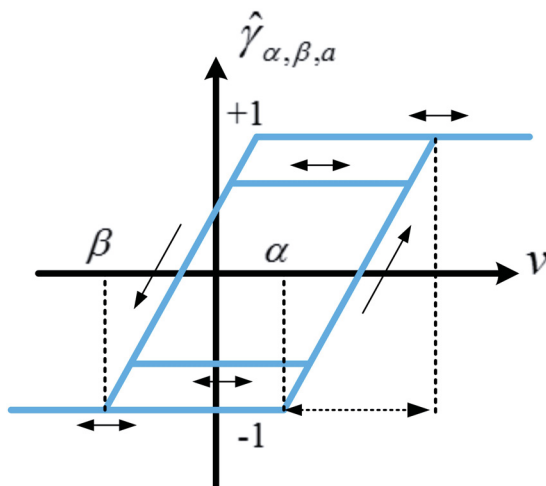
Figure 3.5: KP kernel

In comparison with Preisach model and PI model, the KP model is seldomly unitized to represent the hysteresis effect in the smart materials due to its complex structure. Banks [61] investigated the properties of the KP model and employed this model in describing the hysteresis in SMA, similar work can also be found in [62].

Duhem Model

The Duhem model was proposed by P. Duhem for description of the thermodynamical processes in 1897. This differential equation-based hysteresis model focuses on the fact the

output can change its character when the input changes direction. The Duhem model is given by

$$\dot{B}(t) = \alpha \left| \dot{H} \right| [f(H) - B] + \dot{H} g(H) \tag{3.8}$$

where $\alpha > 0$ is a constant, H is the applied magnetic field and B is the flux density, $f(H)$ and $g(H)$ are continuous functions. Equation (3.8) confirms Duhem model has a form of rate-independent hysteresis. In additions the functions $f(H)$ and $g(H)$ have to meet the following three conditions: [63]

1) $f(\cdot)$ is piecewise smooth, monotone increasing, odd function of H, with $\lim_{H \to \infty} \dot{f}(H) < \infty$;

2) $g(\cdot)$ is piecewise continuous, even function, with $\lim_{H \to \infty} g(H) = \lim_{H \to \infty} \dot{f}(H)$;

3) $\dot{f}(H) > g(H) > \alpha e^{\alpha H} \int_{H}^{\infty} |\dot{f}(\eta) - g(\eta)| e^{-\alpha \eta} d\eta$ for all $H > 0$.

In the literature, the Duhem model is often utilized to describe saturated hysteresis effect in the SMA [64] actuators by selecting different functions $f(v)$ and $g(v)$.

Bouc-Wen Model

The Bouc-Wen hysteresis model is expressed as

$$\dot{z} = -\alpha|\dot{x}|z^n - \beta\dot{x}|z^n| + A\dot{x}, \ for \ n \ odd \tag{3.9}$$

$$\dot{z} = -\alpha|\dot{x}|z^{n-1}|z| - \beta\dot{x}z^n + A\dot{x}, \ for \ n \ even \tag{3.10}$$

where α, β, and A are parameters that govern the scale and general shape of the hysteresis loops, z is the output, x denotes the input. In the literature, the Bouc-Wen model has been widely used in the field of structural engineering, since they greatly facilitate deterministic and stochastic dynamic analysis of real structures with reasonable accuracy [65]. Bouc-Wen model is also used to describe the hysteresis in piezoelectric materials [66].

3.2 The Development of an Asymmetric Hysteresis Model for the Magnetostrictive Actuator

From experimental results reported in Chapter 1, the input and output responses of the magnetostrictive actuator show asymmetric hysteretic characteristics. Among above reviewed hysteresis models, except for the Preisach model, all the models can only describe symmetric hysteresis effects. In order to describe the asymmetric hysteresis effect, the original models should be modified. Inspired by the modeling approaches reported in [57] [59] [60], an asymmetric shifted Prandtl-Ishlinskii (ASPI) model is proposed, which is constructed by three components: a PI model, a shift model and an auxiliary function. The advantages of the proposed model are 1) it is able to represent the asymmetric hysteresis behavior in magnetostrictive actuators, 2) it facilitates the inverse cancelation by utilizing the available results in [1] and [67]. Before introducing the proposed model, an analysis regarding to the asymmetric hysteretic responses in the magnetostrictive actuator is presented first.

3.2.1 The Asymmetric Hysteretic Behaviors in the Magnetostrictive Actuator

From Figure 1.7 we can see that the input-output hysteresis loop is not symmetric. In order to analyze the symmetry property of hysteresis loops, a vertical gap function is defined as

$$\Phi[u] = |\Gamma_{asc}[u, \zeta_0] - \Gamma_{des}[u, \zeta_1]| \tag{3.11}$$

where $u \in \mathbb{R}$, $\mathbb{R}$ is the set of real numbers; $\Gamma_{asc}[\cdot, \zeta_0]$ is defined as the ascending branch of the hysteresis loop, $\Gamma_{des}[\cdot, \zeta_1]$ is defined as the descending branch of the hysteresis loop; ζ_0, ζ_1 denote the internal state of the hysteresis operator. Figure 3.6 shows the hysteresis loop and its vertical gap function curve.

Property 1: If a hysteresis loop $\Gamma[\cdot, \zeta]$ is symmetric, then its vertical gap function $\Phi[u]$ ($u \in [-u_0, u_0]$, $u_{max} = u_0$, $u_{min} = -u_0$) is symmetric with the center line $u = 0$.
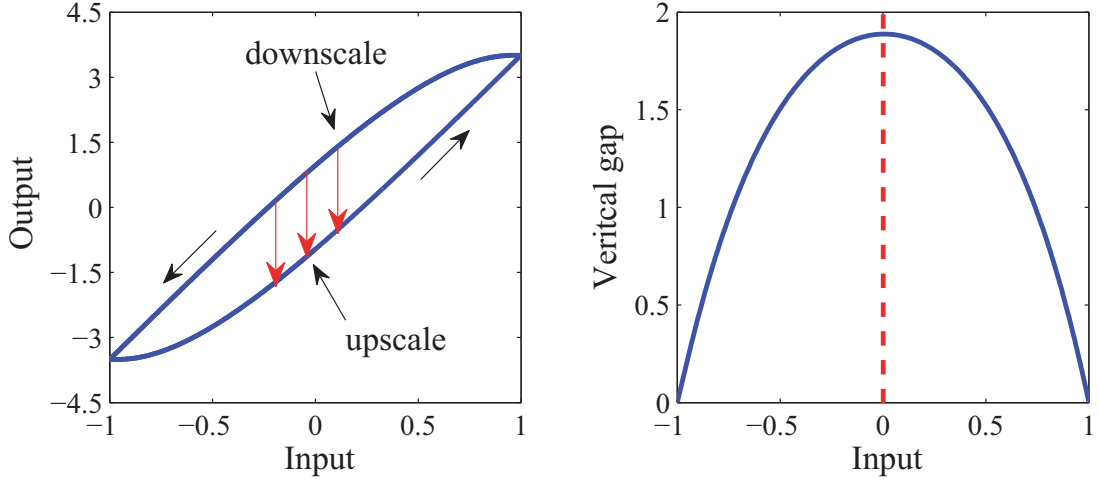
Figure 3.6: The symmetric hysteresis curve and its vertical gap function curve

Proof: In order to prove this property, we have to prove that $\forall\ u_e \in \mathbb{R}$ and $0 \leq u_e \leq u_0$, $\Phi[u_e] = \Phi[-u_e]$. For any $u_e \in \mathbb{R}$ we have,

$$\Phi[u_e] = |\Gamma_{asc}[u_e, \zeta_0] - \Gamma_{des}[u_e, \zeta_1]| \qquad (3.12)$$

Since the hysteresis loop $\Gamma[\cdot, \zeta]$ is symmetric with respect to the origin, it satisfies

$$\Gamma_{asc}[u_e, \zeta_0] = -\Gamma_{des}[-u_e, -\zeta_0] \qquad (3.13)$$

$$\Gamma_{des}[u_e, \zeta_1] = -\Gamma_{asc}[-u_e, -\zeta_1] \qquad (3.14)$$

Substituting (3.13) and (3.14) into (3.12), we have

$$\begin{aligned} \Phi[u_e] &= |-\Gamma_{des}[-u_e, -\zeta_0] + \Gamma_{asc}[-u_e, -\zeta_1]| \\ &= \Phi[-u_e] \end{aligned} \qquad (3.15)$$

In Figure 3.6, because the hysteresis loop is symmetric, according to *Property 1*, the vertical gap function is symmetric with the center line $u = 0$.

Property 2: If the vertical gap function $\Phi[u]$ ($u \in [-u_0, u_0]$, $u_{max} = u_0$, $u_{min} = -u_0$) of a hysteresis loop $\Gamma[\cdot, \zeta]$ is not symmetric with its center line $u = 0$, then the hysteresis operator is asymmetric.
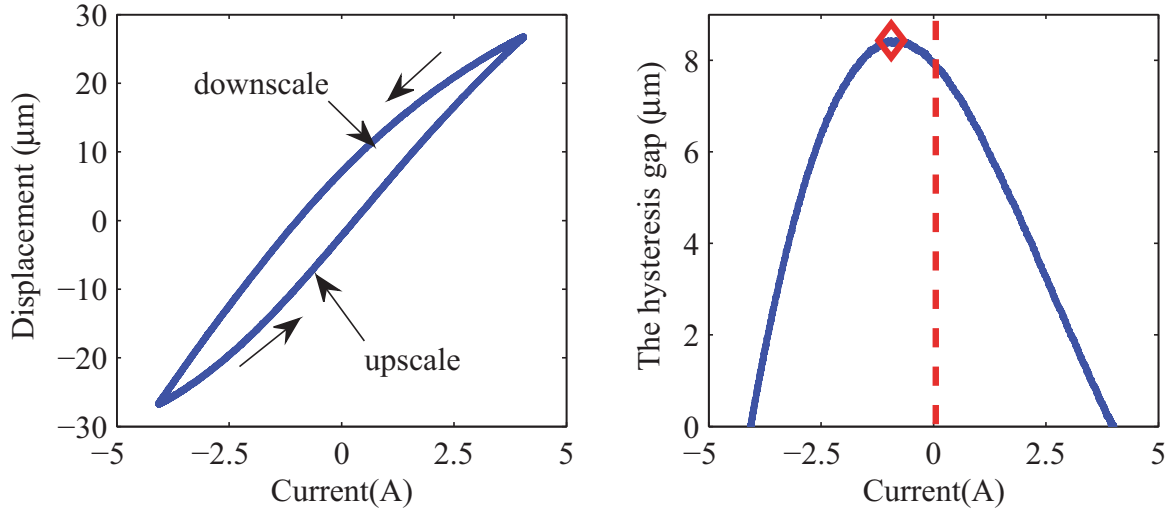
Figure 3.7: The asymmetric hysteresis curve of the magnetostrictive actuator and its vertical gap function curve

Figure 3.7 shows the input-output relation of the magnetostrictive actuator and its vertical gap function curve. Due to the asymmetric property of the vertical gap curve, the hysteresis loop of the magnetostrictive actuator is asymmetric according to Property 2. Figure 3.8 shows the vertical gap curve under different input amplitudes which indicates the asymmetric hysteresis property in the magnetostrictive actuator.

3.2.2 The Asymmetric Shifted Prandtl-Ishlinskii (ASPI) Model

In order to extend the PI model to describe the asymmetric hysteresis effect, still possessing its unique property of being analytically invertible, an asymmetric shifted Prandtl-Ishlinskii (ASPI) model is proposed in this section, which is composed of three components: a Prandtl-Ishlinskii (PI) model, a shift model and an auxiliary function. The purpose for introducing the shift model is to change the symmetric characteristics of the ASPI model and the auxiliary function is used for representing the saturated phenomenon. The ASPI model is defined as

$$u(t) = \Pi[v](t) = P[v](t) + \Psi[v](t) + g(v)(t) \tag{3.16}$$

53
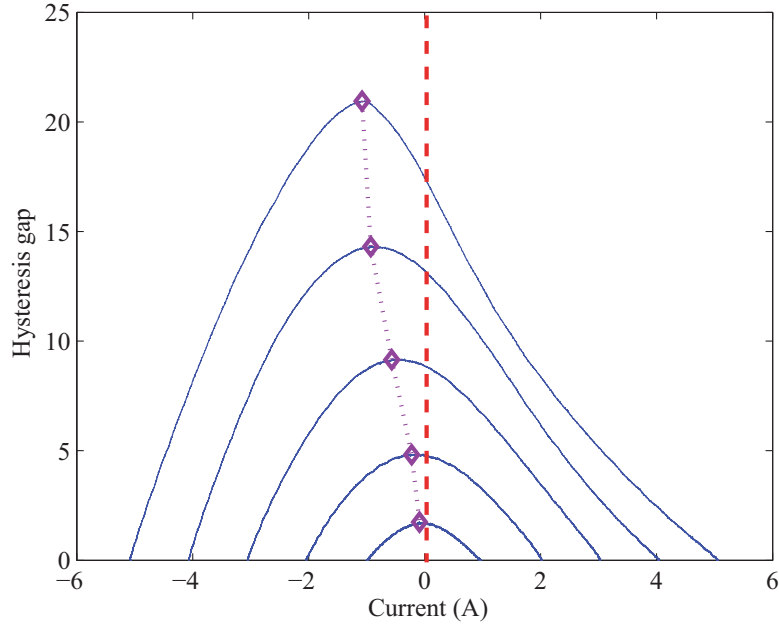
Figure 3.8: The vertical gap curves of hysteresis effect in magnetostrictive actuator

where the first term $P[v](t)$ is the PI model defined in (3.2), and the second term $\Psi[v](t)$ is defined as the superposition of the weighted shift operators:

$$\Psi[v](t) = \int_{C_0}^{C_1} \chi(c)\Psi_c[v](t)dc \tag{3.17}$$

where $\chi(c) \geq 0$ is the density function with $\int_{C_0}^{C_1} c\chi(c)dc = L_\chi < \infty$. $\Psi_c[v](t)$ is the shift operator defined as

$$\Psi_c[v](0) \quad = \quad \psi_c(v(0), 0) \tag{3.18}$$

$$\Psi_c[v](t) \quad = \quad \psi_c(v(t), \psi_c[v](t_i)) \tag{3.19}$$

for $t_i < t \leq t_{i+1}, 0 \leq i \leq N - 1$, with

$$\psi_c(v, w) = max(cv, min(v, w)) \tag{3.20}$$

where $0 = t_0 < t_1 < \ldots < t_N$ is the same partition of $[0, t_N]$ as defined in (3.5). $c \in \mathbb{R}_+$, $\mathbb{R}_+ := \{x \in \mathbb{R} | x \geq 0\}$ is a parameter to determine the shape of the shift operator. When

54

$c > 1$, $\Psi_c[v](t)$ is called left shift operator, see Figure 3.9(a); when $0 < c < 1$, $\Psi_c[v](t)$ is called right shift operator, see Figure 3.9(b). The last term $g(v)(t)$ in (3.16) is an auxiliary function, which assists to represent the saturation behavior of hysteresis nonlinearity. Figure 3.10 shows responses of the PI model and the ASPI model with selected density functions $p(r)$, $\chi(c)$ as well as auxiliary function $g(v)$ in Table 3.1.

Table 3.1: Coefficients of the PI model and the ASPI model

	The PI model	The ASPI model
$p(r)$ $r \in [0, 4]$	$0.4e^{-0.01(r+\frac{1}{6})}$	$0.4e^{-0.01(r+\frac{1}{6})}$
$\chi(c)$ $c \in [1, 4]$		$0.02e^{-0.1(c-1)}$
$g(v)$		$0.8arctan(3v - 2)$
		$-0.05v^2 + 0.05v$

Some of the essential properties of the ASPI model can be described as follows:

Rate Independent: The ASPI model $w[v](t)$ is rate independent. For all $v \in C_{pm}[0, T]$, $C_{pm}[0, T]$ denotes space of monotone, continuous functions on $[0, T]$, and all admissible time transformation $\tau : [0, T] \to [0, T]$ with $\tau(0) = 0$ and $\tau(T) = T$ the elementary shift operator satisfies

$$w[v \circ \tau] = w[v] \circ \tau \tag{3.21}$$

Monotonicity: The ASPI model $w[v](t)$ is a monotone operator. For a given input $v \in C[0, T]$, $C[0, T]$ denotes space of continuous functions on $[0, T]$, for arbitrary $T > 0$ and any initial condition ζ_0, the following property holds

$$(w[v(\cdot), \zeta_0](T) - w[v(\cdot), \zeta_0](0)) \cdot (v(T) - v(0)) \geq 0 \tag{3.22}$$

Discussion on the Selection of Shift Model $\Psi[v]$ and Function $g(v)$

The purpose for introducing the shift model is to describe the asymmetric hysteresis. In order to demonstrate characteristics of the asymmetric hysteresis, the vertical gap function can be
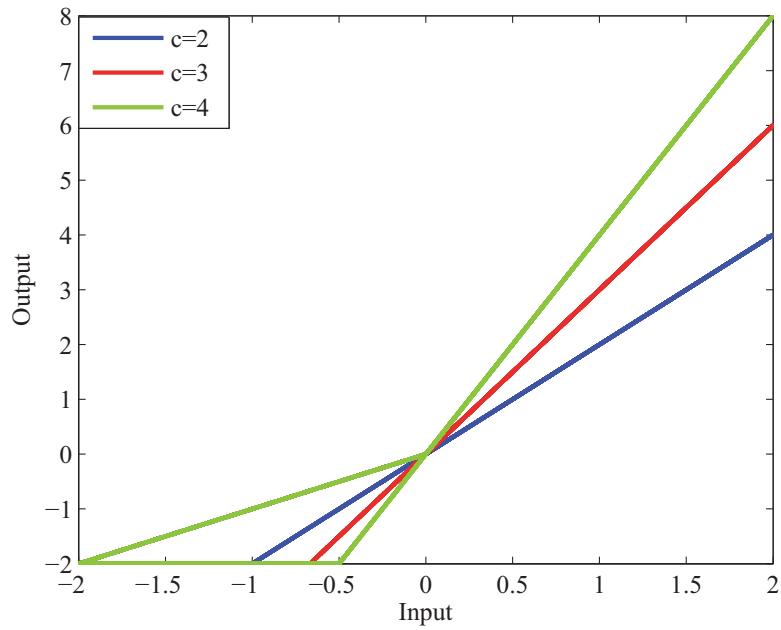
(a) The left shift operator
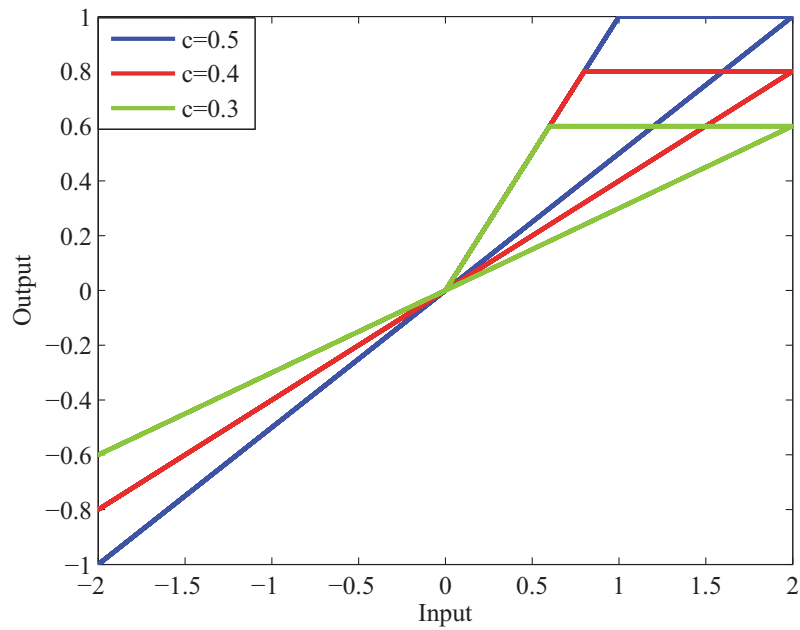
(b) The right shift operator

Figure 3.9: The shift operator
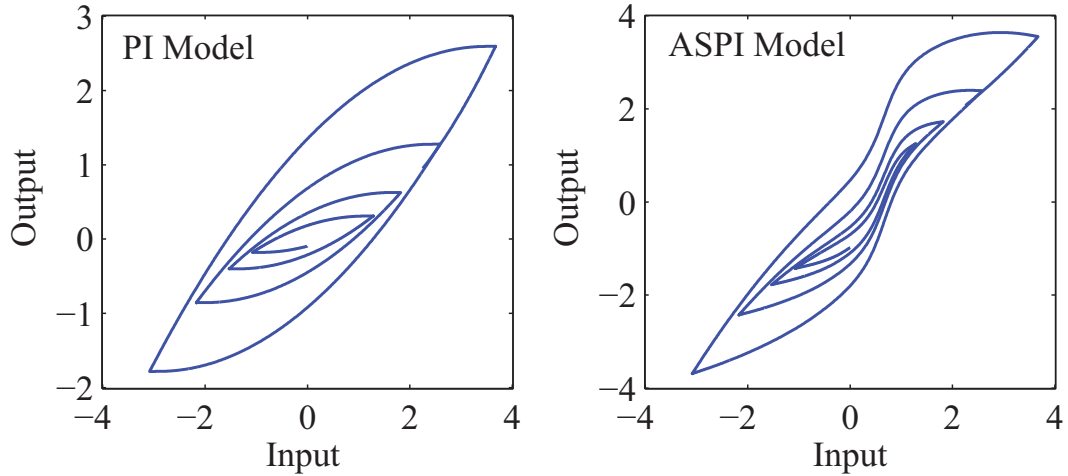
Figure 3.10: Input-output responses of the PI model and the ASPI model

utilized. Figure 3.11 shows the vertical gap value of the shift operators where v_p denotes the input value as the vertical hysteresis gap reaches its peak value. For an asymmetric hysteresis, if v_p is at the left of the center line $v = 0$, $v \in [-v_0, v_0]$, it is called left asymmetric hysteresis. Otherwise, it is called right asymmetric hysteresis. Therefore, we can superpose left shift operators with $c > 1$ to describe the left asymmetric hysteresis and right shift operators with $0 < c < 1$ to describe the right asymmetric hysteresis.

Remark: As a matter of fact, the right asymmetric hysteresis $\Gamma[v]$ can be transformed into the left asymmetric hysteresis by using $\Pi[v] = -\Gamma[-v]$. Therefore, we can always select the left shift operators ($c > 1$) to represent the asymmetric hysteresis. As an illustration, to get the left asymmetric hysteresis, Figure 3.12 demonstrates the superposition of the left shift operators with the PI model to describe the left asymmetric hysteresis.

Since the PI model and the shift model are the monotone models, the derivatives of the upscale of the hysteresis loops described by these models are monotone under piecewise monotone input signal $v(t)$. However, for saturated asymmetric hysteresis, the derivative of the upscale of the hysteresis loop is non-monotone, see Figure 3.13. Thus, we introduce the auxiliary function $g(v)$ into the ASPI model to change the monotone property of the derivative of the upscale in the ASPI model. For such a purpose, $g(v)$ needs to satisfy the

57
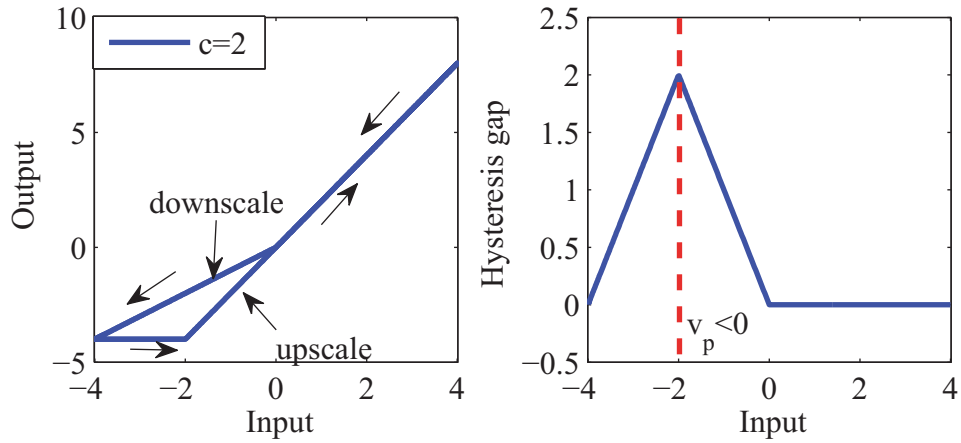
(a) The left shift operator and its hysteresis gap
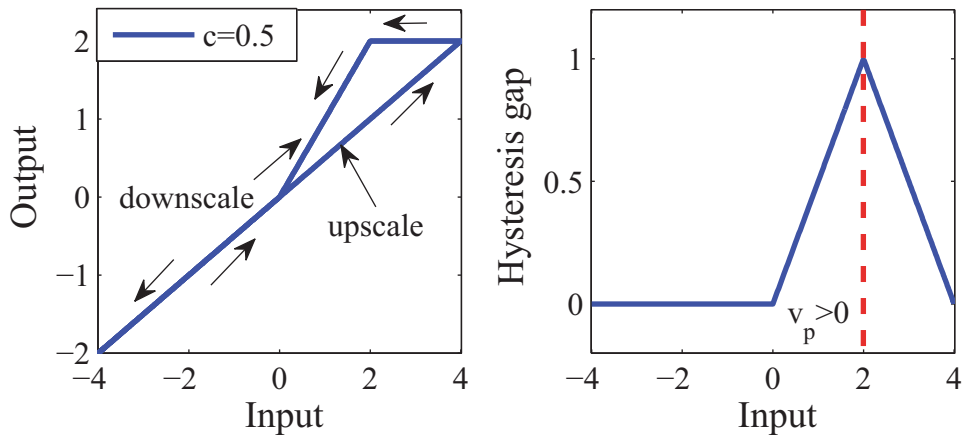
(b) The right shift operator and its hysteresis gap

Figure 3.11: The shift operator and its hysteresis gap function
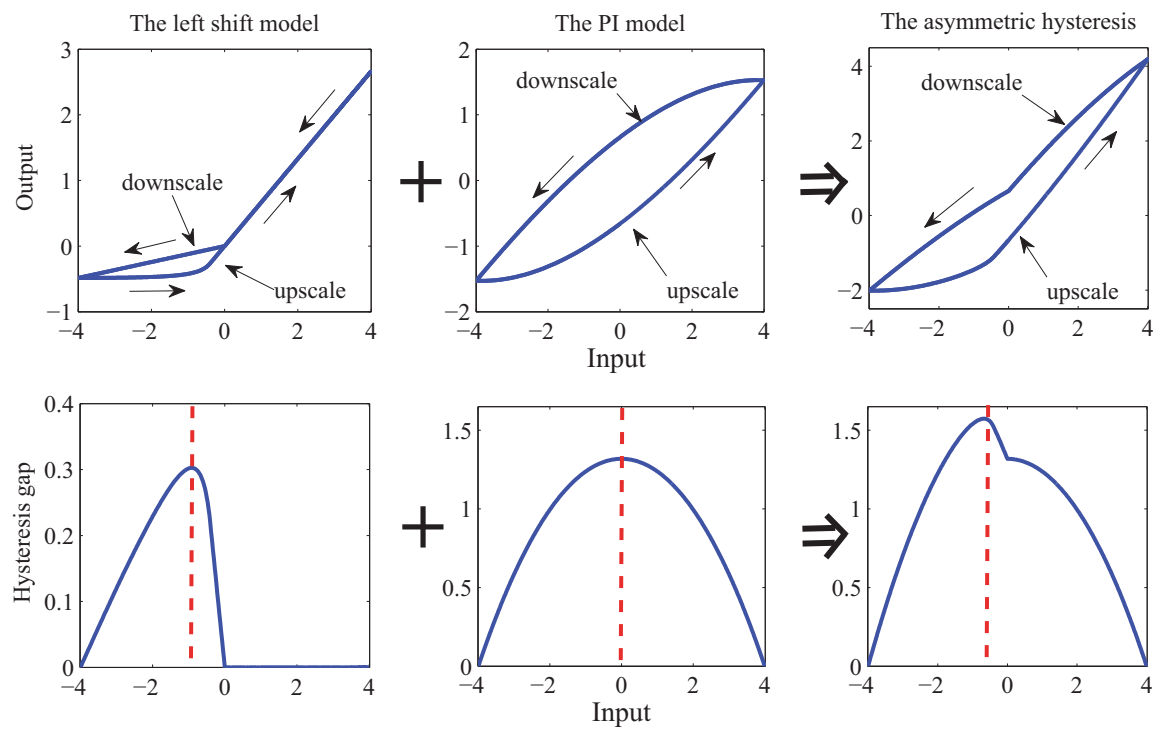
Figure 3.12: The modeling illustration for the asymmetric hysteresis phenomenon
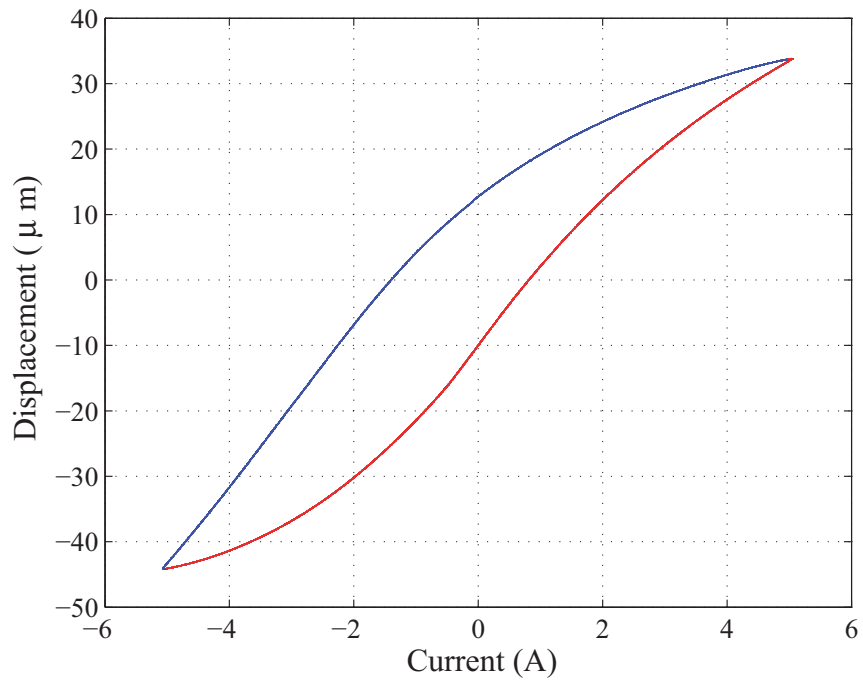
(a) The upscale of the magnetostrictive actuator
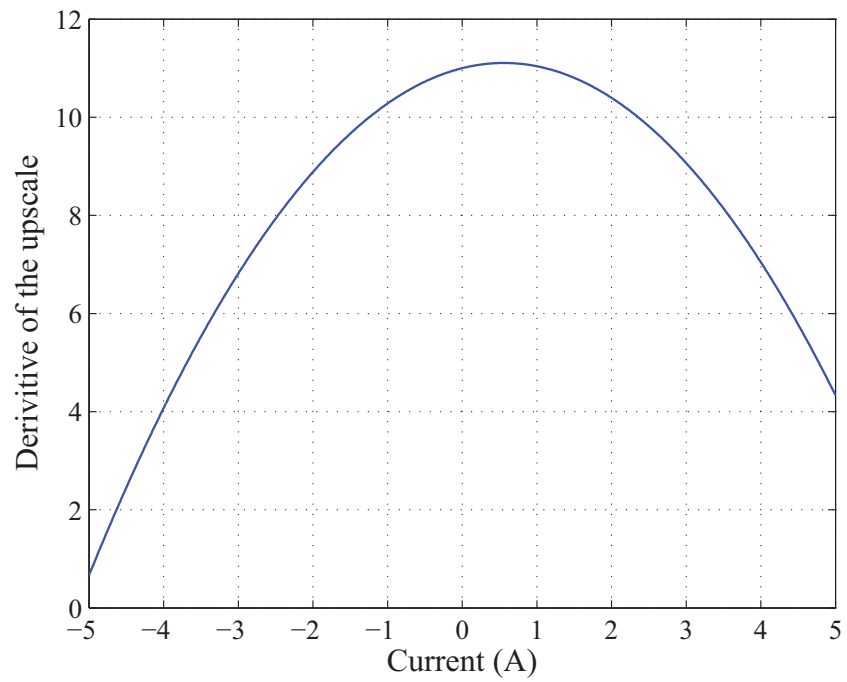
(b) The derivative of the upscale

Figure 3.13: The derivative of the upscale of the hysteresis loop in magnetostrictive actuators

following condition:

Condition 1:

1) for the monotonic increase input $v(t)$, $g'(v) > -(P'[v] + \Psi'[v])$;

2) $g(\frac{v_1+v_2}{2}) > \frac{g(v_1)+g(v_2)}{2}$, where $v_1, v_2 \in [v_{min}, v_{max}]$.

    Remarks:

1) The selection of the $g(v)$ is not unique, any function can be qualified as far as it is Lipschitz continuous, derivative and satisfying the above condition.

2) Similar to the PI model, the exact shape of the hysteresis depends on the selection of the density functions, c, $g(v)$, which can be determined once the hysteresis loops are available.

3.3 Concluding Remarks

In this chapter, a literature review including a historical overview of the hysteresis and available hysteresis models has been presented to give a general status on the hysteresis modeling. Inspired by the reviewed modeling approaches, an asymmetric shifted Prandtl-Ishlinskii (ASPI) model has been therefore proposed, which is constructed by three components: a PI model, a shift model and an auxiliary function. The advantages of the proposed model are 1) it is able to represent the asymmetric hysteresis behavior in magnetostrictive actuators, 2) it facilitates the inverse construction. The model identification and experimental verification will be conducted in the next chapter to demonstrate the effectiveness of the proposed hysteresis model.

Chapter 4

Model Parameters Identification and Model Validation

In Chapter 2, a dynamic model both considering the nonlinear hysteresis effect and the dynamic behaviors was proposed to describe the input output dynamic responses of the magnetostrictive-actuated system. To particularly describe the asymmetric hysteresis effect in the magnetostrictive actuator, an asymmetric shifted Prandtl-Ishlinskii (ASPI) model was proposed in Chapter 3. Therefore, in this chapter, the model parameters identification and the model verification are conducted on the magnetostrictive-actuated experimental platform to verify the proposed modeling strategy.

The model identification is taken into two steps: the identification of the hysteresis component and the identification of the dynamic component. To identify the hysteresis part, a designed decreasing sinusoid signal is applied to the actuator and the input and output experimental data are utilized to determine the parameters of the hysteresis model. To identify the dynamic part, the frequency response of the magnetostrictive-actuated system is obtained, and the parameters of the dynamic part can be found based on the obtained frequency response figure. The identified model then is verified by applying a series of excitation signals with different amplitudes and frequencies. The experimental results illus-

trate that the dynamic model has an excellent agreement with the dynamic behavior of the magnetostrictive actuator.

4.1 Model Parameters Identification

From (2.15) and (2.16), one has

$$\dddot{x} + \rho_2\ddot{x} + \rho_1\dot{x} + \rho_0 x \quad = \quad b(i - \Pi[x]) \tag{4.1}$$

where $\rho_2 = \frac{L_a b_s + R_0 m}{L_a m}$, $\rho_1 = \frac{L_a k_s + T_{em} T M m + R_0}{L_a m}$, $\rho_0 = \frac{k_s R_0}{L_a m}$, $b = \frac{R_0 T_{em}}{L_a m}$. Because the displacement x can be represented as a function of supplied current $i(t)$, i.e. $x(t) = \zeta(i(t))$, the term $i - \Pi[\zeta[i]]$ in (4.1) can be defined as a new hysteresis nonlinearity $\Gamma[i](t)$

$$\Gamma[i](t) = u(t) = i(t) - \Pi[x](t) \tag{4.2}$$

We finally have the model of the magnetostrictive actuated dynamic system as

$$\dddot{x} + \rho_2\ddot{x} + \rho_1\dot{x} + \rho_0 x = b\Gamma[i](t) \tag{4.3}$$

Figure 4.1 shows the cascading structure of the dynamic model. This cascading structure
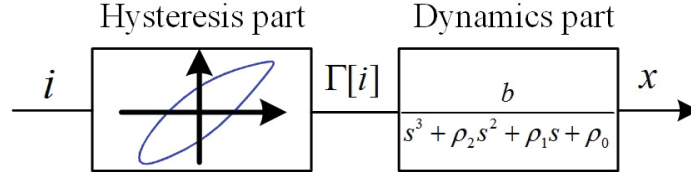
Figure 4.1: The structure of the dynamic model

where a nonlinear component followed by a linear system is called Hammerstein model. In the literature, there are numerous papers working towards the identification of the Hammerstein model, and the available are the iterative method [68]; overparameterization method [69]; stochastic method [70] and so on. However, these approaches are only applicable for identifying simple nonlinear component, such as deadzone or backlash. For the hysteresis, to

our best knowledge, it is still an unsolved question. Therefore, in this section, we avoid to identify the parameters of the hysteresis model and dynamic model together, instead we identify them separately. To this end, we have to normalize one part first, in this section, we normalize the dynamic part.

The s domain expression of the dynamic part is expressed as

$$G(s) = \frac{X(s)}{\Gamma(s)} = \frac{b}{s^3 + \rho_2 s^2 + \rho_1 s + \rho_0} \tag{4.4}$$

where ρ_2, ρ_1, ρ_0 and b are unknown parameters. By performing the normalization, the numerator of the (4.4) is divided by a term b/ρ_0 as

$$G_1(s) = \frac{\rho_0}{s^3 + \rho_2 s^2 + \rho_1 s + \rho_0} \tag{4.5}$$

To keep the equivalence of the model, the hysteresis part is multiplied by the term b/ρ_0, see Figure 4.2. Then we conduct the model parameters identification.
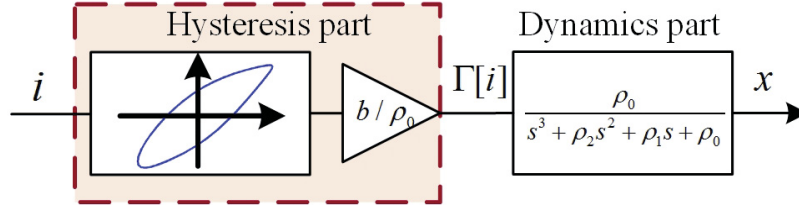
Figure 4.2: The structure of the dynamic model after normalization

Step 1: Identification of the hysteresis part. In Chapter 3, we have proposed an asymmetric hysteresis model ASPI model to describe the hysteresis behaviors in the magnetostrictive actuator. To facilitate the identification, the numerical expression of the ASPI model (3.16) is written as

$$
\begin{aligned}
u(t) &= P[v](t) + \Psi[v](t) + g(v)(t) \\
&= p_0 v(t) + \sum_{j=1}^{n} p_j F_{r_j}[v](t) + \sum_{j=1}^{m} q_j \Psi_{c_j}[v](t) + g(v)(t)
\end{aligned}
\tag{4.6}
$$

where p_j denotes the weight of the play operator; $F_{r_j}[v](t)$ is the play operator at the threshold of r_j; n is the number of the play operator used for identification. q_j denotes the weight

of the elementary shift operator; $\Psi_{c_j}[v](t)$ is the elementary shift operator at the slope of c_j; m is the number of the elementary shift operator used for identification. $g(v)(t)$ is an auxiliary function, which is selected as

$$g(v)(t) = -a_3 v(t)^3 - a_2 v(t)^2 - a_1 v(t) - a_0 \qquad (4.7)$$

The thresholds r_j were selected as $r_j = 0.3j$ $(j = 1, 2, ...n)$, where the current is a designed decreasing sine signal as $i(t) = 5e^{-0.1t} sin(2\pi t)$, see Figure 4.3(a). The weights p_j in (4.11) can be found by the following constrained quadratic optimization:

$$min\{[C\Lambda - d]^T [C\Lambda - d]\} \qquad (4.8)$$

with the constraints

$$p(j) \geq 0, \quad j \in \{0, 1, 2, ..., N\} \qquad (4.9)$$

where $\Lambda = [p_0, ...p_{m+n+4}]^T$, $C = [F_{r_1}, ..., F_{r_N}]$, $N = m + n + 4$, d is the output of the magnetostrictive actuator under a designed amplitude decreasing sinusoidal input signal. Then, the nonlinear least-square optimization toolbox in MATLAB was employed to identify the above parameters and the results are shown in Table 4.1. Figure 4.3(b) and Figure 4.3(c) show the comparison between the experimental data and the model.

Remark 1: Different initial values have been tried in order to obtain the minimum mean squared error, which is defined as

$$e_{MSE} = \frac{1}{n} \sum_{i=1}^{n} (u - u_{exp})^2 \qquad (4.10)$$

Remark 2: 9 play operators in (4.11) were employed in the identification. In fact, different numbers have been tried considering the calculation cost and modeling accuracy. Figure 4.4 shows the relation between the number of play operators and the related mean squared error.

Remark 3: Different orders of function $g(v)$ have been tried and the mean squared error were listed in Table.4.2. Because the third order of $g(v)$ shows lower MSE, therefore, $g(v) = -a_3 v^3 - a_2 v^2 - a_1 v - a_0$ was utilized in (4.11).

Table 4.1: Coefficients of the ASPI model

Numbers	r_j	p_j	c_j	q_j	a_j
0	0	0.9002			0
1	0.3	0.8445	1.1	1.3809	0
2	0.6	0.4276	1.2	0	0.3106
3	0.9	1.4821	1.3	0	0.0417
4	1.2	0.6097	1.4	0	
5	1.5	1.3596	1.5	0	
6	1.8	1.2051	1.6	0	
7	2.1	1.0574	1.7	0	
8	2.4	0.2835	1.8	1.0056	
9	2.7	0.1636			

Table 4.2: Coefficients of the auxiliary function

$g(v)$	e_{MSE}
$-a_1 v - a_0$	1.2885
$-a_2 v^2 - a_1 v - a_0$	0.3737
$-a_3 v^3 - a_2 v^2 - a_1 v - a_0$	0.2811
$-a_4 v^4 - a_3 v^3 - a_2 v^2 - a_1 v - a_0$	0.2811
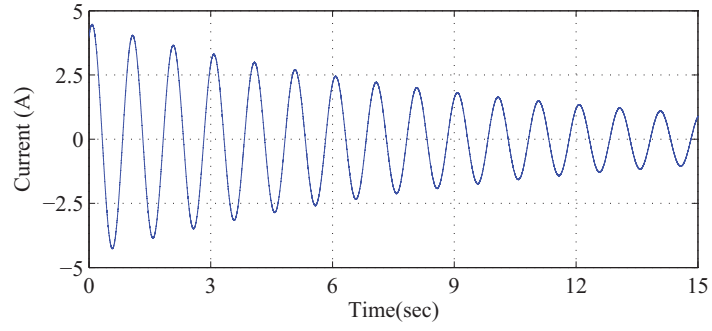
(a) Input signal
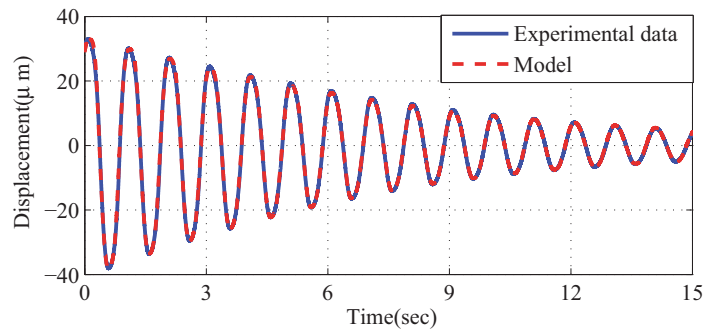
(b) Comparison of the output between the experimental data and
the model
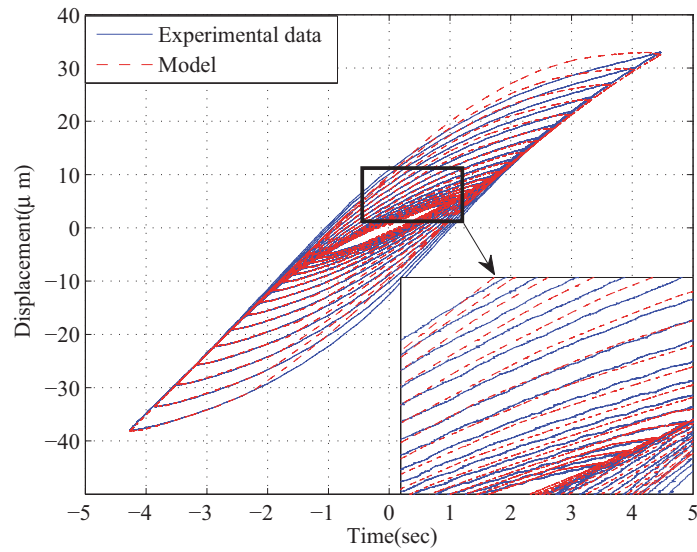
(c) Comparison of the input and output responses between the ex-
perimental data and the model

Figure 4.3: Comparison of experimental data and the model

67
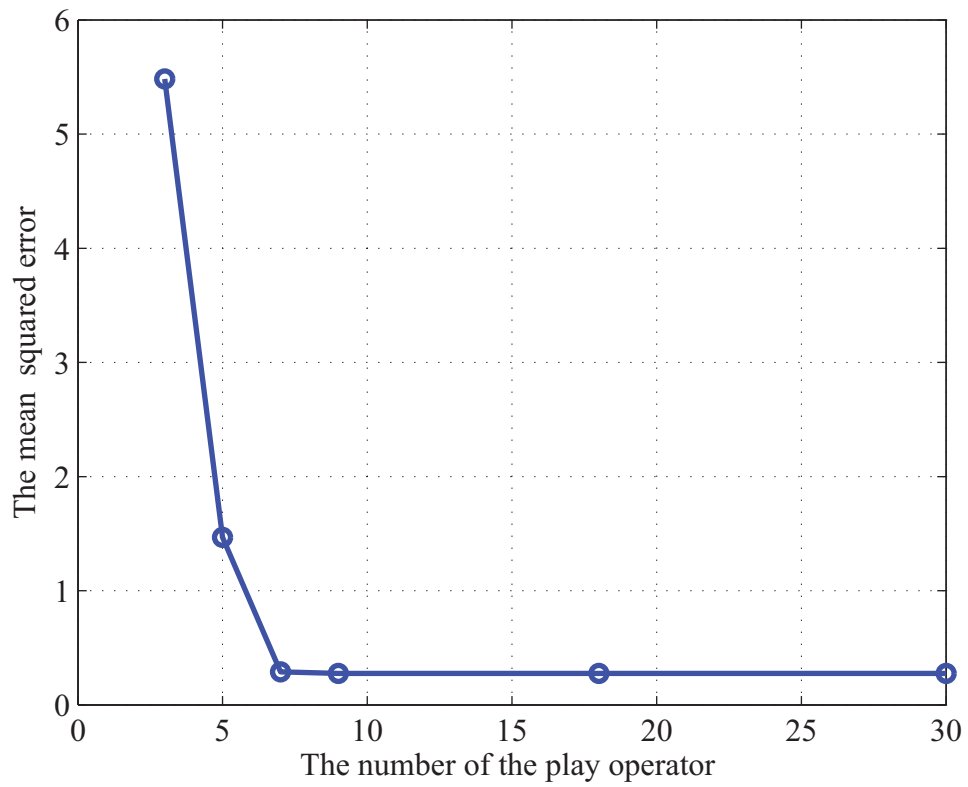
Figure 4.4: The mean squared error with different play operators

Therefore, we have

$$
\begin{aligned}
u(t) &= P[v](t) + \Psi[v](t) + g(v)(t) \\
&= p_0 v(t) + \sum_{j=1}^{n} p_j F_{r_j}[v](t) + \sum_{j=1}^{m} q_j \Psi_{c_j}[v](t) + g(v)(t) \quad (4.11)
\end{aligned}
$$

with

$$
g(v)(t) = -a_3 v(t)^3 - a_2 v(t)^2 - a_1 v(t) - a_0 \quad (4.12)
$$

where the identified parameters p_j, q_j and a_j can be found in Table 4.1.

Step 2: Identification of the dynamic part. We first decompose $G_1(s)$ as

$$
G_1(s) = \frac{\tau}{s + \tau} \cdot \frac{\omega_n^2}{s^2 + 2\xi\omega_n s + \omega_n^2} \quad (4.13)
$$

with $\rho_2 = 2\xi\omega_n + \tau$, $\rho_1 = \omega_n^2 + 2\xi\omega_n\tau$, $\rho_0 = \tau\omega_n^2$. The objective is to identify the parameters of τ, ξ, ω_n. To this end, a frequency response (1 to 500Hz) of the magnetostrictive actuator is obtained in Figure 4.5, where the applied mechanical load is 16Kg.
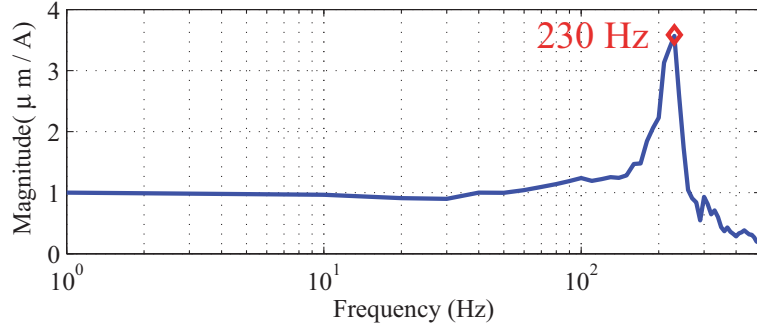
Figure 4.5: Amplitude/frequency characteristics of the system

From the magnitude response in Figure 4.5, we can find that $\omega_n = 230 \times 2\pi rad/s$. Then, the least square approach is utilized to identify the parameters as $\xi = 0.13$ and $\tau = 800 \times 2\pi$, and $G_1(s)$ is expressed as

$$
G_1(s) = \frac{1.05 \times 10^{10}}{s^3 + 5402 s^2 + 3.98 \times 10^6 s + 1.05 \times 10^{10}} \quad (4.14)
$$

4.2 Model Validation

The model validation is conducted on the experimental platform reported in Chapter 1, Section 1.3.1. The applied mechanical load is 16 Kg. We first verify the dynamic model with the operation of the magnetostrictive actuator in low frequency, which means the input and output responses only show hysteresis effect. Figures 4.6(a), 4.7(a), and 4.8(a) show comparisons of the experimental data and the ASPI model under sine input signals with amplitudes 2A to 4A. Figures 4.6(b), 4.7(b), and 4.8(b) show the modeling error which is defined as

$$e_m(t) = \frac{100(u_e(t) - u(t))}{max(v(t)) - min(v(t))} \tag{4.15}$$

where $u_e(t)$ and $u(t)$ denote the output of the magnetostrictive actuator and the ASPI model. From the comparison results and the modeling errors (less than 5%), it can be concluded that the proposed ASPI model shows a good agreement with the experimental data. Moreover, the triangular input signal is also applied, which indicates the effectiveness of the proposed ASPI model in different input signal, see Figure 4.9. To validate the dynamic part, we first obtain the frequency response test on the model. Figure 4.10 shows the comparison of the frequency responses between the experimental data and the developed model. From the comparison, it can be seen that the model can capture the main characteristics of the frequency responses of the magnetostrictive actuated dynamic system. Figures 4.11 and 4.12 demonstrate the comparisons of the experimental data and the model with the sinusoid input signal under different frequency (1Hz, 10Hz, 50Hz, 100Hz, 200Hz) and with triangular input signal under different frequency (10Hz, 50Hz, 150Hz, 200Hz). To validate the transient responses of the model, a square wave is also applied to the actuator. Moreover, a harmonic input $y = 2.16sin(0.35 \times 2\pi f_0 t) + 2.7sin(0.1 \times 2\pi f_0 t + \frac{\pi}{2} f_0)$ $(f_0 = 1, 401)$ is also applied to verify the model with complex input signals. From the comparisons of above the results, it is clearly shown that the proposed model shows an excellent agreement with the experimental data.
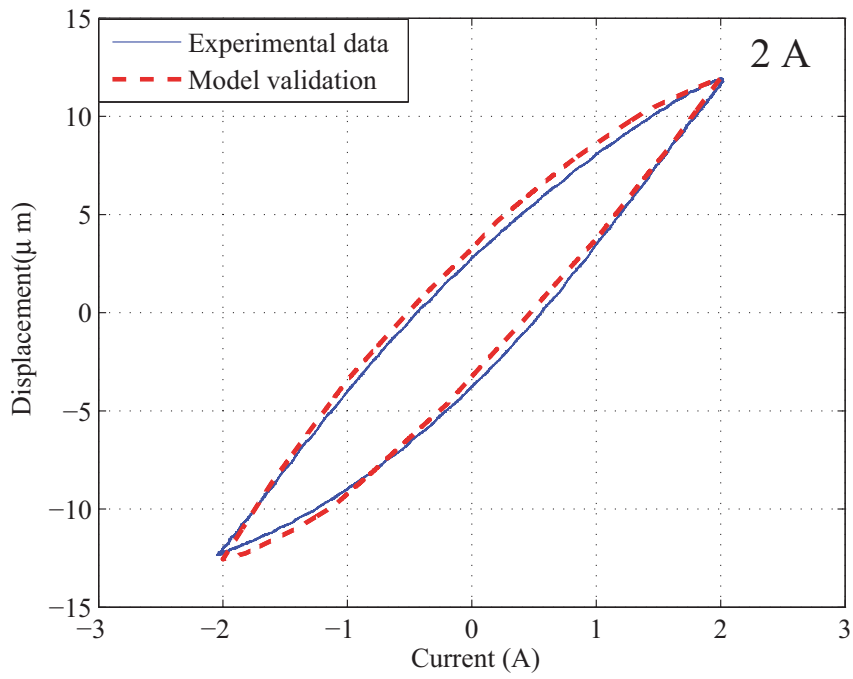
(a) Comparison of the experimental data and ASPI model
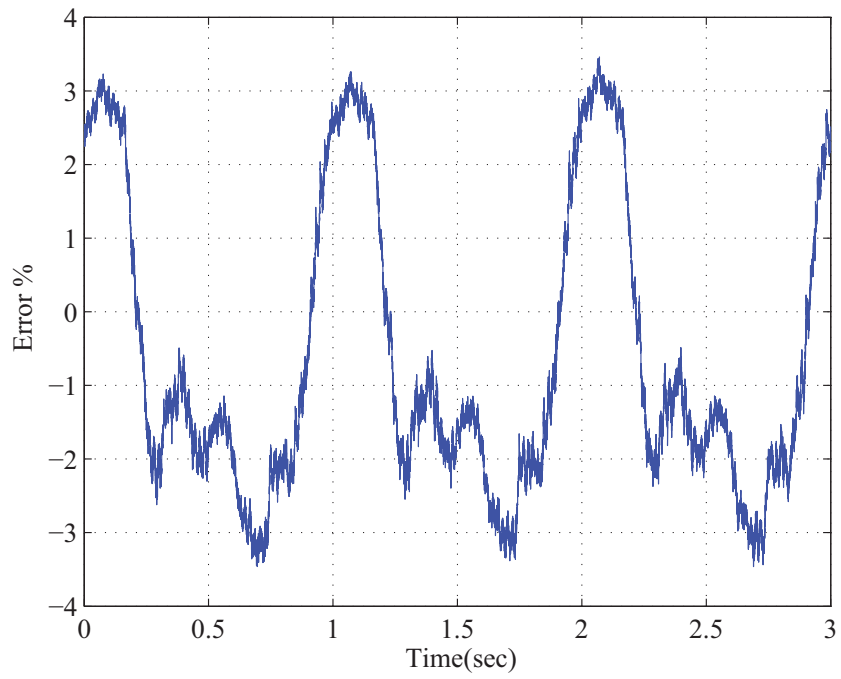
(b) Modeling error

Figure 4.6: Model validation with sinusoidal input $2sin(2\pi t)$
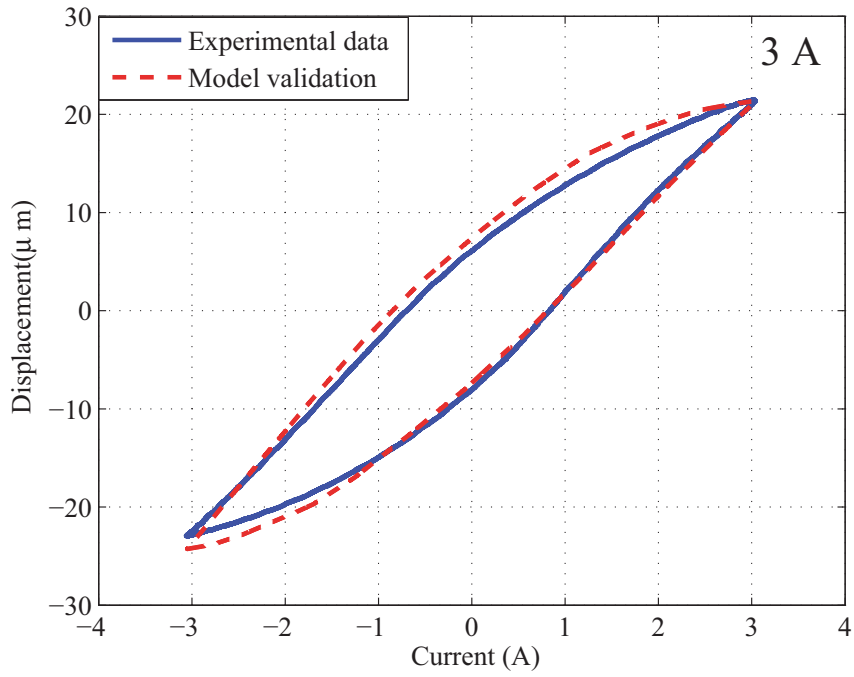
(a) Comparison of the experimental data and ASPI model
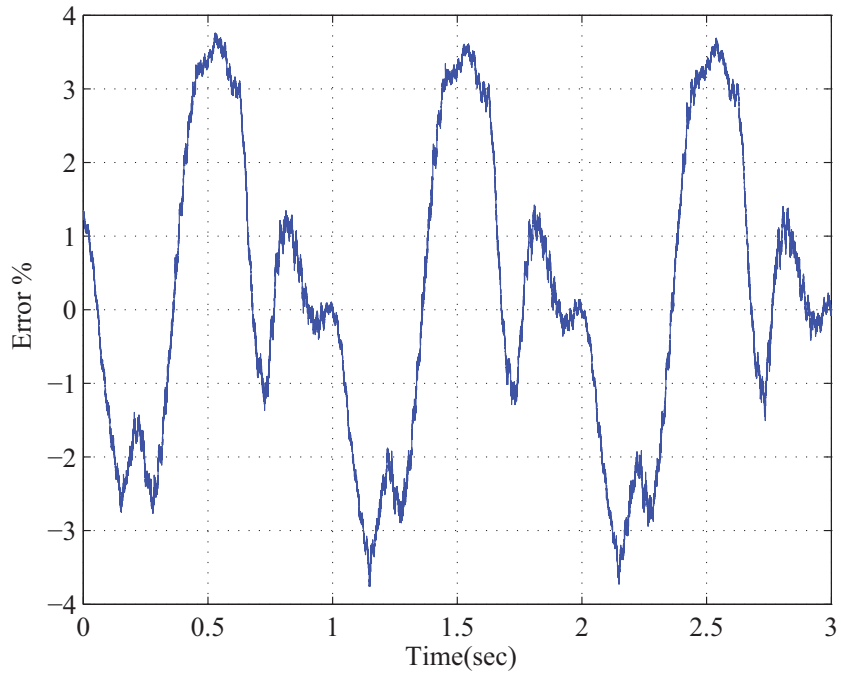
(b) Modeling error

Figure 4.7: Model validation with sinusoidal input $3sin(2\pi t)$
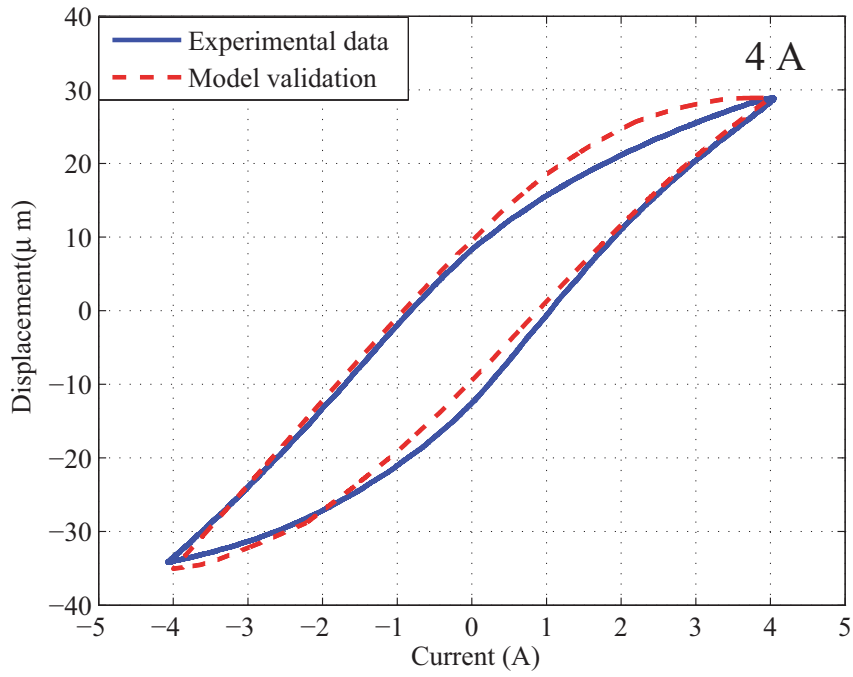
(a) Comparison of the experimental data and ASPI model
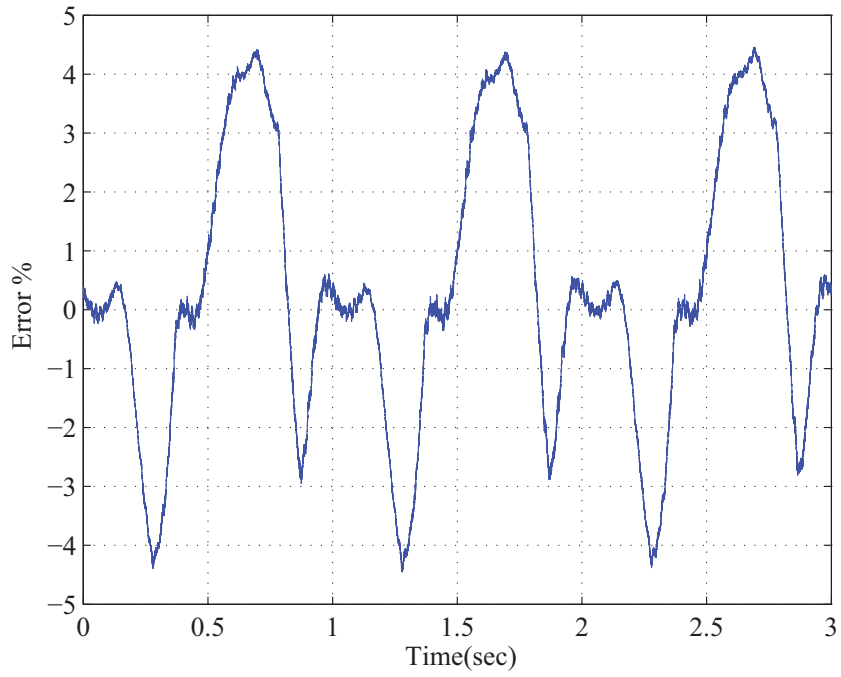
(b) Modeling error

Figure 4.8: Model validation with sinusoidal input $4sin(2\pi t)$
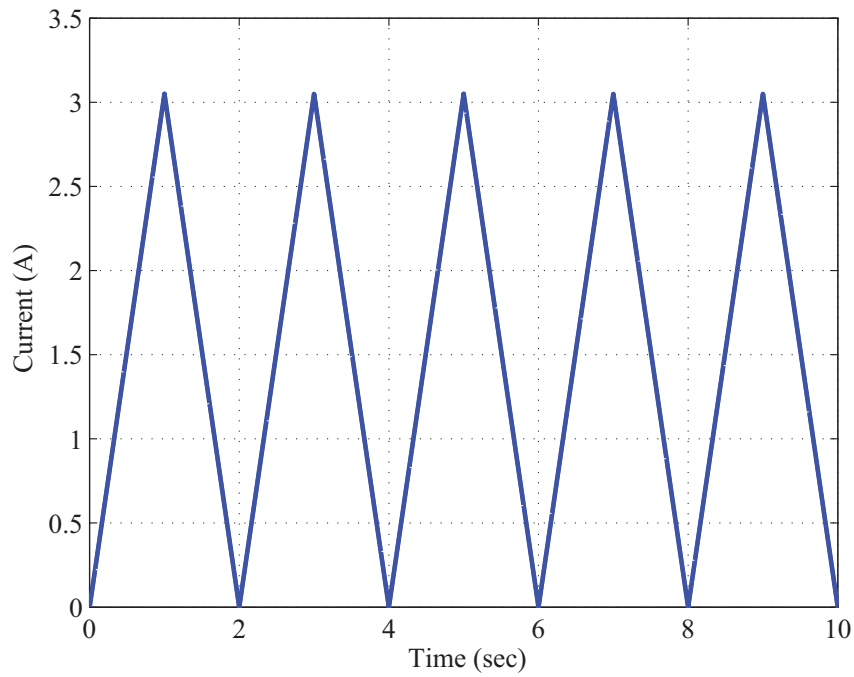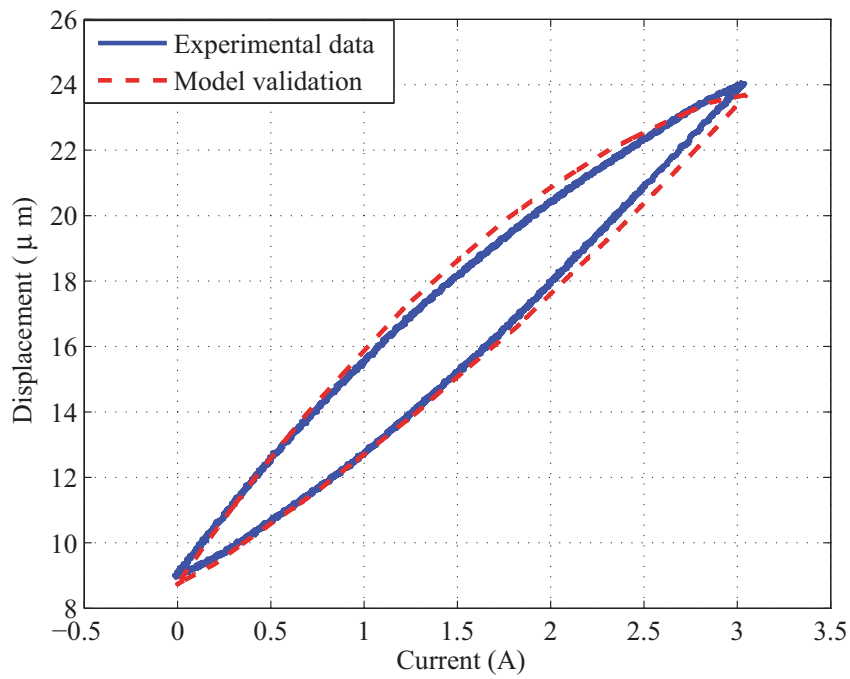
(a) Input signal

(b) Comparison of experimental data and the model

Figure 4.9: Model validation with triangular input signal
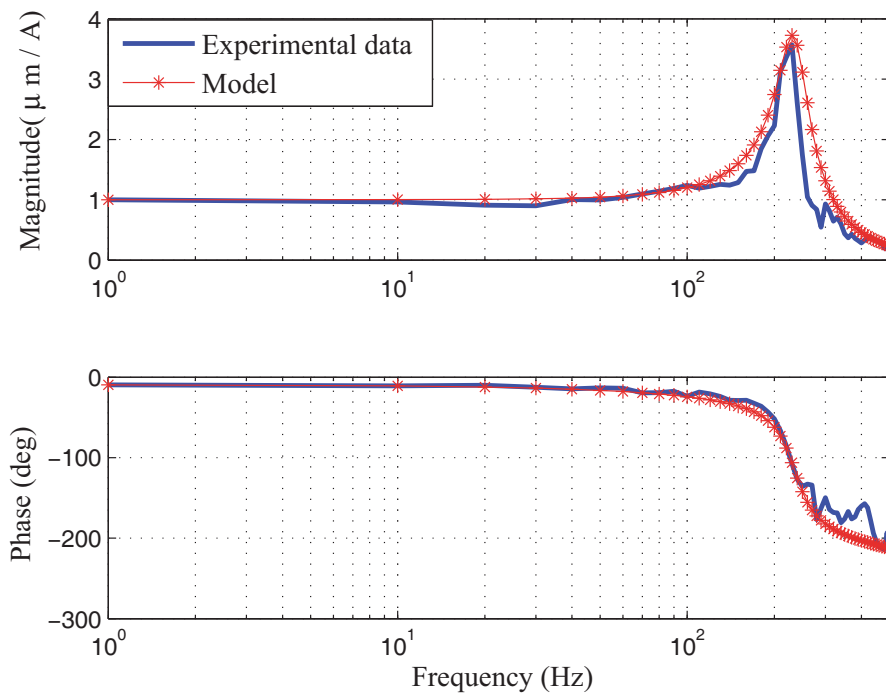
Figure 4.10: The comparison of the frequency response of the system and the dynamic model
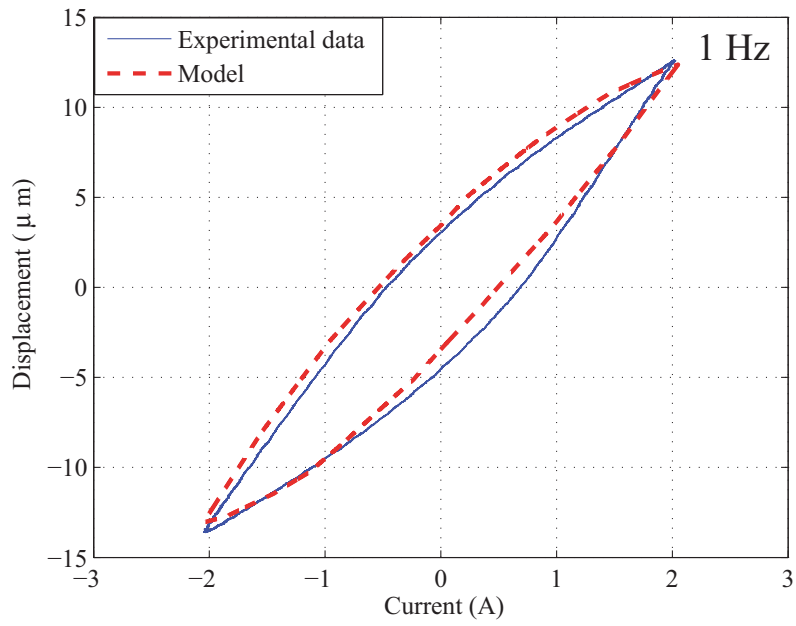
(a) $1Hz$
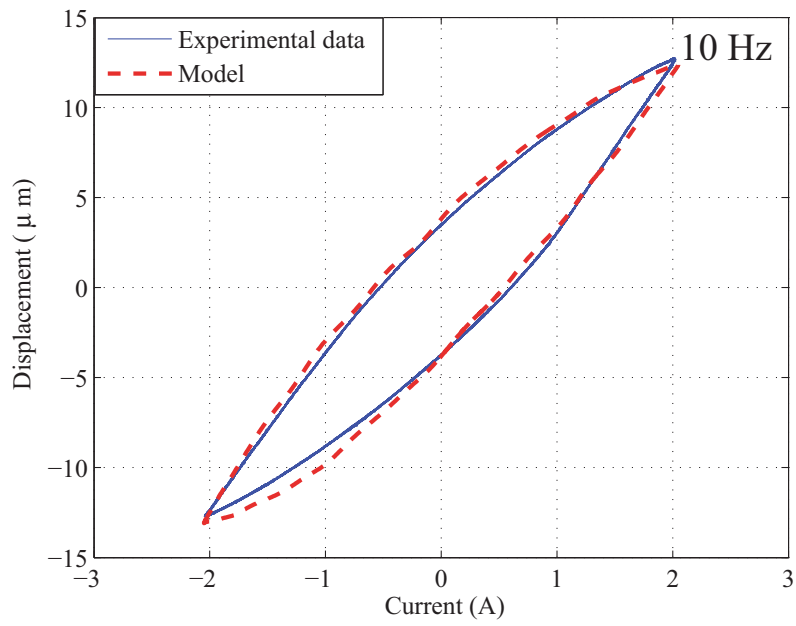
(b) $10Hz$
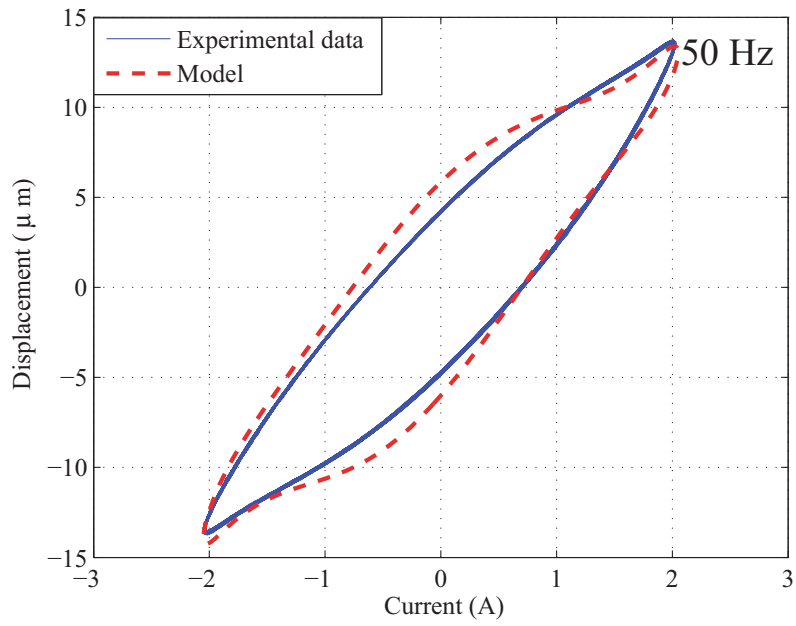
(c) $50Hz$
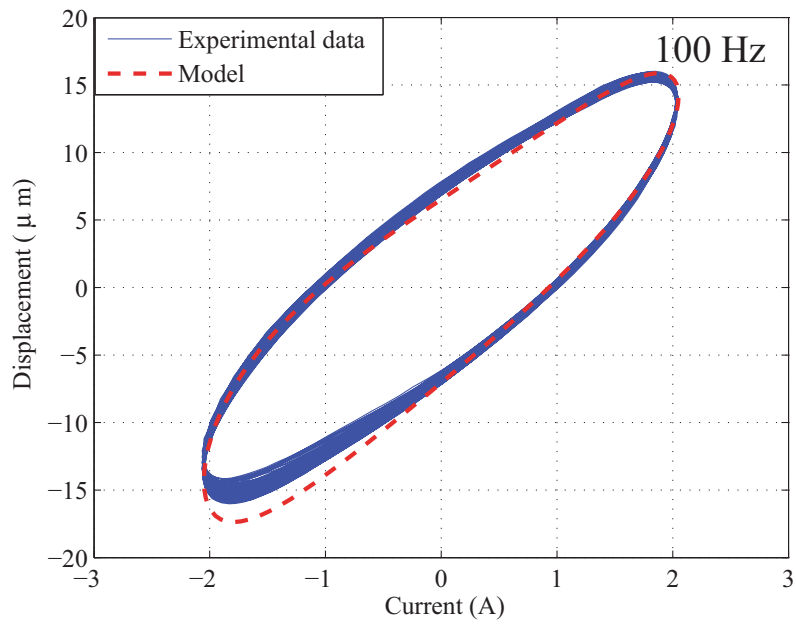
(d) $100Hz$
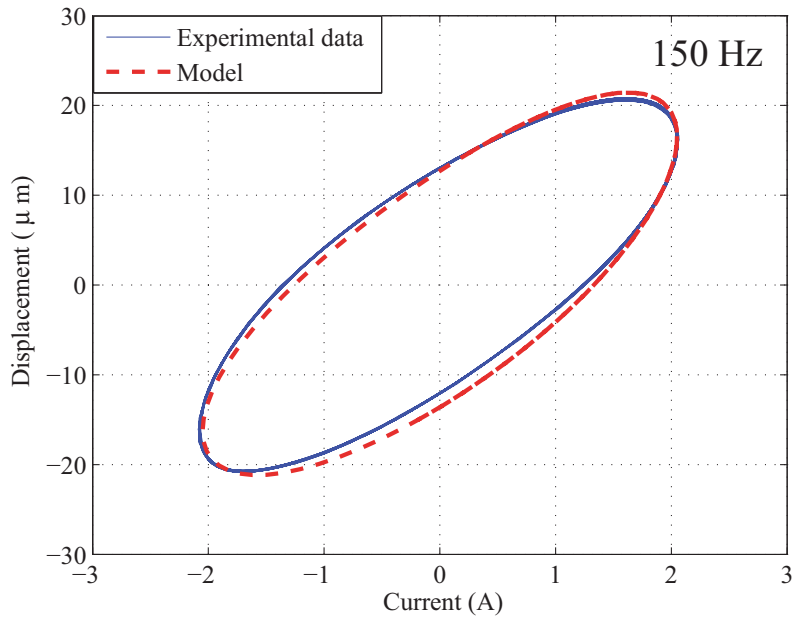
(e) $150Hz$
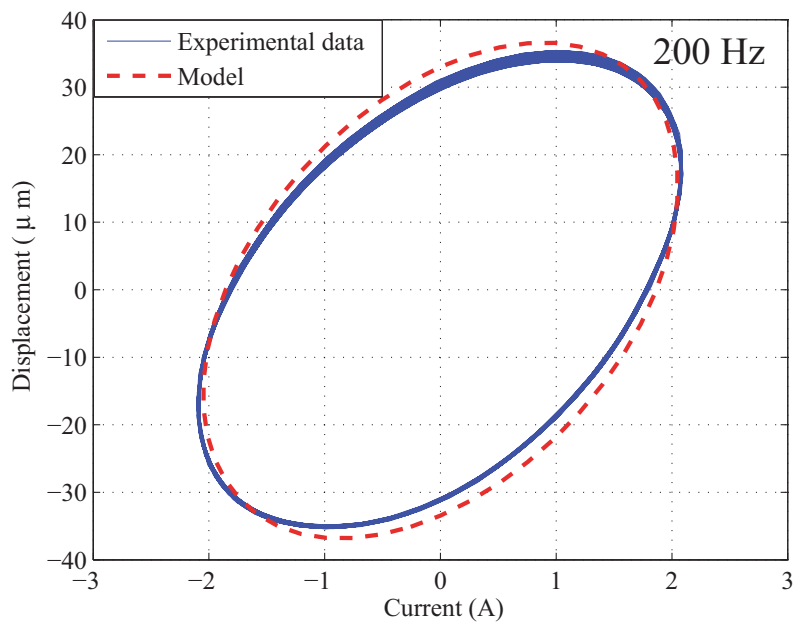
(f) $200Hz$

Figure 4.11: Model verification with sinusoid signal under different input frequency
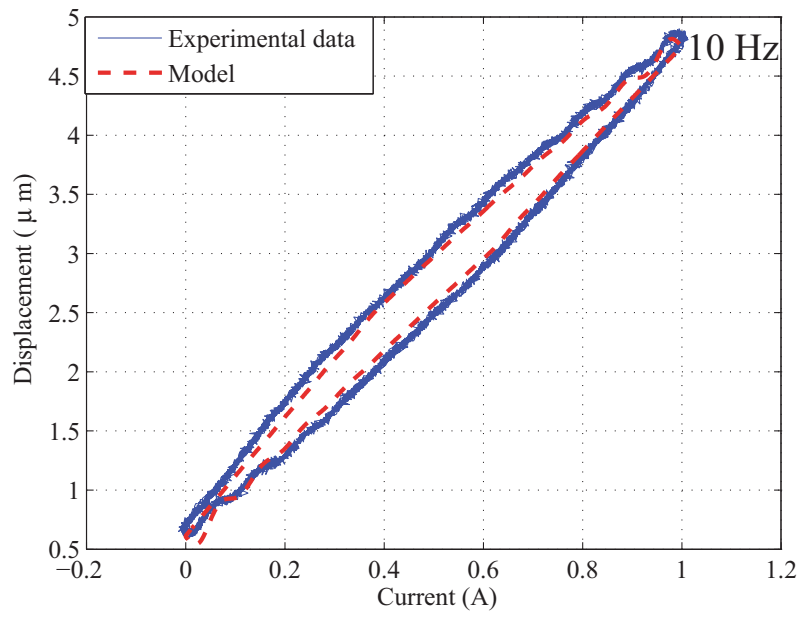
(a) $10Hz$
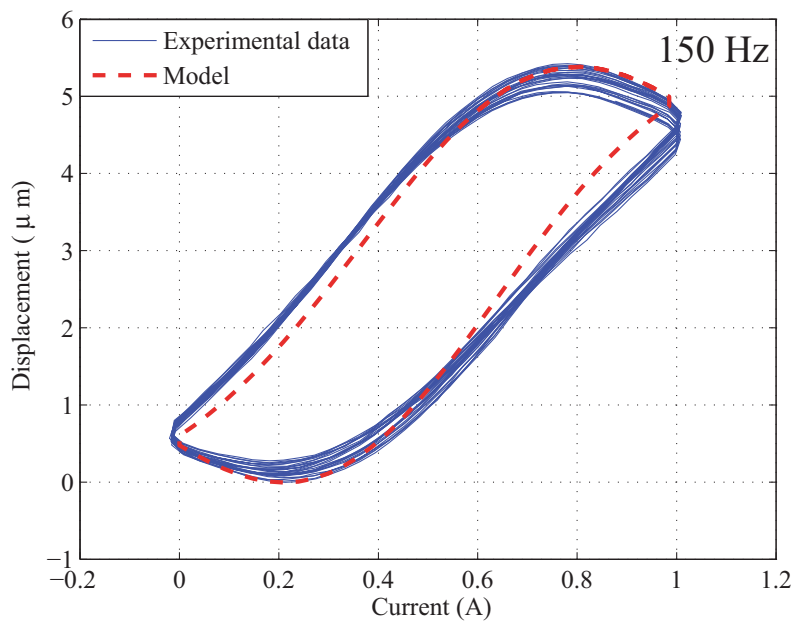
(b) $150Hz$
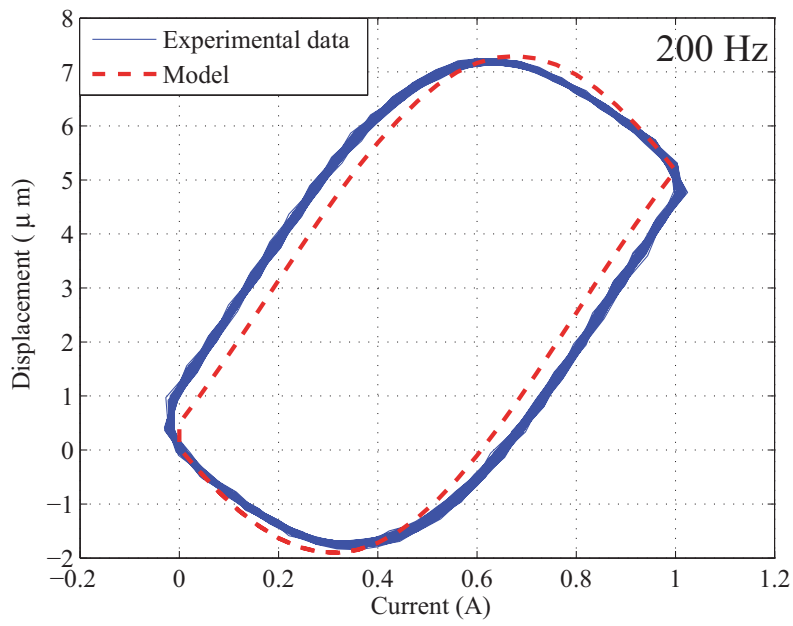
(c) $200Hz$

Figure 4.12: Model verification with triangular signal under different input frequency
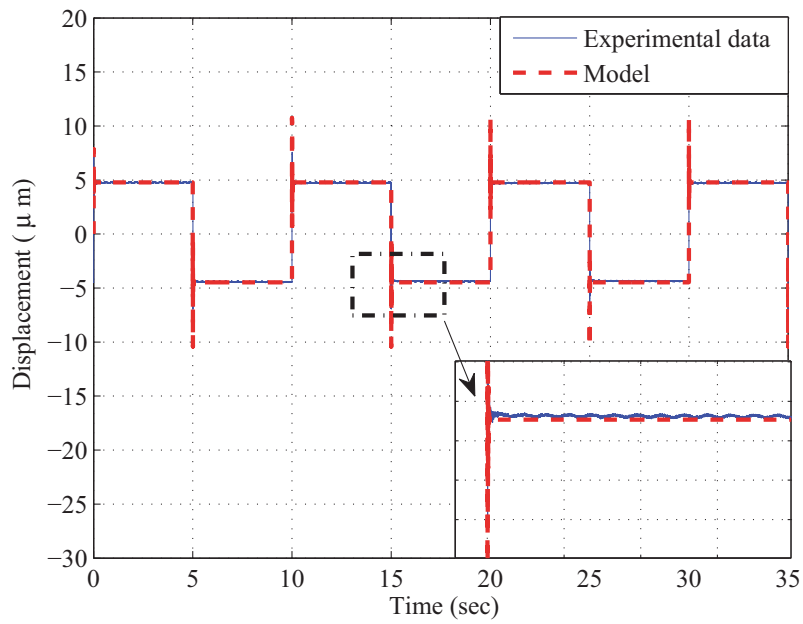
Figure 4.13: Model verification with square wave

80
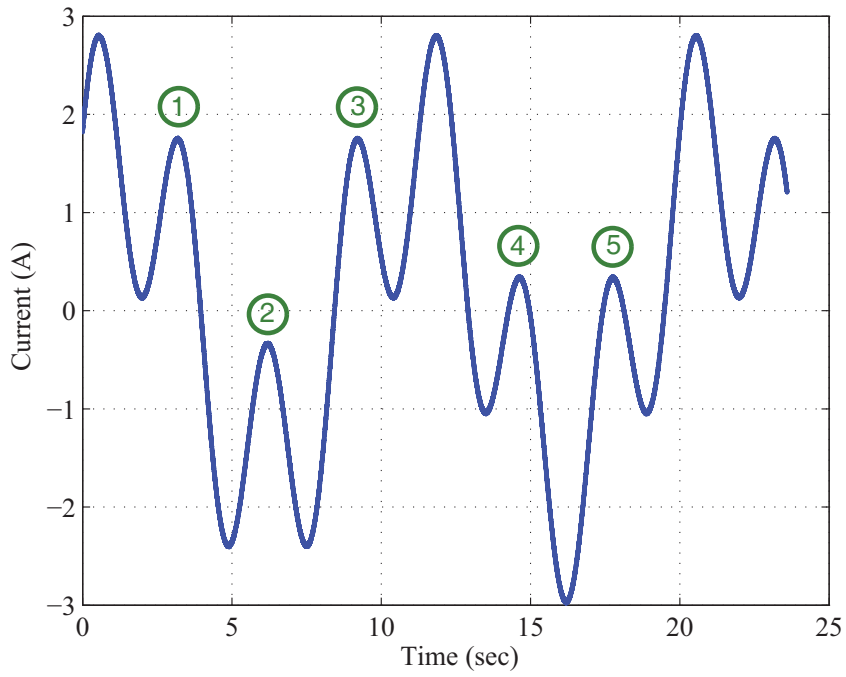
(a) Input signal
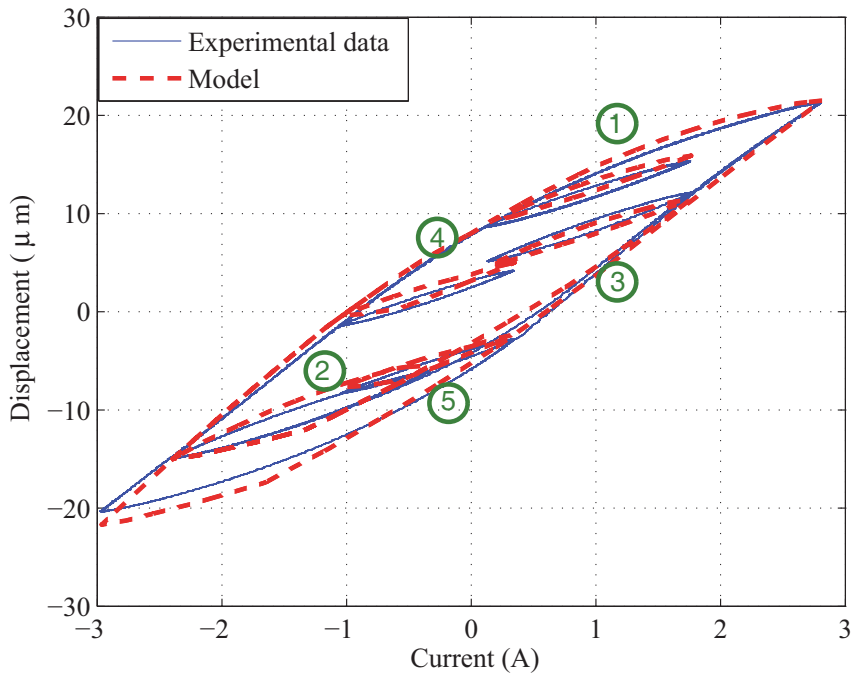
(b) Comparison of experimental data and the model

Figure 4.14: Model validation with complex harmonic input

4.3   Concluding Remarks

In this chapter, the model parameters identification and experimental verification have been conducted to demonstrate the effectiveness of the proposed dynamic model. Different input signals with different input frequencies were applied to magnetostrictive actuators. From the comparisons between the model and experimental data, it illustrates that the proposed model has an excellent agreement with the experimental data.

Chapter 5

Compensation of Hysteresis Nonlinearity with Inverse Approaches

In previous chapters, a cascading model structure (dynamic component preceded by a hysteresis model) is proposed to describe the complex nonlinear dynamic behaviors of the magnetostrictive-actuated systems. From the experimental results, we find it is this preceded hysteresis that generates undesired and detrimental effects, which will deteriorate the performance of the magnetostrictive actuator and cause inaccuracy and oscillations. Therefore, in this chapter we specifically fucus on open-loop inverse compensation strategy for remedying the hysteresis phenomenon based on the cascaded hysteresis model.

In the literature, two compensation approaches are generally used: direct construction of complete inverse function of the hysteresis function (model) [67] [57], and use of an inverse multiplicative structure [1] [71] of the models to compensate the complicated component in the model, for which the development of inverse function for the complicated function is not required.

In Section 5.1, a literature review on the strategy of constructing the inverse compensator is presented. In Section 5.3, the direct inverse construction is constructed to compensate the hysteresis effect described by the ASPI model. In Section 5.2, the inverse multiplicative

structure is applied to find the inverse compensator for the Preisach model.

5.1 The Review of Feedforward Inverse Compensation with Open-loop Schemes

The common approach for remedying the hysteresis nonlinearity is to use an open loop control technique, i.e., construct a hysteresis inverse [1] [67] [57] [72] [73] [74] in putting in cascade as a compensator to cancel the hysteresis effect. Figure 5.1 illustrates the general structure of the feedforward inverse compensation. For construction of the hysteresis inverse, two approaches are generally used: direct construction of complete inverse of the hysteresis model [57] [67], and the inverse multiplicative structure [1] [71]. Direct construction of inverse hysteresis model is mainly for the Prandtl-Ishlinskii (PI) model. When the hysteresis is represented by differential equations such as Bouc-Wen model [1] or the Preisach model, the direct inverse is either impossible or extremely difficult to be obtained. In this case, the inverse multiplicative structure technique developed in [1] [71] can be used to compensate the complicated function in the model. In the following development, the two inverse compensation approaches are briefly reviewed.
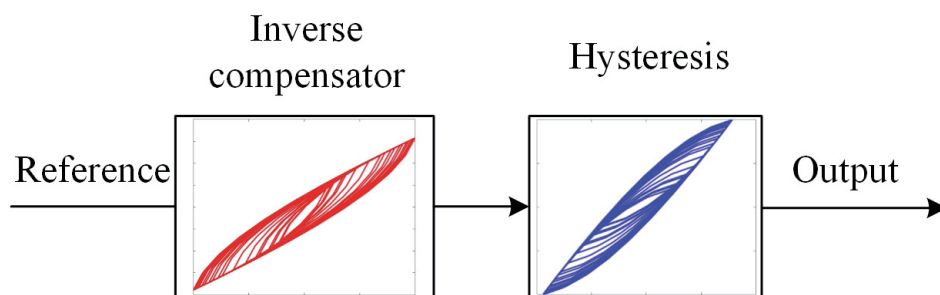
Figure 5.1: Feedforward inverse compensation structure

5.1.1 The Direct Inverse Compensation Approach

In the direct inverse construction approach, only the inverse of the PI model was reported [67] in which the properties of the initial loading curve of the PI model were adopted for constructing the analytical solution for the inverse. In this section, we briefly present this available result as follows.

In [67], the definition of the PI model is given as

$$P[v](t) = p_0 v(t) + \int_0^{\Lambda} p(r) F_r[v](t) dr \tag{5.1}$$

where p_0 is a positive constant; $p(r)$ is a given density function, satisfying $p(r) \geq 0$ with $\int_0^{\infty} r p(r) dr < \infty$. $F_r[v]$ is the play operator. The initial loading curve of the PI model is defined as follows

$$\varphi(r) = p_0 r + \int_0^r p(\kappa)(r - \kappa) d\kappa \tag{5.2}$$

The initial loading curve reflects the characteristics of the output of the PI model starting at the initial condition. And the first derivative and second derivative of the initial loading curve function satisfy

$$\varphi'(0) = p_0 \tag{5.3}$$

$$\varphi''(r) = p(r) \tag{5.4}$$

Therefore, the inverse of the PI model [67] is derived as

$$P[u]^{-1}(t) = \bar{p}_0 u(t) + \int_0^{\bar{\Lambda}} \bar{p}(r) F_r[u](t) dr \tag{5.5}$$

where,

$$\bar{p}_0 = \frac{1}{p_0} \tag{5.6}$$

$$\bar{p}(r) = (\varphi^{-1})''(r) \tag{5.7}$$

In order to implement the inverse compensation numerically, we have the numerical expression of the PI model as

$$P[v](t) = p_0 v(t) + \sum_{j=1}^{n} p_j F_{r_j}[v](t) \tag{5.8}$$

The direct inverse expression of the PI model is expressed as

$$P^{-1}[u](t) = \bar{p}_0 v(t) + \sum_{i=1}^{n} \bar{p}_i F_{\bar{r}_i}[u](t) \tag{5.9}$$

where $\bar{r}_i$, $\bar{p}_0$ and $\bar{p}_i$ can be found as

$$\bar{r}_i = p_0 r_i + \sum_{l=1}^{i} \sum_{j=1}^{l-1} p_j (r_l - r_{l-1}) \tag{5.10}$$

$$\bar{p}_0 = 1/p_0 \tag{5.11}$$

$$\bar{p}_i = -\frac{p_i}{(p_0 + \sum_{j=1}^{i} p_j)(p_0 + \sum_{j=1}^{i-1} p_j)} \tag{5.12}$$

Therefore, as long as we find the parameters of $\bar{r}_i$, $\bar{p}_0$, and $\bar{p}_i$ in (5.10) based on the parameters in the PI model (5.8), the direct inverse of the PI model can be obtained. An illustration example is given as follows. A PI model with the thresholds and weights which are shown in Table 5.1. According to (5.10), the corresponding $\bar{r}_i$, $\bar{p}_0$, and $\bar{p}_i$ are computed in Table 5.1. Figure 5.2 shows the input and output relationship of the PI model, the direct inverse of the PI model as well as the compensation results.

Table 5.1: Coefficients of the PI model and its direct inverse

Numbers	r_i	p_i	$\bar{r}_i$	$\bar{p}_i$
0	0	1	0	1
1	0.25	0.5	0.25	-0.1667
2	0.5	0.5	0.55	-0.119
3	0.75	0.5	0.9	-0.0893

As we mentioned before, the direct inverse compensation approach can only be applied to the PI model and the extended PI models such as the modified PI model [57], the generalized PI model [60], etc. If the hysteresis effect shown in the cascading model structure reported in Chapter 2 is described by other hysteresis models, i.e. Preisach model or Bouc-Wen model, this direct inverse compensation approach may generate approximating error or not be
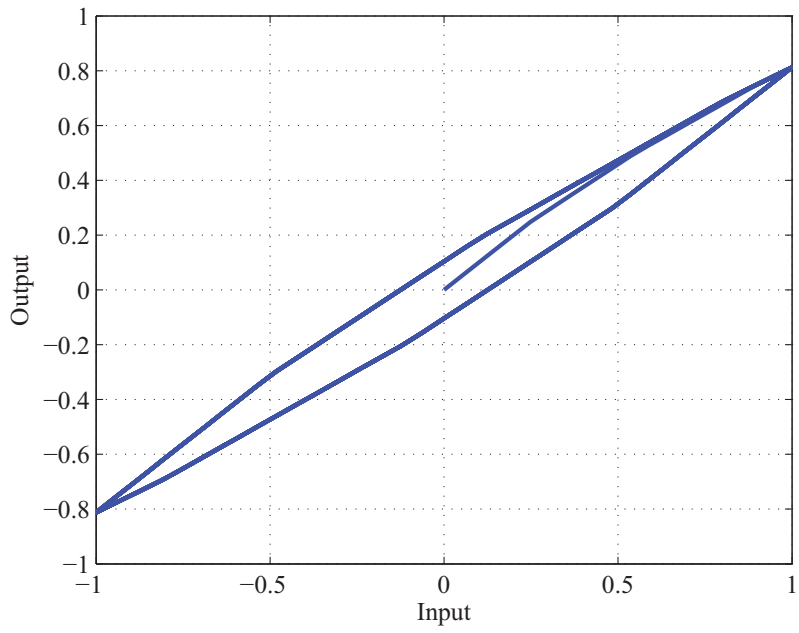
(a) The I/O of the direct inverse PI model
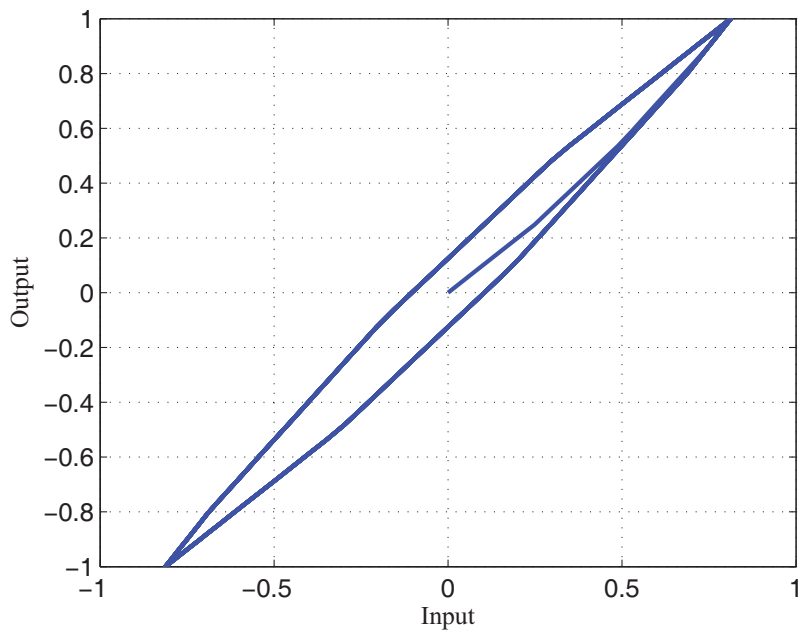
(b) The I/O of the PI model

87
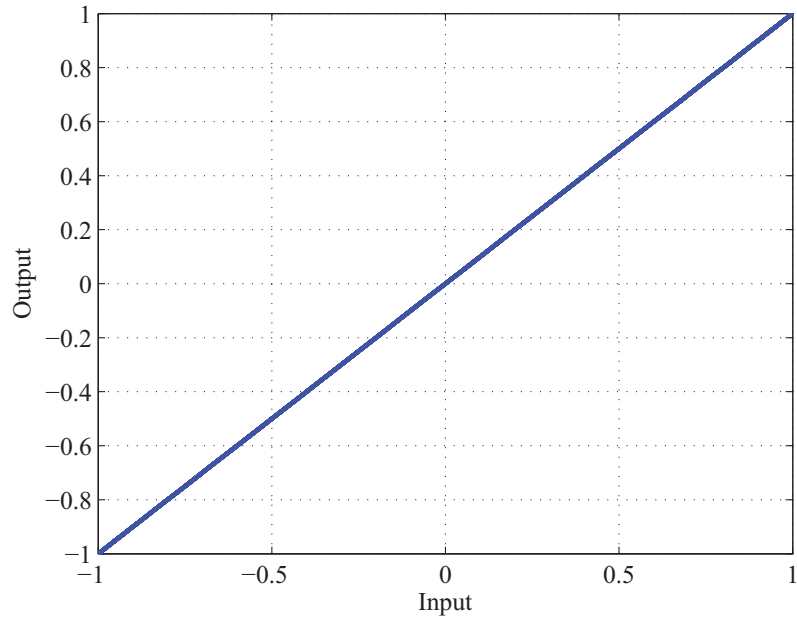
(c) The I/O of the combination of the PI model and the direct inverse PI model

Figure 5.2: The simulation of the inverse compensation of the PI model

applicable. Therefore, the second inverse compensation approach, the inverse multiplicative structure technique [1], is considered.

5.1.2 The Inverse Multiplicative Structure Approach

The inverse multiplicative structure technique was first reported in [1] for constructing the inverse of the Bouc-Wen hysteresis model. The advantages of the inverse multiplicative structure compensator are 1) it does not require the direct inverse calculations of the hysteresis model; 2) no additional computation is required. Therefore, the inverse multiplicative structure provides the possibility to construct the inverse for complex hysteresis models, such as the Preisach model. A brief overview of the inverse multiplicative structure technique in [1] is presented first.

In [1], the Bouc-Wen model is utilized to describe the hysteresis effect in piezoelectric

actuators, which is defined as

$$y(t) = d_p U - H(U) \tag{5.13}$$

where,

$$H(U) = h(t)$$

$$\frac{dh}{dt} = A_{bw}\frac{dU}{dt} - B_{bw}|\frac{dU}{dt}|h - \Gamma_{bw}\frac{dU}{dt}|h| \tag{5.14}$$

and A_{bw}, B_{bw}, and Γ_{bw} are parameters that govern the scale and general shape of the hysteresis loops, y is the displacement output, U denotes the input. The inverse multiplicative structure compensator is obtained as

$$U = \frac{1}{d_p}(y_r + H(U)) \tag{5.15}$$

where y_r is the desired output. The structure of the compensator is shown in Figure 5.3. A simulation is given to demonstrate the compensation result of the inverse multiplicative structure for the Bouc-Wen model. Figures 5.4(a) and 5.4(b) show the input and output relationship of the Bouc-Wen model and the inverse multiplicative structure compensator, where $b_p = 2$, $A_{bw} = 2$, $B_{bw} = 1.5$, and $\Gamma_{bw} = 0.1$ in (5.13) and (5.14). The linear relationship shown in Figure 5.4(c) indicates the Bouc-Wen hysteresis has been completely canceled.
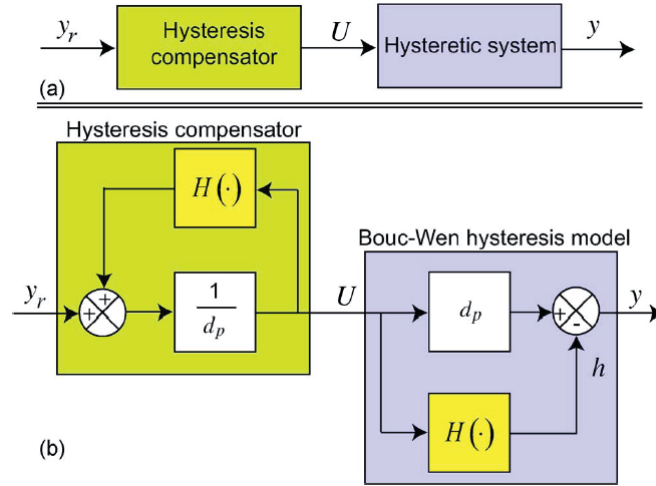
Figure 5.3: Hysteresis compensation. (a) General principle. (b) The proposed structure [1]
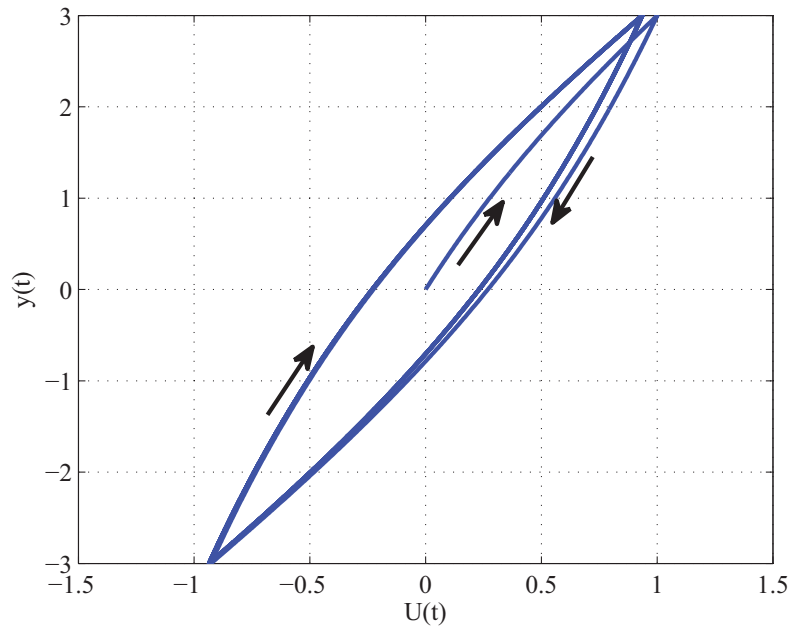
(a) The Bouc-Wen Hysteresis
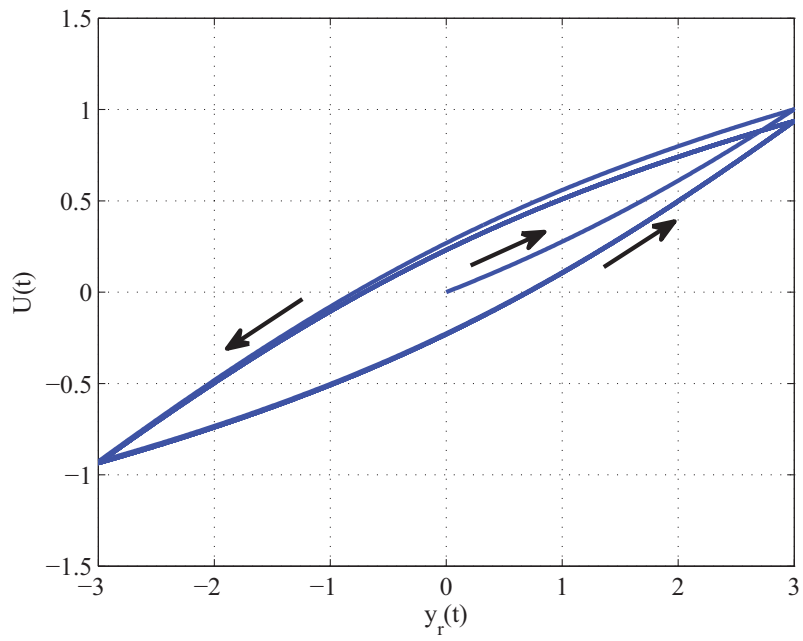
(b) The inverse multiplicative structure compensator
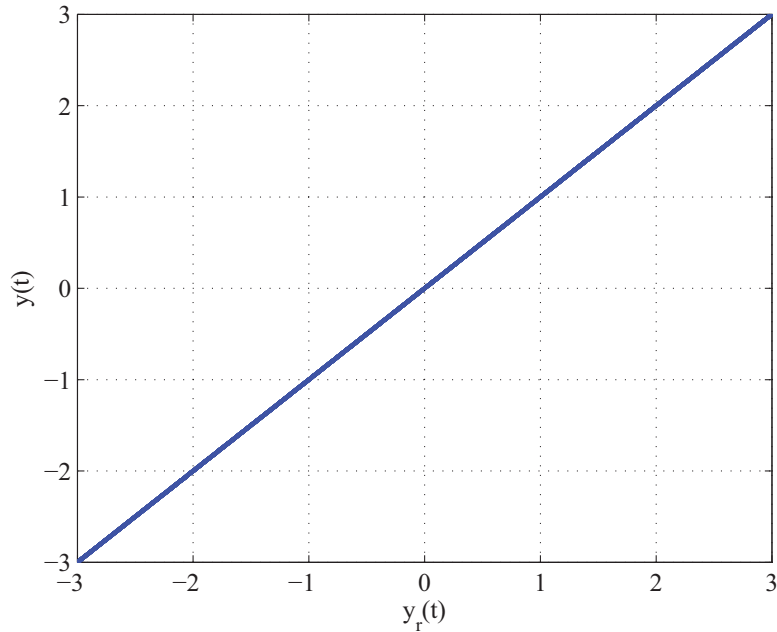
(c) The compensation result

Figure 5.4: The inverse multiplicative structure compensator for Bouc-Wen model

5.2 The Inverse Multiplicative Structure Compensator for the Preisach Model

In the literature, the Preisach model is a very popular model to describe the hysteresis behaviors. If we use the Preisach model to represent the hysteresis effect in the cascading model structure in (4.3) of Chapter 4, the challenge addressed here is how to construct its feedforward inverse compensator. In the literature, some results have obtained for the inverse construction of the Preisach model. However, since the input signal is implicitly involved in the Preisach model, the results are mainly numerical inversion algorithms [2] [75]. The application of these approximate inverse models would thus yield considerable compensation errors under excitations at higher frequencies. Therefore, it would be desirable if the inverse multiplicative structure technique [1] developed for the Bouc-Wen model can be utilized for the Preisach model inverse construction. However, unlike the Bouc-Wen model, the input

signal in the Preisach model is implicitly involved into its complex dual integral formulation and does not possess the required multiplicative structure.

Therefore, in this section, we attempt to develop an inverse compensator for the Preisach model using the inverse multiplicative structure technique [1]. For such a purpose, by exploiting the properties of the Preisach model, it is decomposed as two parts: non-memory part and memory part. Based on this separation, it only requires to solve the inverse of the non-memory part to obtain an explicit expression of the input signal, making it possible to use the inverse multiplicative structure technique. Then, by solving the exact inverse of the non-memory part, the entire inverse of the Preisach model has been developed. To validate the result, the inverse model is applied in a cascade configuration with the Preisach hysteresis model using the laboratory-measured input-output characteristics of the magnetostrictive actuator to study its effectiveness as an open-loop feedforward hysteresis nonlinearity compensator. The experimental results validated the effectiveness of the proposed inverse compensation method.

5.2.1 The Preisach Model

The Preisach model was first developed in 1935 by F. Preisach [41] for the purpose of describing the hysteresis effect in ferromagnetic materials. A detailed discussion on this model can be found in the monograph [49]. The Preisach model is constructed by superposing relay operators as [49]

$$u(t) = \Gamma[v](t) = \iint_{T_0} \mu(r,s)\hat{\gamma}_{s-r,s+r}[v](t)drds \tag{5.16}$$

where $\hat{\gamma}_{s-r,s+r}[v](t)$ denotes the relay operator as

$$\hat{\gamma}_{s-r,s+r}[v](t) = \begin{cases} +1 & \text{if } v(t) > s+r \\ -1 & \text{if } v(t) < s-r \\ \hat{\gamma}_{s-r,s+r}[v](t^-) & \text{if } s-r \leq v(t) \leq s+r \end{cases}$$

92

$t^- = \lim_{\varrho > 0, \varrho \to 0} t - \varrho$, s and r are two parameters that determine switching values $+1$ (the switch is "on") and -1 (the switch is "off"), $v(t)$ denotes the input signal, $\mu(r, s)$ is the density function of the Preisach model, which is selected by designers. Without losing the generality, in the following development $\mu(r, s)$ is defined on a compact support [51]: $T = \{(r, s) \in T_0 | r - R \le s \le -r + R, R > 0\}$ with a bound $R > 0$, and $\mu(r, s)$ is equal to zero outside the triangle T, T_0 denotes the set $\{(s, r)| -\infty < s < \infty, r \ge 0\}$.

5.2.2 The Inverse Construction of the Preisach Model Using the Inverse Multiplicative Structure

It is obvious that the inverse multiplicative structure technique cannot be directly applied to the Preisach model (5.16) due to the input signal $u(t)$ which is implicitly involved in its complex double integral formulation. To utilize the above technique, the task in the following development is to re-formulate the Preisach model (5.16) into a form similar to the Bouc-Wen model (5.13), i.e., obtain an explicit expression of the input signal from its implicit form, so that the inverse multiplicative technique can be applied. To this end, a Preisach plane (r-s plane) [49] on which the geometric interpretation of the Preisach model can be best visualized is introduced first.

Consider the isosceles right triangle $T = \{(r, s) \in T_0 | r - R \le s \le -r + R, R > 0\}$ on the r-s plane, as illustrated in Figure 5.5, for any $v(t)$, $-R \le v(t) \le R$, the triangle T is subdivided by a interface $L(t)$ into two parts: $S^+(t)$, all switches $\hat{\gamma}_{s-r,s+r}[v](t)$ within this area are on $(\hat{\gamma}_{s-r,s+r}[v](t) = +1)$; $S^-(t)$, all switches $\hat{\gamma}_{s-r,s+r}[v](t)$ are off $(\hat{\gamma}_{s-r,s+r}[v](t) = -1)$. Therefore, based on the geometric interpretation, the Preisach model (5.16) is decomposed as:

$$
\begin{aligned}
u(t) &= \iint_{S+} \mu(r, s)\hat{\gamma}_{s-r,s+r}[v](t)drds + \\
&\quad \iint_{S-} \mu(r, s)\hat{\gamma}_{s-r,s+r}[v](t)drds \\
&= 2\iint_{S+} \mu(r, s)\hat{\gamma}_{s-r,s+r}[v](t)drds - \Delta
\end{aligned}
\tag{5.17}
$$

93
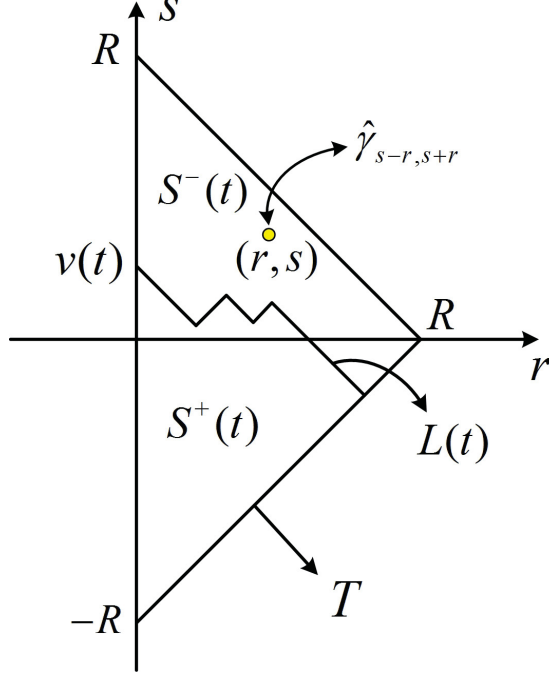
Figure 5.5: The geometric interpretation of the Preisach model

where $\Delta = \iint_T \mu(r,s)\hat{\gamma}_{s-r,s+r}[v](t)drds = \int_0^R \int_{r-R}^{-r+R} \mu(r,s)dsdr$ is a constant. From (5.17) and the geometric interpretations

$$\hat{\gamma}_{s-r,s+r}[v](t) = +1, \quad if \ (r,s) \in S^+(t) \tag{5.18}$$

the model (5.16) can be re-expressed as:

$$u(t) = 2\iint_{S^+} \mu(r,s)drds - \Delta \tag{5.19}$$

for the purpose of calculation.

From (5.19), it follows that the output of the Preisach model $u(t)$ depends on the evolution in time of $S^+(t)$ and $S^-(t)$ governed by the input signal $v(t)$, which implies that the input signal $v(t)$ is implicitly involved in (5.19), causing the challenge for stable controller designs. In order to derive a new expression where the input signal $v(t)$ in (5.19) can be expressed explicitly, a discrete Preisach model is considered. In the literature, there exist several discretization strategies [75] [76] [77]. For our purpose, we adopted the discretization

approach reported in [75], see Figure 5.6. We divide the interval $[0, R]$ into N+1 subintervals of equal width, Δr, and from each interval choose the point, r_i. Then the discrete Preisach model (5.17) is written as

$$
\begin{aligned}
u(t) &= \Gamma_\kappa[v](t) \\
&= 2 \int_{r_0}^{r_1} \int_{r_0-R}^{L[r_0](t)} \mu(r_0, s)\, ds\, dr + ... \\
&\quad 2 \int_{r_i}^{r_{i+1}} \int_{r_i-R}^{L[r_i](t)} \mu(r_i, s)\, ds\, dr + ... \\
&\quad 2 \int_{r_N}^{r_{N+1}} \int_{r_N-R}^{L[r_N](t)} \mu(r_N, s)\, ds\, dr - \Delta_\kappa \\
&= 2\Delta r \sum_{i=0}^{N} \int_{r_i-R}^{L[r_i](t)} \mu(r_i, s)\hat{\gamma}_{s-r_i, s+r_i}[v](t)\, ds - \Delta_\kappa \qquad (5.20)
\end{aligned}
$$

where $\Delta_\kappa = \Delta r \sum_{i=0}^{N} \int_{r_i-R}^{-r_i+R} \mu(r_i, s)\, ds$ is a constant. $L[r_i](t)$ denotes the values on the interface $L(t)$, see Figure 5.6, and we have $L[r_0](t) = v(t)$.
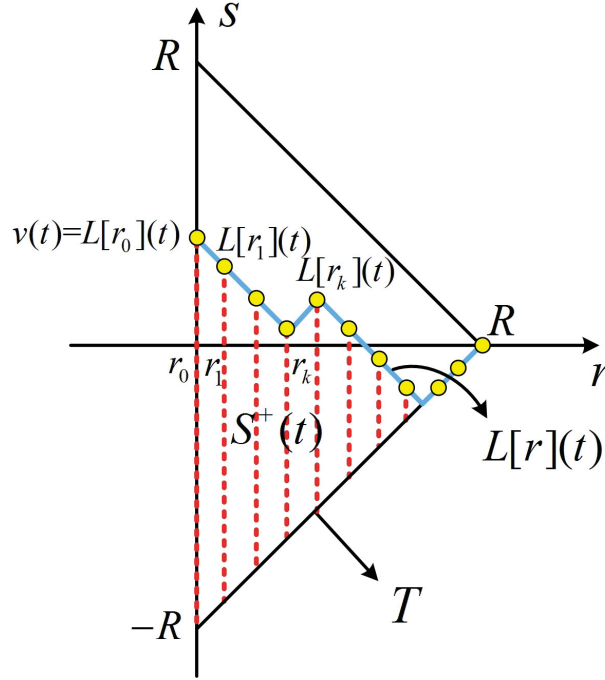
Figure 5.6: The discretization in geometric interpretation of the Preisach model

Remark: The discretization procedure of the original Preisach model is based on the

definition of the integral. When the number of the integgral subintervals goes to infinity, the error $e_\Gamma(t)$ between the original Preisach model $\Gamma[v](t)$ in (5.19) and the discrete Preisach model $\Gamma_\kappa[v](t)$ in (5.20) will converge to zero,

$$\lim_{N\to\infty} \Gamma[v](t) - \Gamma_\kappa[v](t) = \lim_{N\to\infty} e_\Gamma(t) = 0 \tag{5.21}$$

Therefore, if we select a sufficiently large N, we regard the discrete Preisach model is equivalent to the original Preisach model.

With the help of r-s plane, in the following development we will further explore the model (5.20) to obtain a new expression that is suitable for controller design where the input signal can be explicitly expressed in the Preisach model. By further examining the geometric interpretation of the Preisach model in Figure 5.6, the model (5.20) on the area $S^+(t)$ in r-s plane can be further divided into two parts: $\Gamma_{r_0}^+$ and $\sum_{i=1}^N \Gamma_{r_i}^+[v](t)$. In this case, (5.20) can be re-written as

$$u(t) = 2(\Gamma_{r_0}^+[v](t) + \sum_{i=1}^N \Gamma_{r_i}^+[v](t)) - \Delta_\kappa \tag{5.22}$$

where

$$\begin{aligned}
\Gamma_{r_0}^+[v](t) &= (r_1 - r_0) \int_{r_0-R}^{L[r_0](t)} \mu(r_0, s)\hat{\gamma}_s[v]ds \\
&= \Delta r \int_{-R}^{v(t)} \mu_1(s)ds \\
&= \Delta r(\lambda(v) - \lambda(-R)) \tag{5.23}
\end{aligned}$$

where $\lambda(\cdot) = \int \mu_1(s)ds$ and

$$\hat{\gamma}_s[v] = \begin{cases} +1 & \text{if } v(t) \geq s \\ -1 & \text{if } v(t) < s \end{cases}$$

and

$$\Gamma_{r_i}^+[v](t) = (r_{i+1} - r_i) \int_{r_i-R}^{L[r_i](t)} \mu(r_i, s)\hat{\gamma}_{s-r_i,s+r_i}[v](t)ds \tag{5.24}$$

Remark: In (5.23), we denote $\mu(r_0, s) = \mu_1(s)$ because $r_0 = 0$ and $\mu(0, s)$ is only with respect of variable s, we therefore replace $\mu(r_0, s)$ with $\mu_1(s)$ just for convenience. Equation (5.22)

96

can be further written as

$$u(t) = 2\Delta r \lambda(v) + G \tag{5.25}$$

where $G = 2\sum_{i=1}^{N} \Gamma_{r_i}^+[v](t) - 2\Delta r \lambda(-R) - \Delta_\kappa$. Now, the Preisach model (5.25) is in a structure similar to the Bouc-Wen model (5.13). By applying the inverse multiplicative structure technique, the inverse (feedforward) compensator of the Preisach model (5.25) can be obtained as

$$u = \lambda^{-1}\left(\frac{u_r - G}{2\Delta r}\right) \tag{5.26}$$
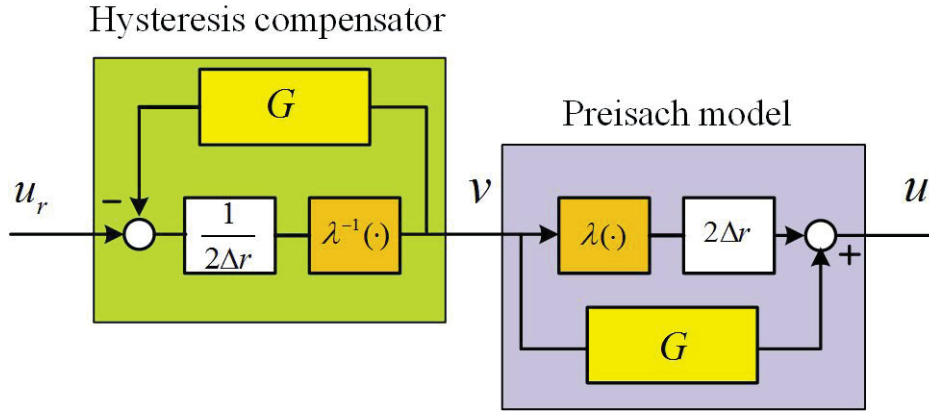
Figure 5.7: The inverse multiplicative structure for the Preisach model

The scheme of the inverse compensator is shown in Figure 5.7. The only difference is the inclusion of λ^{-1}, which makes it possible to obtain the explicit expression of the input signal $v(t)$ from the Preisach model (1), imposing a major challenge. It should be noted that unlike the Bouc-Wen hysteresis model, whose input signal $v(t)$ is explicit already because its structure is fixed and the shape depends on the coefficients of the model, the input signal $v(t)$ of the Preisach model can only be obtained by calculating λ^{-1}. The analytical form of λ^{-1} cannot be determined a priori, depending on the density functions $\mu(\cdot)$. This is because the shape of the Preisach model is determined by the selection of the density functions $\mu(\cdot)$, which is not unique. The analytical form of λ^{-1} can only be obtained after the density functions $\mu(\cdot)$ is selected with a specific magnetostrictive actuator. For example, the common used density function for the Preisach model are $\mu(s) = a$ (a is a constant), the

exponential function [49] $\mu(s) = ae^{-s}$, as well as the lorentzian function [50] $\mu(s) = \frac{k}{1+(s-a)^2}$ (a, k are constants). Their corresponding $\lambda(s)$ functions and the exact inverse expressions $\lambda^{-1}(s)$ are listed in Table. 5.2 as illustrations.

Table 5.2: $\lambda(s)$ function and its exact inverse $\lambda^{-1}(s)$

$\mu(s)$	$\lambda(s)$	$\lambda^{-1}(s)$
a	as	$\frac{s}{a}$
ae^{-s}	$-ae^{-s}$	$ln\frac{-a}{s}(s<0)$
$\frac{k}{1+(s-a)^2}$	$k\arctan(s-a)$	$tan(\frac{s}{k})+a$

5.2.3   Experimental Validation

The experimental validation is conducted on the experimental platform reported in Chapter 1, Section 1.3.1. In order to implement the inverse compensator (5.26) in the dSPACE, we first need to identify the discrete Preisach model in (5.25) as

$$u = 2\Delta r \lambda(v) + G \qquad (5.27)$$

where $G = 2\sum_{i=1}^{N} \Gamma_{r_i}^{+}[v](t) - 2\Delta r \lambda(-R) - \Delta_\kappa$.

To this end, the density function on the line $r = 0$ is selected as

$$\mu(s) = a_1 e^{-s} \qquad (5.28)$$

where a_1 is a coefficient and $a_1 > 0$. Then, according to Table.5.2

$$\lambda(s) = -a_1 e^{-s} \qquad (5.29)$$

Δr is selected as 0.05. G is further discretized as

$$G = \sum_{k=1}^{M} W_k[v]\mu_k + b_1 \qquad (5.30)$$

98

where $W_k[v]$ denotes the delay operator, μ_k denotes identified coefficient. The number of μ_k is $K = L(L+1)/2$, where L is discretization level. L is sufficiently large, the Preisach model with identified weights would correspond smoothly with the experimental data. $b_1 = -2\Delta r\lambda(-R) - \Delta_\kappa$, which is a constant.

Then, we have

$$
\begin{aligned}
u &= -2\Delta r a_1 e^{-v} + \sum_{k=1}^{M} W_k[v]\mu_k + b_1 \\
&= \mathbf{W^T}[v]\mu_k
\end{aligned}
\tag{5.31}
$$

where $\mathbf{W}[v] = [-2\Delta r e^{-v}, w_1, w_2, ... w_M, 1]^T$, $\mu_k = [a_1, v_1, v_2, ..., v_M, b_1]^T$. In $\mathbf{W}[v]$, the input signal v and the bound of the triangle area R are all available, $w_1, w_2, ..., w_M$ are calculated from the relay operators defined in (5.16) with the input signal v, therefore, $W[v]$ can be determined. The parameter μ_k of the Preisach model is unknown and needs to be determined by the following constrained quadratic optimization:

$$
min\{[\mathbf{C}\mu_k - \mathbf{d}_k]^T[\mathbf{C}\mu_k - \mathbf{d}_k]\}
\tag{5.32}
$$

with the constraints

$$
\mu_k \geq 0
\tag{5.33}
$$

$$
\mathbf{C} = \begin{pmatrix} \boldsymbol{W}^T[1] \\ \boldsymbol{W}^T[2] \\ \vdots \\ \boldsymbol{W}^T[k] \end{pmatrix}
$$

where $\mathbf{d}_k = [d_1, d_2...d_3]^T$ is the output of the magnetostrictive actuator under a designed decreasing input signal as $4.5sin(2\pi t)e^{-0.2t}$. Then, a nonlinear least-square optimization function *lsqnonneg* in MATLAB was employed to find the parameters μ_k. Let the bound of the triangle T be $R = 5$ and the discretization level L=200. Then, the total number of the discrete components becomes $M = L(L+1)/2 - L = 19900$. Figure 5.8 illustrates the identified weights $\boldsymbol{v}[n](n = 2, 3, ...M)$, and μ_1 is identified as $a_1 = 8.4$, $b_1 = 62.33$. Figure 5.9

99
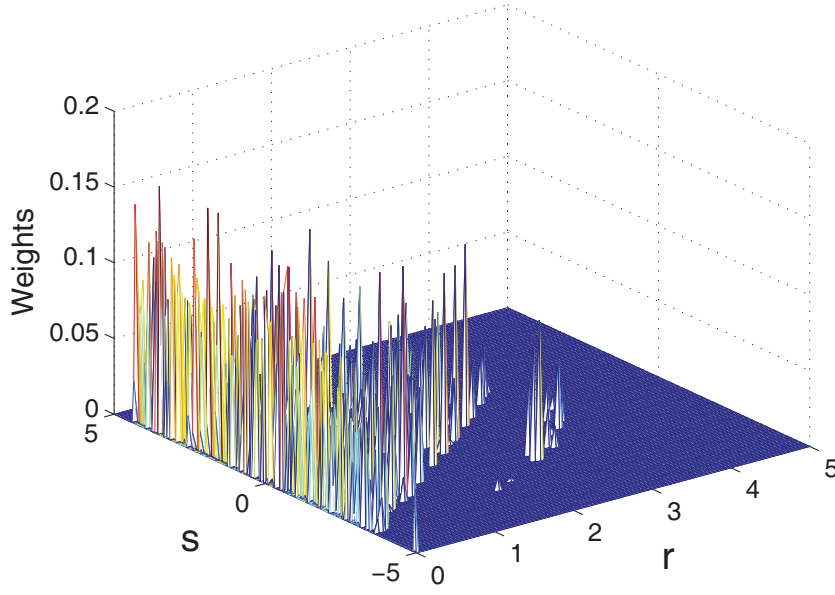
Figure 5.8: The identified weights

shows the comparison of output of the magnetostrictive actuator and the Preisach model. The modeling error is defined as

$$e_m(t) = \frac{100(\mu(t) - y(t))}{max(\mu(t))} \tag{5.34}$$

where $\mu(t)$ and $y(t)$ are the output of the magnetostrictive actuator and the Preisach model. The hysteresis loops are shown in Figure 5.9(b). As is shown in Figure 5.9(a), the output of the Preisach model corresponds well with the experimental data and the maximum error is less than 0.6% of the total range.

Based on the identified results, we have

$$u = 2 \times 0.05\lambda[v] + G \tag{5.35}$$

where,

$$\lambda[v] = -8.4e^{-v} \tag{5.36}$$

$$G = \sum_{k=1}^{M} W_k[v]\mu_k + 62.33 \tag{5.37}$$

100
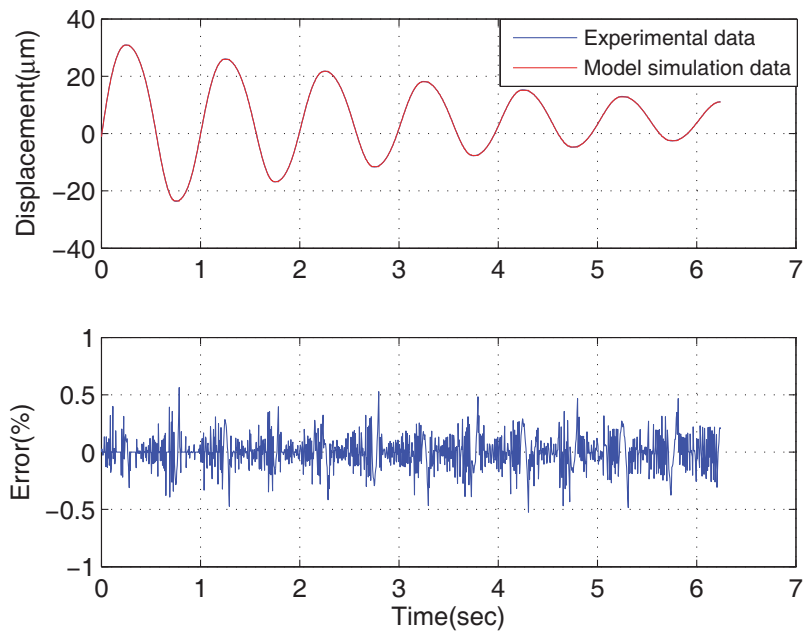
(a) Displacement vs time.
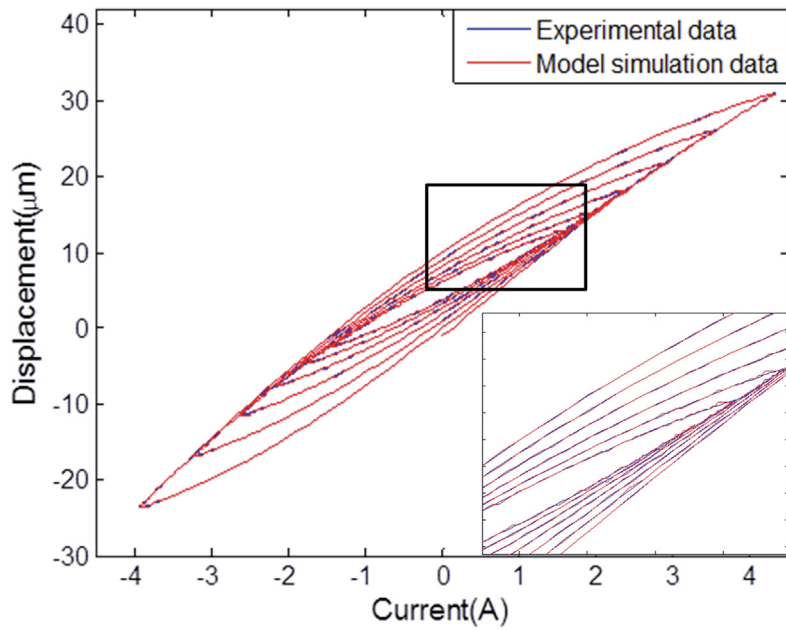
(b) Hysteresis loop.

Figure 5.9: Comparison of experimental data and the Preisach model

101

The inverse multiplicative structure compensator can be expressed as

$$
\begin{aligned}
v &= \lambda^{-1}\left[\frac{u_r - G}{2 \times 0.05}\right] \\
&= \ln\frac{0.84}{G - u_r}
\end{aligned}
\tag{5.38}
$$

The inverse compensation and experimental analysis have been carried using hardware-in-the-loop techniques which efficiently connect the embedded system to the real plant. The inverse multiplicative structure was implemented in the Matlab/simulink and the codes were transformed into real-time control codes and downloaded to the dSPACE board. A desired tracking signal u_r was applied to the compensator with an amplitude of 35 μm and a frequency of 1 Hz, and the output together with the actuator gain (0.1429 A μm^{-1}) was applied to the magnetostrictive actuator through the power amplifier. The measured actuator displacement responses was subsequently obtained by using capacitive sensor (Lion Precision, model C23-C) and uploaded into the dSPACE board. Figure 5.10(a) shows the input-output relationship of the inverse multiplicative structure compensator. Figure 5.10(b) shows the input-output responses of the magnetostrictive actuator, and Figure 5.10(c) shows the inverse compensation result. The effectiveness of the inverse multiplicative structure compensator is further evaluated by comparing the time history of the measured displacement responses of the magnetostrictive actuator with and without the feedforward compensator. Figure 5.11 illustrates the comparison of the compensation error of the magnetostrictive actuator with and without the feedforward compensator.

The compensation error indicates a peak error of maximum 1.43% among the total range which significantly lower than that obtained without the compensator 10.51 %. The experimental results suggest that the proposed multiplicative inverse structure of the Preisach model could effectively compensate the hysteretic behavior in the magnetostrictive actuators.

(a)

(b)

103
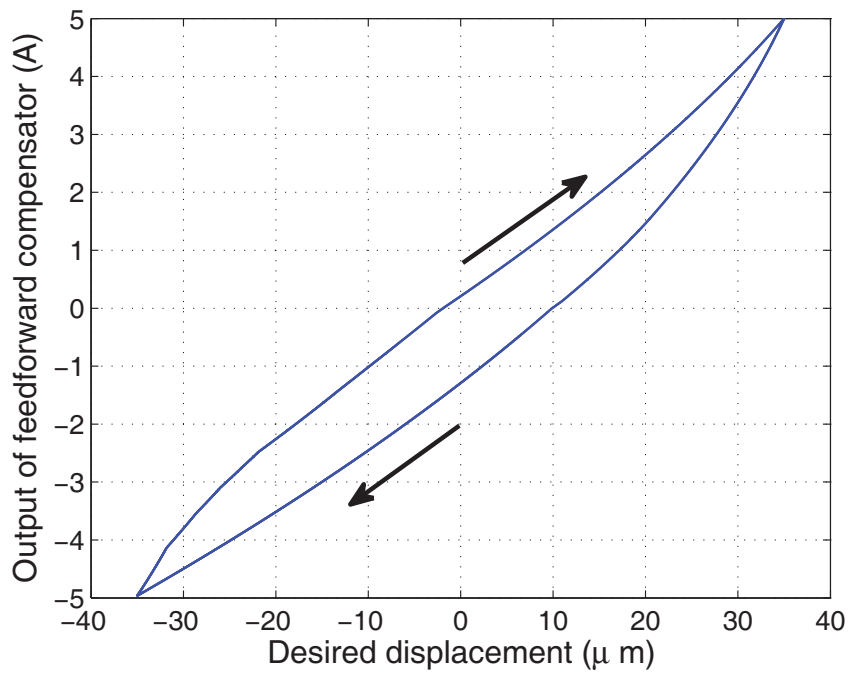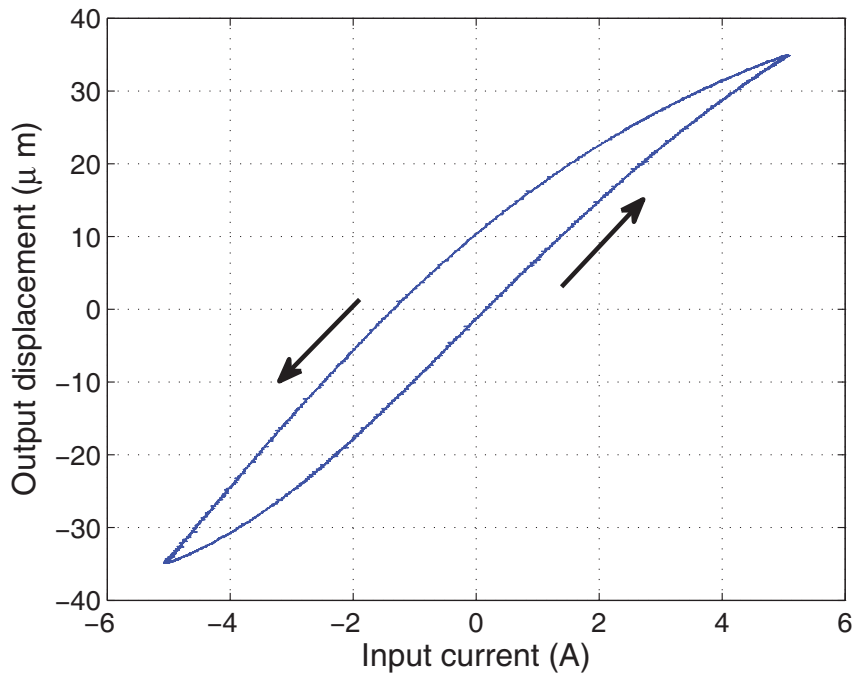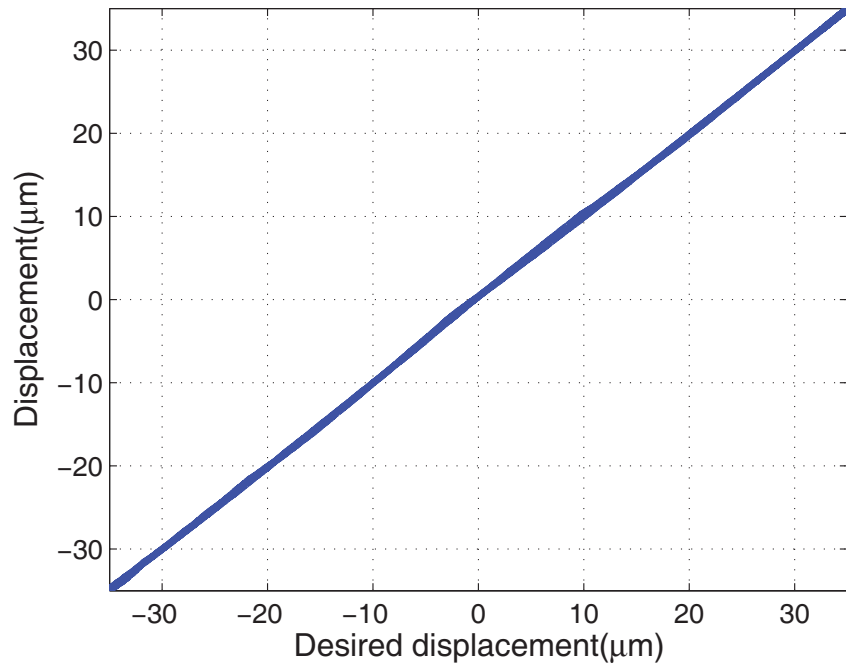
(c)

Figure 5.10: a) Input-output responses of the feedforward compensator b)Input-output responses of the magnetostrictive actuator c) Input-output responses of the magnetostrictive actuator with a compensator
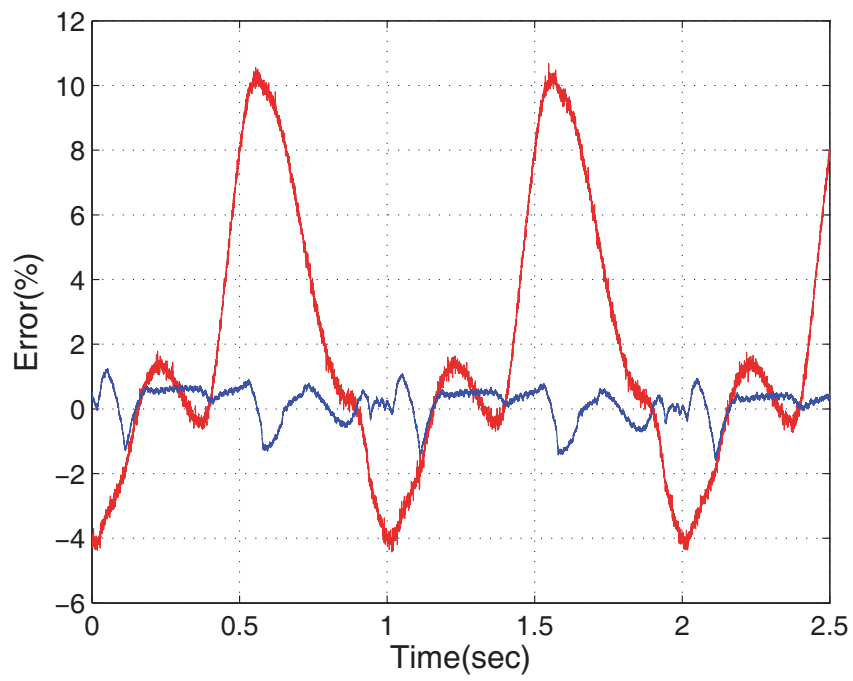
Figure 5.11: The compensation error (red line-without compensator; blue line-with compensator)

5.3 The Direct Inverse Compensation Approach for the ASPI Model

Since inverse multiplicative structure needs the exact knowledge of the hysteresis model, it is very restrict for a practical actuator. In the following development, we will focus on the direct inverse compensation approach, which allows the estimation of the unknown hysteresis. Thus, we use the ASPI model to describe the hysteresis effect in the cascading model structure in (4.3) of Chapter 4, the direct inverse compensation approach can therefore be utilized to compensate the hysteresis in the actuator. In Chapter 3, the ASPI model is developed as

$$u(t) = \Pi[v](t) = P[v](t) + H[v](t) \tag{5.39}$$

where $P[v](t)$ denotes the PI model, $H[v](t) = \Psi[v](t) + g(v)(t)$, $\Psi[v](t)$ is the shift model and $g(v)(t)$ is the auxiliary function.

The objective is that if we can find a Π^{-1} so that $\Pi[\Pi^{-1}[u]](t) = u(t)$, then such a Π^{-1} can be qualified as an inverse of the ASPI model.

Since $u(t)$ in (5.39) is expressed as $u(t) = \Pi[v](t) = P[v](t) + H[v](t)$. Then, $P[v](t)$ can be re-expressed as

$$P[v](t) = u(t) - H[v](t) \tag{5.40}$$

Taking the inverse of P in (5.40) on both sides, one has

$$v(t) = P^{-1}[P[v]](t) = P^{-1}[u - H[v]](t) \tag{5.41}$$

where $P^{-1}[\cdot]$ denotes the inverse model of the PI model, which has been reported in the previous section.

Thus, the inverse of the ASPI model Π^{-1} is obtained

$$\Pi^{-1}[u](t) = P^{-1}[u - H[v]](t) = v(t) \tag{5.42}$$

The merit of the above construction is the utilization of the analytic inverse result for the PI operator in [67]. Only an extra signal $H[v](t)$ is included to the input of P^{-1} for the inverse construction of $\Pi[v](t)$.

The experimental validation is conducted on the experimental platform reported in Chapter 1, Section 1.3.1. The applied mechanical load is 16 Kg. In Chapter 4, numerical expression of the ASPI model is defined as

$$
\begin{aligned}
u(t) &= P[v](t) + H[v](t) \\
&= P[v](t) + \Psi[v](t) + g(v)(t) \\
&= p_0 v(t) + \sum_{j=1}^{n} p_j F_{r_j}[v](t) + \sum_{j=1}^{m} q_j \Psi_{c_j}[v](t) + g(v)(t)
\end{aligned} \tag{5.43}
$$

with

$$
g(v)(t) = -a_3 v(t)^3 - a_2 v(t)^2 - a_1 v(t) - a_0 \tag{5.44}
$$

where the identified parameters p_j, q_j and a_j can be found in Table 4.1 in Chapter 4. According to (5.10), the thresholds and weights of $P^{-1}[\cdot](t)$ are calculated as: $\bar{r}_i = [0, 0.2701, 0.7935, 1.4452, 2.5415, 3.8207, 5.5078, 7.5565, 9.9223, 12.3732]$, $\bar{p}_0 = 1.1109$, $\bar{p}_i = [-0.5377, -0.1128, -0.1867, -0.0391, -0.0567, -0.0314, -0.0196, -0.0044, -0.0024]$. Therefore, the inverse multiplicative structure compensator is therefore implemented as

$$
v(t) = \Pi^{-1}[u](t) = P^{-1}[u - H[v]](t) \tag{5.45}
$$

Figure 5.12 shows the experimental compensation results. The desired input is $u_d = 15\sin(2\pi t)$, the input and output responses of the inverse compensator are shown in Figure 5.12(a). Figure 5.12(b) shows the input and output hysteresis loops. The linear input and output relationship of the combination of the inverse compensator and the actuator in Figure 5.12(c) indicates the proposed inverse compensator can effectively cancel the inherent hysteresis effects in the magnetostrictive actuator. In order to demonstrate the effectiveness of the proposed inverse compensator for overcoming the asymmetric hysteresis, the comparison of the inverse compensation by using the inverse ASPI model and the inverse PI model are conducted, see Figure 5.13(a). The large compensation error caused by the inverse PI

107
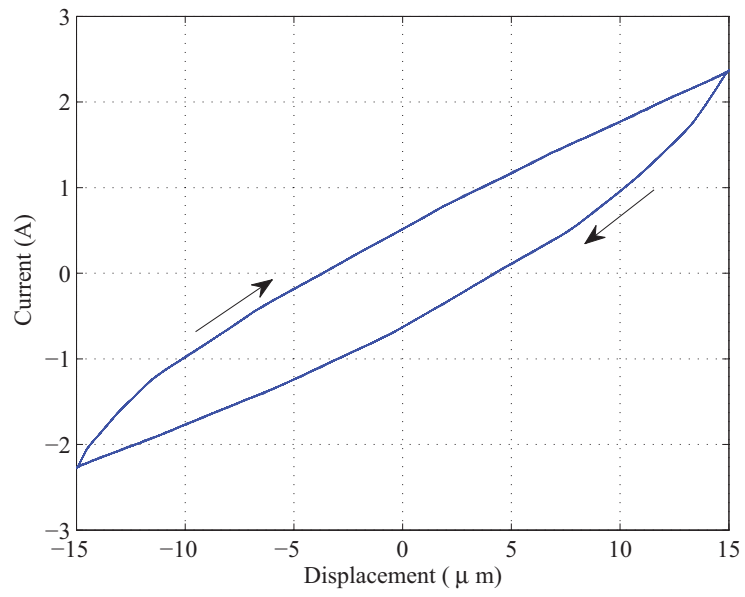
(a) The I/O of the inverse compensator
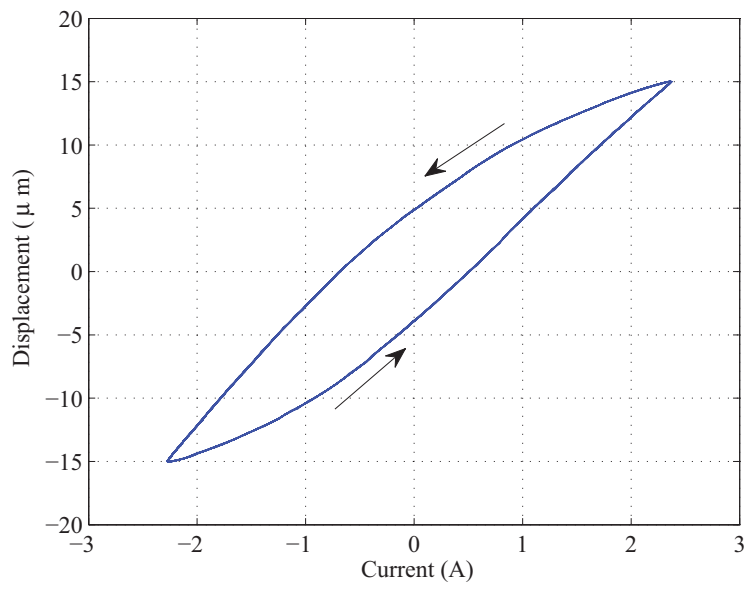
(b) The I/O of the the magnetostrictive actuator
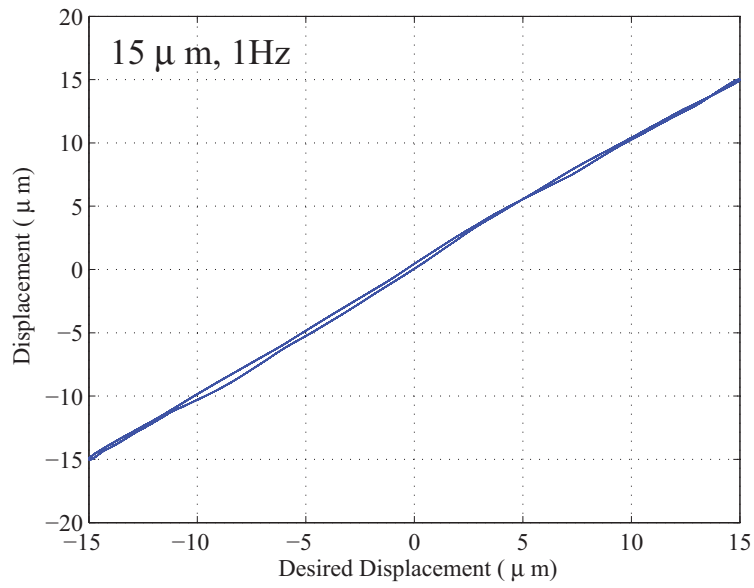
(c) The I/O of inverse compensation results

Figure 5.12: The experimental results of the inverse compensation for the magnetostrictive actuator
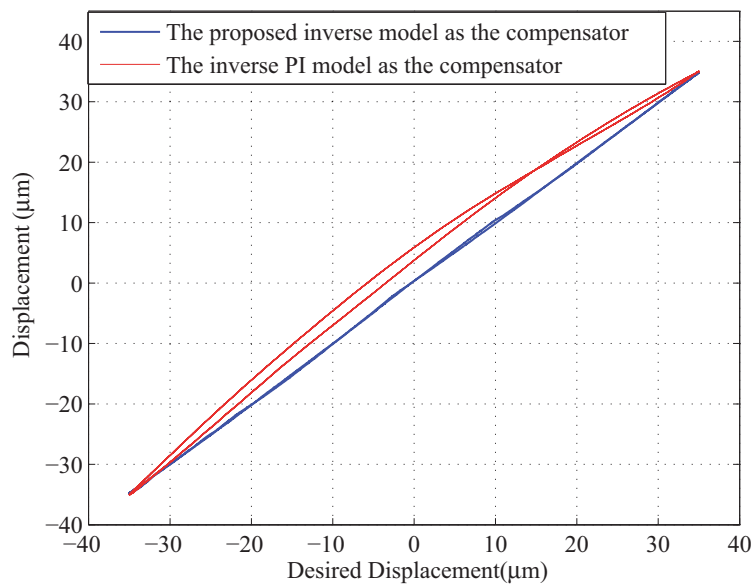
(a) The I/O of of inverse compensation results by using the proposed inverse compensator and the inverse PI model compensator
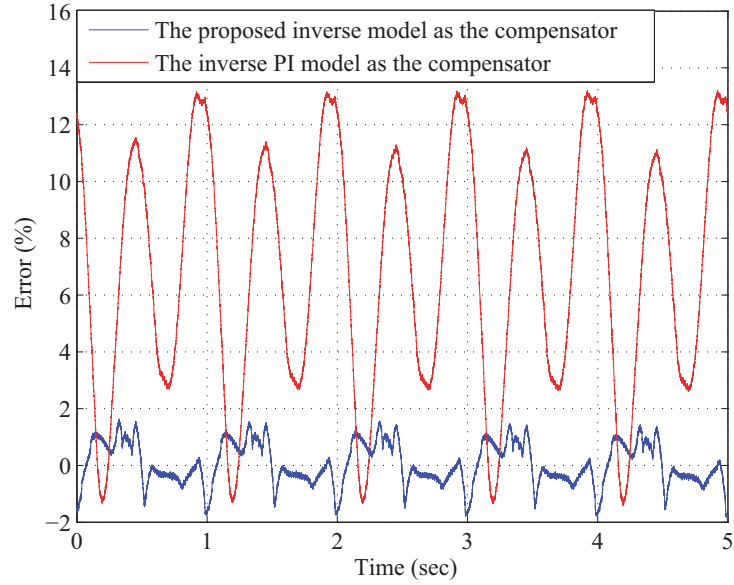
(b) The compensation error

Figure 5.13: The comparison of the inverse compensation results by using the inverse ASPI model and the inverse PI model as a compensator

model in Figure 5.13(b) indicates that the inverse PI model cannot effectively cancel the asymmetric hysteresis effect in the magnetostrictive actuator.

5.4   Concluding Remarks

In this chapter, two inverse compensation approaches: the direct inverse compensation approach and the inverse multiplicative structure have been reviewed. Firstly, we used the Preisach model to represent the hysteresis effect in the cascading model structure, and the inverse multiplicative structure compensator was then applied. However, inverse multiplicative structure needs the exact knowledge of the hysteresis model, which is very restrict for a practical actuator. Considering this point and specially focusing on the asymmetric hysteresis showing in the magnetostrictive actuator, the proposed ASPI model was therefore utilized to describe the asymmetric hysteresis effect in the cascading model structure and

the direct inverse compensation approach was applied to find the inverse of the ASPI model. Both inverse compensation approaches have been examined on the magnetostrictive-actuated platform.

Chapter 6

Inverse Adaptive Control of Magnetostrictive-actuated Dynamic System

When dynamic systems are actuated by smart material based actuators, the systems exhibit hysteresis nonlinearities and corresponding control is becoming a challenging task, especially with magnetostrictive actuators which are dominated by asymmetric hysteresis. Therefore, in this chapter, an inverse compensation based robust adaptive control is developed for the purpose of mitigating the hysteresis effect in the magnetostrictive-actuated dynamic system. Focusing on the asymmetric hysteresis phenomenon, the proposed asymmetric shifted Prandtl-Ishlinskii (ASPI) model and its inverse are utilized to describe and compensate the asymmetric hysteresis behaviors in the magnetostrictive actuator. To guarantee the global stability of the closed loop system and the transient performance of the tracking error, a prescribed adaptive control method will be applied. The effectiveness of the proposed control scheme is validated on the magnetostrictive-actuated experimental platform.

In Section 6.1, the available feedback control of dynamic system preceded by hysteresis nonlinearity is reviewed. The control problem statement is presented in Section 6.2. An

analytical error of the inverse compensation for the asymmetric shifted Prandtl-Ishlinskii (ASPI) model for the purpose of controller design is derived in Section 6.3. The prescribed adaptive control approaches and the experimental validation are reported in Section 6.4 and Section 6.5.

6.1 Review of Feedback Control of Dynamic System Preceded by Hysteresis Nonlinearity

Although the feedforward inverse compensation approaches are very effective to deal with the hysteresis effect due to its simplicity and easy implementation, they only show good performance when the actuators operate in low frequency and without external loads or disturbances occur in the actuated systems. In addition, there always exists a modeling error between the estimated model and the true hysteresis behaviors, therefore, the use of an estimated hysteresis model in deriving the model inverse would be expected to yield some degree of hysteresis compensation error. This error would cause the tracking error in the closed-loop control system. For the purpose of alleviating these drawbacks of open loop compensation, feedback control strategies are desired. In the literature, the feedback control schemes for dealing with the hysteresis include the feedback control without hysteresis inverse compensation and feedback control with hysteresis inverse compensation. The following sections will give the detailed introduction.

6.1.1 Feedback Control without Inverse Construction

Figure 6.1 illustrates the structure of the control strategy without inverse compensator. In this type of control strategy, the hysteresis nonlinearities are normally decomposed as a linear term and an uncertainty term. Due to this division, many available control strategies can be directly applied. In [78], a backlash-like hysteresis model is proposed to describe the hysteresis effect and the solution of the backlash-like model is derived, in which the solution
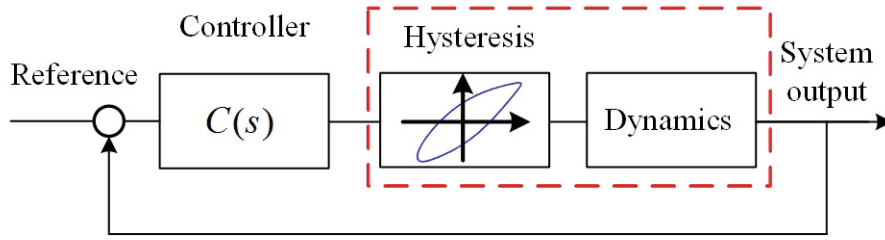
Figure 6.1: Feedback control without inverse construction

can be divided into a linear term and a bounded term. By using the properties of the solution
of the backlash-like model, a robust adaptive control scheme is adopted without constructing
the inverse of the hysteresis model. The stability of the dynamic nonlinear system preceded
by the unknown backlash-like hysteresis is guaranteed. Likewise, in [56], the PI model is
fused with a robust control approach without constructing the inverse of the PI model. The
challenges shown in [56] are that the separated uncertain term of the PI model is not bounded.
However, due to the time-invariability of the density function of the PI model, the uncertain
term can be treated as a parameter and estimated in the adaptive law. Following the work
in [56] and [78], numerous control approaches with the same treatment to the hysteresis are
developed: adaptive backstepping control approaches [79], decentralized adaptive output
feedback control [80], sliding mode control [81] [82] [83], adaptive neural control [84] [85],
adaptive fuzzy output feedback control [86] [87], etc. The advantages of these feedback
control approaches are that they avoid the calculation of the inverse of the hysteresis model.
However, these control methods may result in large control input magnitudes [3] [88], which
is not desirable in real control applications.

6.1.2   Inverse-based Feedback Control

The inverse-based feedback control means the inverse of the hysteresis is constructed first as
a feedforward compensator, then the feedback control approach is applied. The purpose for
developing the inverse of the hysteresis model first is to overcome the influence of the hystere-
sis nonlinearity since the existence of the hysteresis always brings inaccuracy and oscillations

114
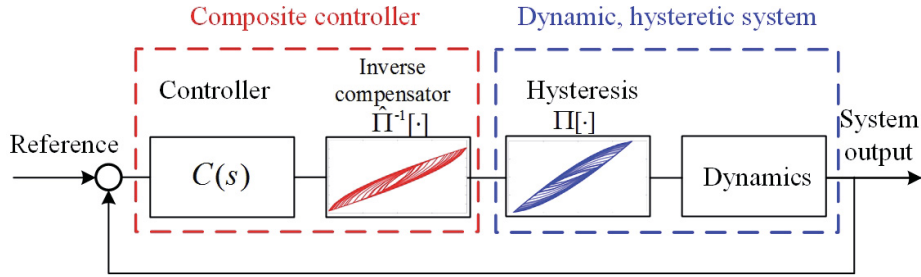
Figure 6.2: Inverse-based feedback control strategy [2] [3]

to the closed system. Figure 6.2 illustrates the general structure of the inverse-based feedback control strategy. As in the real control system, there always exists an modeling error between the estimated model $\hat{\Pi}[\cdot]$ and the true hysteresis $\Pi[\cdot]$. The constructed inverse compensator $\hat{\Pi}^{-1}[\cdot]$ based on the estimated model $\hat{\Pi}[\cdot]$ can not completely cancel the hysteresis nonlinearity $\Pi[\cdot]$ in the system. The incomplete compensation would yield some degrees of inverse compensation error which generally can not be ignored in controller designs. Therefore, the challenge that lies in the inverse-based feedback control strategy is how to handle the inverse compensation error in the controller design.

In [75], a Preisach model is utilized to describe the hysteresis effect of the magnetostrictive actuator, and a fast inverse algorithm is developed for compensating the hysteresis effect, then a PI controller is applied to reduce the inverse compensation error or uncertainty caused by the plants. However, the inverse compensation error is not explicitly expressed and no stability analysis is given in this paper. In [13], a Preisach model is utilized and the numerical inverse compensation approach is adopted. Although the inverse compensation error is provided, the inverse compensation error is in a numerical expression, in which the convergence of the numerical error can not be strictly proved. In addition, the numerical inverse error can not be directly utilized in the adaptive controller design. In [89] and [90], a backlash hysteresis is studied and the analytical inverse of the backlash model is derived. Therefore, the analytical inverse compensation error for backlash hysteresis can be obtained, and an adaptive control scheme is developed based on the analytical compensation error. The global stability of the entire system is also achieved. Along this line, in [91], a PI model

115

is adopted to describe the hysteresis effect and the composition theory developed by Pavel Krejci [44] is applied for deriving the analytical formulation of the compensation error. An adaptive control approach is developed to achieve high tracking performance in the closed-loop control system using the obtained compensation error. Likewise, in [71], a Bouc-Wen model is adopted and a multiplicative inverse structure is utilized to construct the inverse of the Bouc-Wen model. The analytical inverse compensation error is analytical derived using the lemma proposed in [92], finally an adaptive output feedback control strategy is developed based on the inverse compensation error. However, the developed analytical inverse error mentioned above are only for the symmetric hysteresis model (PI model and Bouc-Wen model), it has not yet being exploited for asymmetric hysteresis cases in the literature. While in the magnetostrictive-actuated dynamic system, the hysteresis effect shows asymmetric hysteresis characteristics. Therefore, it is necessary to find the analytical expression of the inverse compensation error for the asymmetric hysteresis model, and develop a feedback controller based on this inverse compensation error.

6.2 Problem Statement

In Chapter 2, the dynamic model for describing the magnetostrictive-actuated dynamic system is developed, where the dynamic part is described in the formation of the transfer function. In order to facilitate the controller design, the transfer function is expressed in the general formation as

$$x^{(n)}(t) + \sum_{i=1}^{k} a_i Y_i(x(t), \dot{x}(t), ..., x^{(n-1)}(t)) = bu(t) \tag{6.1}$$

with the hysteresis nonlinearity output $u(t)$

$$u(t) = \Pi[v](t) \tag{6.2}$$

where $v(t)$ denotes the input, Y_i are known continuous, linear or nonlinear functions. Parameters a_i and control gain b are unknown constants, $\Pi[v](t)$ can be expressed by the proposed

ASPI model in chapter 3 as

$$
\begin{aligned}
u(t) &= P[v](t) + \Psi[v](t) + g(v)(t) \\
&= p_0 v(t) + \sum_{j=1}^{n} p_j F_{r_j}[v](t) + \sum_{j=1}^{m} q_j \Psi_{c_j}[v](t) + g(v)(t) \quad (6.3)
\end{aligned}
$$

with

$$
g(v)(t) = -a_3 v(t)^3 - a_2 v(t)^2 - a_1 v(t) - a_0 \quad (6.4)
$$

where p_j denotes the weight of the play operator; $F_{r_j}[v](t)$ is the play operator at the threshold of r_j; n is the number of the play operator used for identification. q_j denotes the weight of the elementary shift operator; $\Psi_{c_j}[v](t)$ is the elementary shift operator at the slope of c_j; m is the number of the elementary shift operator used for identification. $g(v)(t)$ is the selected auxiliary function.

The control objective is to design a control signal $v(t)$ for system (6.1), such that:

P1: The system state $x(t)$ tracks a desired $x_d(t)$ and all signals in the closed-loop are bounded;

P2: Both transient and steady-state performance of tracking error $e_1(t) = x(t) - x_d(t)$ should be within the prescribed area.

Throughout the chapter the following standard assumptions are required:

Assumption 1: The sign of uncertain parameter b is known. Without losing generality, it is selected as $b > 0$ in this paper.

Assumption 2: The desired trajectory $x_d(t)$ and its (n-1)th-order derivatives are continuous. Furthermore, $[x_d, \dot{x}_d, ..., x_d^n]^T \in \Omega_d \subset R^{n+1}$ with Ω_d being a compact set.

Comparing with general nonlinear control for the system (6.1) only, the control signal $u(t)$ becomes the output of the hysteresis operator $u(t) = \Pi[v](t)$, where the actual control signal is $v(t)$. As it is well known, the hysteresis nonlinearity will deteriorate the system performance and cause inaccuracy or oscillations. Therefore, it imposes great challenges to handle this cascaded term with a basic requirement that $u(t)$ is not available/measurable. The common approach for remedying the effect is to construct a hysteresis inverse as a feedforward compensator. Then the control law can be designed with available control

methods. The inverse compensator using the the direct inverse compensation approach is constructed in Chapter 5 as

$$v(t) = \Pi^{-1}[u](t) = P^{-1}[u - H[v]](t) \tag{6.5}$$

As a matter of fact, the inverse compensator was constructed using estimated ASPI model $\hat{\Pi}[v]$ (there always exists a modeling error between the estimated model and the true hysteresis). Therefore, the inverse compensation error is unavoidable and generally can not be ignored. Therefore, we use $\hat{\Pi}[v]$ to represent the inverse compensator and (6.5) is re-expressed as

$$v(t) = \hat{\Pi}^{-1}[u](t) = \hat{P}^{-1}[u - \hat{H}[v]](t) \tag{6.6}$$

Figure 6.3 shows the complete control scheme in which we can see that if there is no compensation error, the hysteresis $\Pi[v]$ will be completely canceled, which means $u_d(t)$ should equal to $u(t)$. However, due to the existence of the compensation error, $u_d(t)$ is no longer equal to $u(t)$, and hence we define this compensation error as

$$e(t) = u_d(t) - u(t) \tag{6.7}$$

In the following section, a detailed procedure on deriving the expression of the compensation error $e(t)$ is provided.
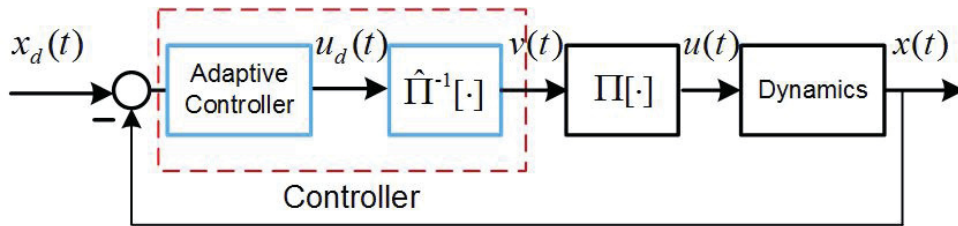
Figure 6.3: The control scheme

6.3 Analytical Error of the Inverse Compensation for the Asymmetric Shifted Prandtl-Ishlinskii (ASPI) Model

As reported in the previous section, use of an estimated hysteresis model in deriving the inverse model would yield some degree of hysteresis compensation error. This error will cause tracking error in the closed-loop control system. To accommodate such a compensation error, the analytical expression of the inverse compensation error should be derived first. In [91], an analytic inverse compensation error of the PI model is developed. However, such an approach is only limited to the symmetric hysteresis case. Focusing on the asymmetric hysteresis, in the following development we will derive the analytic inverse compensation error for the asymmetric shifted Prandtl-Ishlinskii (ASPI) model.

6.3.1 Overview of Composition Theorem Applied to the PI Model

In order to use the composition theorem to find the compensation error of the PI model, we first need to rewrite the PI model as [30]

$$P[u](t) = \varphi'(0)u(t) + \int_0^\Lambda \varphi''(r)F_r[u](t)dr \tag{6.8}$$

where $\varphi(r)$ denotes the initial loading curve which uniquely determines the shape of hysteresis loop described by the PI model and is defined as

$$\varphi(r) = p_0 r + \int_0^r p(\kappa)(r - \kappa)d\kappa \tag{6.9}$$

Thus, $\varphi'(0) = p_0$ is a positive constant, $\varphi''(r) = p(r)$ denotes the density function. According to the composition theorem presented in [44], the composition between two PI models $P_\gamma[\cdot](t)$ and $P_\delta[\cdot](t)$ is expressed as

$$
\begin{aligned}
P_\phi[u](t) &= P_\gamma \circ P_\delta[u](t) \\
&= \phi'(0)u(t) + \int_0^\Lambda \phi''(r)F_r[u](t)dr
\end{aligned}
\tag{6.10}
$$

119

where $\phi(r) = \gamma \circ \delta(r)$, $\gamma(r)$ and $\delta(r)$ denote the initial loading curves of the $P_\gamma[\cdot](t)$ and $P_\delta[\cdot](t)$, separately.

Since in practice, the exact density function $p(r)$ in the PI model may not be available. It needs to be estimated based on the measured data. In this case, the inverse model should be constructed based on the estimated density function, which is denoted as $\hat{p}(r)$. Let $\hat{P}[\cdot](t)$ denotes the estimation of the actual hysteretic behavior $P[\cdot](t)$ as

$$\hat{P}[u](t) = \hat{\varphi}'(0)u(t) + \int_0^\Lambda \hat{\varphi}''(r)F_r[u](t)dr \tag{6.11}$$

where $\hat{\varphi}(r)$ is defined as

$$\hat{\varphi}(r) = \hat{p}_0 r + \int_0^r \hat{p}(\kappa)(r - \kappa)d\kappa \tag{6.12}$$

$\hat{P}^{-1}[\cdot](t)$ denotes the inverse of $\hat{P}[\cdot](t)$ as

$$\hat{P}[u]^{-1}(t) = \hat{\bar{p}}_0 u(t) + \int_0^{\bar{\Lambda}} \hat{\bar{p}}(r)F_r[u](t)dr \tag{6.13}$$

where,

$$\hat{\bar{p}}_0 = \frac{1}{\hat{p}_0} \tag{6.14}$$

$$\hat{\bar{p}}(r) = (\hat{\varphi}^{-1})''(r) \tag{6.15}$$

$$\hat{\varphi}^{-1}(r) = \hat{\bar{p}}_0 r + \int_0^r \hat{\bar{p}}(\xi)(r - \xi)d\xi \tag{6.16}$$

Thus, by applying the composition theorem on the $P[\cdot](t)$ and $\hat{P}^{-1}[\cdot](t)$, yields

$$\begin{aligned} u(t) &= P \circ \hat{P}^{-1}[u_d](t) \\ &= \phi'(0)u_d(t) + \int_0^\Lambda \phi''(r)F_r[u_d](t)dr \end{aligned} \tag{6.17}$$

where u_d is the desired input signal. The compensation error $e_{pi}(t)$ can be analytically written as

$$\begin{aligned} e_{pi}(t) &= u_d(t) - u(t) \\ &= (1 - \phi'(0))u_d(t) - \int_0^\Lambda \phi''(r)F_r[u_d](t)dr \end{aligned} \tag{6.18}$$

6.3.2 Analytical Error of the Inverse Compensation for the Asymmetric Shifted Prandtl-Ishlinskii (ASPI) Model

Due to the presence of the estimation error, we use $\hat{\Pi}[u](t)$ to estimate the true hysteresis phenomenon $\Pi[u](t)$, which is expressed as

$$\hat{\Pi}[v](t) \quad = \quad \hat{P}[v](t) + \hat{H}[v](t) \tag{6.19}$$

where $\hat{H}[v] = \hat{\Psi}[v](t) + \hat{g}(v)(t)$.

The output of the composition between the inverse compensation $\hat{\Pi}^{-1}[u](t)$ and true hysteretic behavior $\Pi[u](t)$ is expressed as

$$u(t) = \Pi \circ \hat{\Pi}^{-1}[u_d](t) = P \circ \hat{P}^{-1}[u_d - \hat{H}[v]](t) + H[v](t) \tag{6.20}$$

According to the combined results in (6.10), (6.20) becomes

$$u(t) \quad = \quad \phi'(0)(u_d - \hat{H}[v](t)) + \int_0^\Lambda \phi''(r)F_r[u_d - \hat{H}[v]](t)dr + H[v](t) \tag{6.21}$$

Because of $E_r[v](t) + F_r[v](t) = v(t)$, where $E_r[v](t)$ denotes the stop operator as:

$$E_r[v](0) \quad = \quad e_r(v(0) - w_{-1}) \tag{6.22}$$

$$E_r[v](t) \quad = \quad e_r(v(t) - v(t_i) + E_r[v](t_i)) \tag{6.23}$$

for $t_i < t \le t_{i+1}$ and $0 \le i \le N - 1$, with

$$e_r(v) = min(r, max(-r, v)) \tag{6.24}$$

w_{-1} is the initial value. Then, we have

$$
\begin{aligned}
u(t) \quad &= \quad \phi'(0)(u_d - \hat{H}[v](t)) + \int_0^\Lambda \phi''(r)(u_d - \hat{H}[v](t))dr \\
&\quad - \int_0^\Lambda \phi''(r)E_r[u_d - \hat{H}[v]](t)dr + H[v](t) \\
&= \quad \phi'(0)(u_d - \hat{H}[v](t)) + (\phi'(\Lambda) - \phi'(0))(u_d - \hat{H}[v](t)) \\
&\quad - \int_0^\Lambda \phi''(r)E_r[u_d - \hat{H}[v]](t)dr + H[v](t)
\end{aligned}
$$

$$= \phi'(\Lambda)u_d - d_b(t) \tag{6.25}$$

where $d_b(t) = \phi'(\Lambda)\hat{H}[v](t) - H[v](t) + \int_0^\Lambda \phi''(r)E_r[u_d - \hat{H}[v]](t)dr$. The estimation (inverse compensation) error $e(t)$ of the ASPI model is therefore expressed as

$$e(t) = u_d(t) - u(t) = (1 - \phi'(\Lambda))u_d(t) + d_b(t) \tag{6.26}$$

It should be noted that if the estimated hysteresis operator $\hat{\Pi}[\cdot](t)$ is equal to the true hysteresis $\Pi[\cdot](t)$, it yields $\phi(r) = r$, $\phi'(r) = 1$, $\phi''(r) = 0$, then in (6.26) $\phi'(\Lambda) = 1$, $d_b(t) = 0$, leading to $e(t) = 0$. Before showing the way to utilize the estimation error in the next section, the following lemma is exploited to facilitate the robust controller design.

Lemma: The term $d_b(t)$ in (6.26) is bounded, i.e. $|d_b(t)| \leq D_1$ where D_1 is a bounded constant, for any time $t \geq 0$.

Proof: Based on the definition of the stop operator [30], one has

$$|E_r[\cdot](t)dr| \leq r \leq \Lambda \tag{6.27}$$

From (6.27), we have

$$\begin{aligned}
\int_0^\Lambda \phi''(r)E_r[u_d - \hat{H}[v]](t)dr &\leq \Lambda \int_0^\Lambda \phi''(r)dr \\
&\leq \Lambda(\phi'(\Lambda) - \phi'(0)) \tag{6.28}
\end{aligned}$$

Thus,

$$|\int_0^\Lambda \phi''(r)E_r[u_d - \hat{H}[v]](t)dr| \leq |\Lambda(\phi'(\Lambda) - \phi'(0))| \tag{6.29}$$

Here, we slightly modify the $H[v]$ term in the ASPI model as

$$\begin{aligned}
\hat{H}[v] &= R_1 sat(\frac{\hat{H}_1[v]}{R_1}) \\
\hat{H}_1[v] &= \hat{\Psi}[v](t) + \hat{g}(v)(t) \tag{6.30}
\end{aligned}$$

Since $H[v]$ is a designed term, we just put a bound to the function. Moreover, if the output of $\hat{H}_1[v]$ is less than the bound R_1, $\hat{H}[v] = \hat{H}_1[v]$, and normally R_1 can be set as a sufficiently large value. According to the definition in (6.30), it yields

$$-R_1 \leq H[v] \leq R_1 \tag{6.31}$$

122

$$-\phi'(\Lambda)R_1 \le \phi'(\Lambda)\hat{H}[v] \le \phi'(\Lambda)R_1 \tag{6.32}$$

From (6.31) and (6.32), we have

$$|\phi'(\Lambda)\hat{H}[v] - H[v]| \le |(\phi'(\Lambda) + 1)R_1| \tag{6.33}$$

Therefore, based on (6.29) and (6.33),

$$|d_b(t)| \le |(\phi'(\Lambda) + 1)R_1| + |\Lambda(\phi'(\Lambda) - \phi'(0))| = D_1 \tag{6.34}$$

6.4 Prescribed Adaptive Control

Different from the standard procedure of backstepping control presented in the literature [56] [79] [93], the transient and steady-state performance of tracking error are incorporated in the design procedure of prescribed adaptive control. This control approach is originally developed in [94], which is the first time that provides a systematic procedure to accurately compute the required bounds, thus making tracking error converge to a predefined arbitrarily small residual set, with convergence rate no less than a pre-specified value, exhibiting a maximum overshoot less than a sufficiently small preassigned constant [94] [95].

To show the feasibility for the controller design with the inverse compensation, in this section, as a demonstration, a prescribed adaptive control approach is adopted to ensure the transient and steady-state performance of the system (6.1). In the literature, most of controller design techniques can theoretically guarantee the boundedness of the closed-loop system and the tracking error can converge to a residual set around zero. However, the transient performance of the systems (e.g., overshoot, undershoot, and convergence rate) has not been systematically studied [96]. In [94] [95], Bechlioulis and Rovithakis proposed a novel control approach by introducing a prescribed performance function, which will lead to global stability and yield the tracking error converge to a predefined arbitrarily small residual set, with convergence rate no less than a pre-specified value and the maximum overshoot less than a sufficiently small preassigned constant.

6.4.1 Prescribed Performance Function and Error Transformation

The performance function is introduced in [94] for the purpose of depicting a convergent zone in which the trajectory of tracking error which starts from a point in the zone remains for all future time, see Figure 6.4. The performance function is a decreasing smooth function, which is defined as $\rho : R^+ \to R^+$ with $\lim_{t \to \infty} \rho(t) = \rho_\infty > 0$.

It is noted that the control objective P2 can be guaranteed by satisfying

$$\underline{M}\rho(t) < e_1(t) < \overline{M}\rho(t) \tag{6.35}$$

for all $t \geq 0$, where $\underline{M} < 0, \overline{M} > 0$ are selected parameters. $\overline{M}\rho(0)$ and $\underline{M}\rho(0)$ represent the upper bound of the maximum overshoot and the lower bound of the undershoot. The constant ρ_∞ denotes the maximum tracking error at the steady state. Thus, the performance function and the parameters $\overline{M}, \underline{M}$ prescribe the convergent zone for the transient and steady state performance of the tracking error.
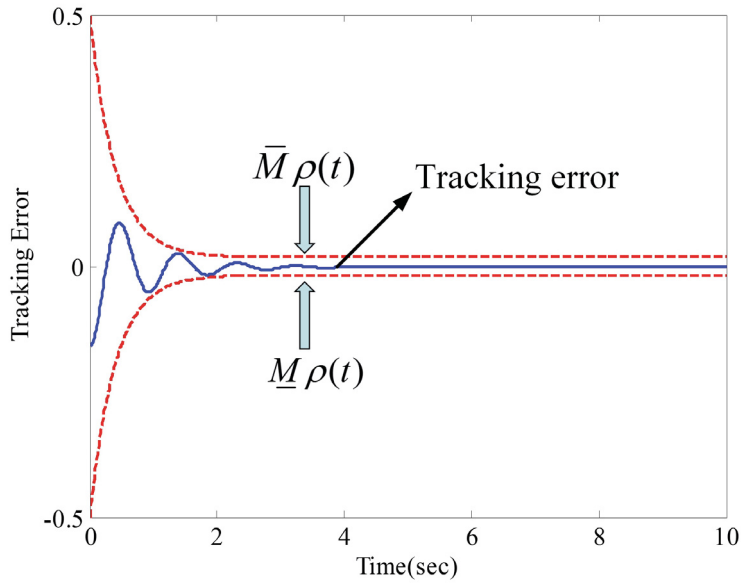
Figure 6.4: The prescribed performance of tracking error

In order to meet the requirements P1 and P2 together with condition (6.35), an error transformation is developed [94] by transforming the original nonlinear system (6.1) into an

equivalent unconstraint one. Define $S(\cdot)$ a smooth and strictly increasing function and z_1 a transformed error as

$$e_1(t) = \rho(t)S(z_1) \tag{6.36}$$

$S(\cdot)$ conforms the following conditions:

1) $\underline{M} < S(z_1) < \overline{M}$

2) $\lim_{z_1 \to +\infty} S(z_1) = \overline{M}$, $\lim_{z_1 \to -\infty} S(z_1) = \underline{M}$

Since $S(\cdot)$ is strictly increasing as well as $\rho(t) > 0$, the inverse transformation can be written as:

$$z_1 = S^{-1}\left(\frac{e_1(t)}{\rho(t)}\right) \tag{6.37}$$

Assume $z_1(t)$ remains bounded $z_1 \in L_\infty$, $\forall t \geq 0$, then $\underline{M} < S(z_1) < \overline{M}$ holds, and hence the condition (6.35) can be guaranteed. A candidate function $S(\cdot)$ is selected as

$$S(z_1) = \frac{\overline{M}e^{z_1} + \underline{M}e^{-z_1}}{e^{z_1} + e^{-z_1}} \tag{6.38}$$

Conduct inverse transformation on (6.38), yielding

$$z_1 = S^{-1}\left(\frac{e_1(t)}{\rho(t)}\right) = \frac{1}{2}ln\frac{e_1(t)/\rho(t) - \underline{M}}{\overline{M} - e_1(t)/\rho(t)} \tag{6.39}$$

Then the derivative of z_1 with respect to time can be written as

$$
\begin{aligned}
\dot{z}_1 &= \frac{\partial S^{-1}}{\partial \frac{e_1(t)}{\rho(t)}}\left(\frac{e_1(t)}{\rho(t)}\right) \\
&= \frac{1}{2}\left[\frac{1}{e_1(t)/\rho(t) - \underline{M}} - \frac{1}{e_1(t)/\rho(t) - \overline{M}}\right]\left(\frac{\dot{e}_1(t)}{\rho(t)} - \frac{e_1(t)\dot{\rho}(t)}{\rho^2(t)}\right) \\
&= r_1(\dot{x}_1 - \dot{x}_d - e_1(t)\dot{\rho}(t)/\rho(t))
\end{aligned} \tag{6.40}
$$

where $r_1 = \frac{1}{2\rho(t)}\left[\frac{1}{e_1(t)/\rho(t) - \underline{M}} - \frac{1}{e_1(t)/\rho(t) - \overline{M}}\right]$. It is noted that both $e_1(t)$ and $\rho(t)$ in (6.40) are available and they can be involved in controller design.

6.4.2   Prescribed Adaptive Controller Design

The system (6.1) can be re-written as

$$\dot{x}_1 = x_2$$

$$\dot{x}_2 \;=\; x_3$$

$$\vdots \tag{6.41}$$

$$\dot{x}_{n-1} \;=\; x_n$$

$$\dot{x}_n \;=\; \boldsymbol{a}^T\boldsymbol{Y} + bu(t)$$

where $\boldsymbol{a} = [-a_1, -a_2, \cdots, -a_k]^T$ and $\boldsymbol{Y} = [Y_1, Y_2, \cdots, Y_k]^T$. The parameters $\boldsymbol{a}$, b are unknown. $u(t)$ denotes the system input with the inverse compensation as

$$u(t) = \phi'(\Lambda)u_d - d_b(t) \tag{6.42}$$

Considering the time derivative of transformed error (6.40) and nonlinear system (6.41), the transformed nonlinear system dynamics are given by:

$$\dot{z}_1 \;=\; r_1(x_2 - \dot{x}_d - e_1(t)\dot{\rho}(t)/\rho(t))$$

$$\dot{x}_2 \;=\; x_3$$

$$\vdots$$

$$\dot{x}_{n-1} \;=\; x_n$$

$$\dot{x}_n \;=\; \boldsymbol{a}^T\boldsymbol{Y} + b_p u_d(t) - d(t) \tag{6.43}$$

where $b_p = b\phi'(\Lambda)$, $d(t) = bd_b(t)$. Thus, the entire transformed dynamic system can be further written as:

$$\dot{z}_1 \;=\; r(x_2 - \dot{x}_d - e_1(t)\dot{\rho}(t)/\rho(t))$$

$$\dot{z}_2 \;=\; x_3 - \ddot{x}_d - \dot{\alpha}_1$$

$$\vdots$$

$$\dot{z}_{n-1} \;=\; x_n - x_d^{n-1} - \dot{\alpha}_{n-2}$$

$$\dot{z}_n \;=\; \mathbf{a}^T\boldsymbol{Y} + b_p u_d(t) - d(t) - x_d^n - \dot{\alpha}_{n-1} \tag{6.44}$$

The controller design is achieved by using the recursive back-stepping technique and is summarized as follows. The control law is developed as

$$u_d(t) \;=\; \hat{\zeta}u_{d1}(t) \tag{6.45}$$

with

$$u_{d1}(t) = -k_n z_n - z_{n-1} + \dot{\alpha}_{n-1} + x_d^{(n)} - \hat{\boldsymbol{a}}^T \boldsymbol{Y} + sgn(z_n)\hat{D} \tag{6.46}$$

where,

$$z_1 = \frac{1}{2}ln\frac{e_1(t)/\rho(t) - \underline{M}}{\overline{M} - e_1(t)/\rho(t)} \tag{6.47}$$

$$z_i = x_i - x_d^{(i-1)} - \alpha_{(i-1)}, i = 2, 3, ..., n \tag{6.48}$$

$$\alpha_1 = -k_1 z_1/r_1 + e_1(t)\dot{\rho}(t)/\rho(t) \tag{6.49}$$

$$\alpha_2 = -k_2 z_2 + \dot{\alpha}_1 - r_1 z_1 \tag{6.50}$$

$$\alpha_i = -k_i z_i + \dot{\alpha}_{i-1} - z_{i-1} \tag{6.51}$$

where k_i are positive designed parameters. The parameters $\hat{\zeta}$, $\hat{D}$ and the vector $\hat{\boldsymbol{a}}$ are updated by the following adaptation laws:

$$\dot{\hat{\zeta}} = -\eta_\zeta u_{d1}(t)z_n \tag{6.52}$$

$$\dot{\hat{\boldsymbol{a}}} = \boldsymbol{\Gamma_a} \boldsymbol{Y} z_n \tag{6.53}$$

$$\dot{\hat{D}} = -\eta_D |z_n| \tag{6.54}$$

where $D = bD_1$ and D_1 is the bound defined in the Lemma in Section 6.3.2. The stability of the closed-loop system is established in the following theorem.

Theorem 2: For the transformed nonlinear system (6.1) preceded by ASPI model in (6.42), the prescribed adaptive controller presented by (6.45)-(6.54) guarantees that

(i) All signals in the closed-loop system remain bounded;

(ii) The tracking control with prescribed performance condition (6.35) is preserved.

Proof: From (6.40), and (6.47)-(6.51), and with $b_p u_d(t) = b_p\hat{\zeta} u_{d1} = u_{d1} - b_p\tilde{\zeta} u_{d1}$, we have

$$z_1\dot{z}_1 = rz_1 z_2 - k_1 z_1^2 \tag{6.55}$$

$$z_2\dot{z}_2 = z_2 z_3 - k_2 z_2^2 - rz_1 z_2 \tag{6.56}$$

$$z_i\dot{z}_i = z_i z_{i+1} - k_i z_i^2 - z_{i-1} z_i \tag{6.57}$$

$$z_n\dot{z}_n = z_n(-k_n z_n - z_{n-1} + \tilde{\boldsymbol{a}}^T \boldsymbol{Y} + sgn(z_n)\hat{D}$$
$$-d(t) - b_p\tilde{\zeta} u_{d1}) \tag{6.58}$$

127

where $\tilde{\zeta} = \zeta - \hat{\zeta}$, $\tilde{\mathbf{a}} = \mathbf{a} - \hat{\mathbf{a}}$. Let $\tilde{D} = D - \hat{D}$. To establish the global boundedness, the following Lyapunov function candidate is adopted

$$V(t) = \sum_{i=1}^{n} \frac{1}{2} z_i^2 + \frac{1}{2} \tilde{\boldsymbol{a}}^T \boldsymbol{\Gamma}_{\boldsymbol{a}}^{-1} \tilde{\boldsymbol{a}} + \frac{b_p}{2\eta_\zeta} \tilde{\zeta}^2 + \frac{1}{2\eta_D} \tilde{D}^2 \tag{6.59}$$

The derivative of $V(t)$ with regard to the time is

$$
\begin{aligned}
\dot{V}(t) &= -\sum_{i=1}^{n} k_i z_i^2 + \tilde{\boldsymbol{a}}^T \boldsymbol{Y} z_n - b_p \tilde{\zeta} u_{d1} z_n + sgn(z_n) \hat{D} z_n \\
&\quad -d(t) z_n + \tilde{\boldsymbol{a}}^T \boldsymbol{\Gamma}_{\boldsymbol{a}}^{-1} \dot{\tilde{\boldsymbol{a}}} + \frac{b_p}{\eta_\zeta} \dot{\tilde{\zeta}} \tilde{\zeta} + \frac{1}{\eta_D} \dot{\tilde{D}} \tilde{D} \\
&\leq -\sum_{i=1}^{n} k_i z_i^2 + \tilde{\boldsymbol{a}}^T (\boldsymbol{Y} z_n + \boldsymbol{\Gamma}_{\boldsymbol{a}}^{-1} \dot{\tilde{\boldsymbol{a}}}) - b_p \tilde{\zeta} (u_{d1} z_n \\
&\quad -\frac{1}{\eta_\zeta} \dot{\tilde{\zeta}}) - \tilde{D} (|z_n| - \frac{1}{\eta_D} \dot{\tilde{D}}) \\
&= -\sum_{i=1}^{n} k_i z_i^2 \tag{6.60}
\end{aligned}
$$

Equations (6.59) and (6.60) show that $V(t)$ is nonincreasing. Therefore, $z_i (i = 1, ..., n)$, $\hat{\zeta}$, $\hat{\boldsymbol{a}}$, and $\hat{D}$ are bounded. By utilizing the Lasalle-Yoshizawa theorem in [97] to (6.60), it further follows that $z_i \to 0 (i = 1 = 1, ..., n)$ as $t \to \infty$, which concludes the tracking error is bounded within the prescribed zone.

6.5 Experimental Results

In this section, the prescribed adaptive controller designed above will be verified in the magnetostrictive-actuated dynamic system reported in Chapter 1, Section 1.3.1 with a mechanical load 16 Kg. The inverse compensator is first constructed and implemented in the dSPACE. Then the prescribed adaptive controller is also applied in the dSPACE to suppress the inverse compensation error and meanwhile improve the control precision. Finally, the experimental results will be provided to demonstrate the effectiveness of the developed control scheme.

6.5.1 Asymmetric Hysteresis Modeling and Its Inverse Compensation

In Chapter 3, the proposed ASPI model is expressed as

$$
\begin{aligned}
\hat{\Pi}[v](t) &= \hat{P}[v](t) + \hat{H}[v](t) \\
&= \hat{p}_0 v(t) + \sum_{i=1}^{n} \hat{p}_i F_{r_i}[v](t) + R_1 sat((\sum_{j=1}^{m} \hat{q}_i \Psi_{c_j}[v](t) + \hat{g}(v)(t))/R_1) \quad (6.61)
\end{aligned}
$$

with

$$
\hat{g}(v)(t) = -\hat{a}_3 v(t)^3 - \hat{a}_2 v(t)^2 - \hat{a}_1 v(t) - \hat{a}_0 \tag{6.62}
$$

The identified parameters $\hat{p}_i$ $\hat{c}_i$, $\hat{q}_i$, $\hat{a}_i$ of the ASPI model can be found in Table 4.1 in Chapter 4, and R_1 is selected as 100. Based on above parameters, the direct inverse compensator is therefore implemented as

$$
v(t) = \hat{\Pi}^{-1}[u](t) = \hat{P}^{-1}[u - \hat{H}[v]](t) \tag{6.63}
$$

where

$$
\hat{P}[u]^{-1}(t) = \hat{\bar{p}}_0 u(t) + \sum_{i=1}^{n} \hat{\bar{p}}_i F_{\hat{\bar{r}}_i}[v](t) \tag{6.64}
$$

$$
\hat{\bar{r}}_i = p_0 \hat{r}_i + \sum_{l=1}^{i} \sum_{j=1}^{l-1} b_j(\hat{r}_l - \hat{r}_{l-1}) \tag{6.65}
$$

$$
\hat{\bar{p}}_0 = 1/\hat{p}_0 \tag{6.66}
$$

$$
\hat{\bar{p}}_i = -\frac{\hat{p}_i}{(\hat{p}_0 + \sum_{j=1}^{i} \hat{p}_j)(\hat{p}_0 + \sum_{j=1}^{i-1} \hat{p}_j)} \tag{6.67}
$$

Therefore, the thresholds and weights of $P^{-1}[\cdot](t)$ are calculated as: $\hat{\bar{r}}_i[0, 0.2701, 0.7935, 1.4452, 2.5415, 3.82075.5078, 7.5565, 9.9223, 12.3732]$, $\hat{\bar{p}}_0 = 1.1109$, $\hat{\bar{p}}_i = [-0.5377, -0.1128, -0.1867, -0.0391, -0.0567, -0.0314, -0.0196, -0.0044, -0.0024]$.

The inverse compensator was implemented in the Matlab/Simulink and the codes were transformed into real-time control codes and downloaded to the dSPACE board. A desired tracking signal $u_d(t) = B_1 sin(2\pi t)$, $B_1 = 5, 10, 15$ was applied to the compensator. In Chapter 5, we have demonstrated that with the desired input $u_d = 15sin(2\pi t)$, the compensation

129

result with the proposed inverse compensator shows an approximate linear relationship, see Figure 6.5. However, due to the existence of the modeling error, the inverse compensation error is unavoidable, see Figures 6.6 and 6.7 with different desired input amplitudes. To accommodate this compensation error, the prescribed adaptive control scheme was therefore applied.
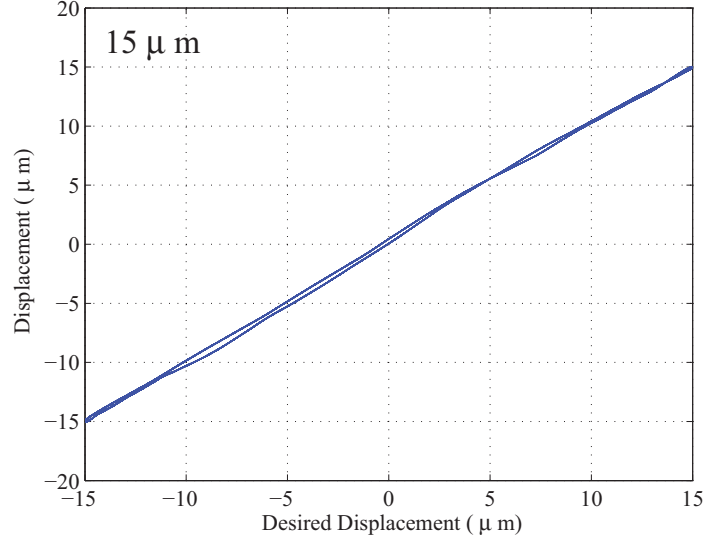
Figure 6.5: The inverse compensator with desired input $u_d(t) = 15sin(2\pi t)$

6.5.2 The Implementation of the Prescribed Adaptive Control

The entire control scheme is illustrated in Figure 6.3. Since in experiments we only focus on the low frequency application, the dynamic model of the magnetostrictive actuated system is first reduced to a first-order system [98], namely we select $n = 1$, $Y = x(t)$ in (6.41). Similar treatment also can be found in [99], [100]. The control objective is to force the output of the magnetostrictive-actuated system to follow the desired signal $x_d = 5sin(t)$ and ensure the transient and steady-state performance of the tracking error within the prescribed function area. The prescribed performance function is selected as $\rho = (1 - 0.07)e^{-t} + 0.07$ with $\overline{M} = 10$, $\underline{M} = -10$. The parameters in the control and adaptive laws are selected as
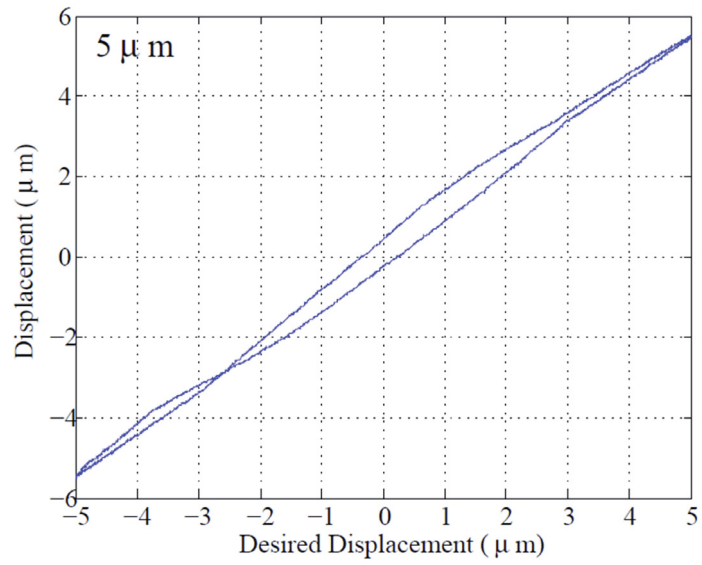
Figure 6.6: The inverse compensator with desired input $u_d(t) = 5sin(2\pi t)$
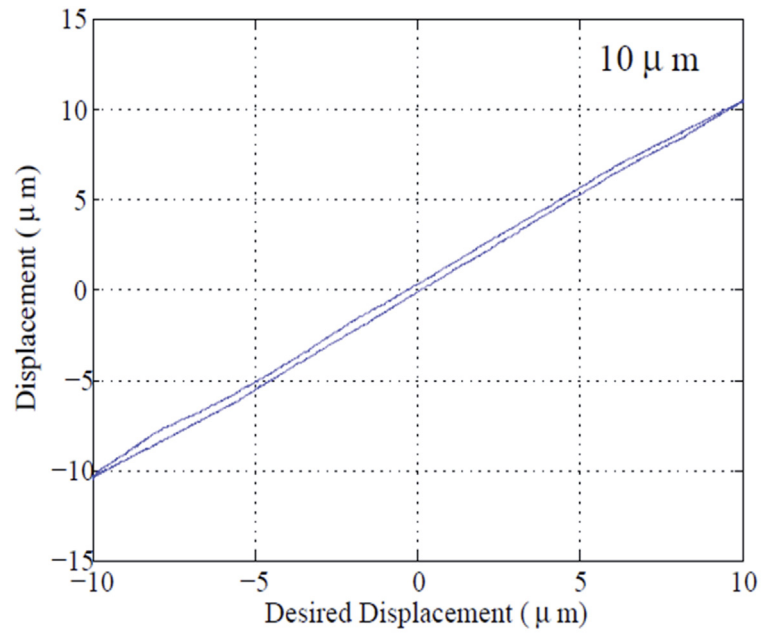
Figure 6.7: The inverse compensator with desired input $u_d(t) = 10sin(2\pi t)$

131
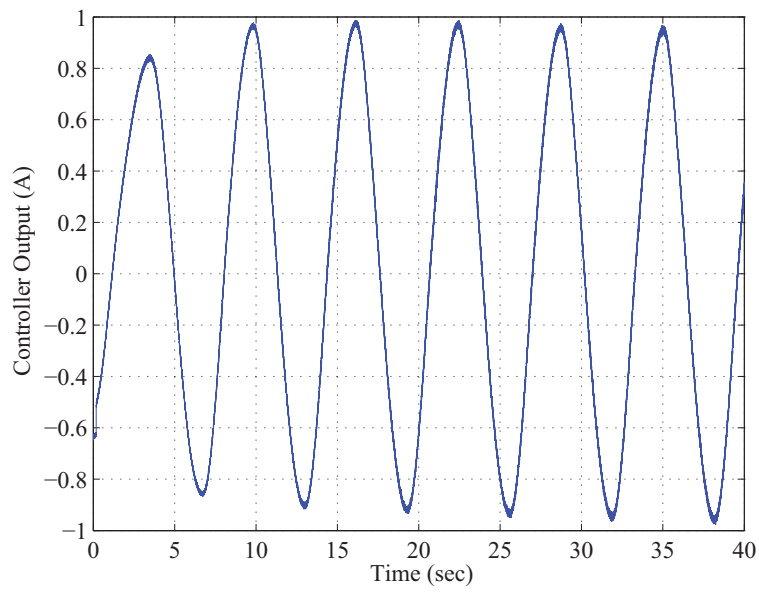
Figure 6.8: The control input signal to the system
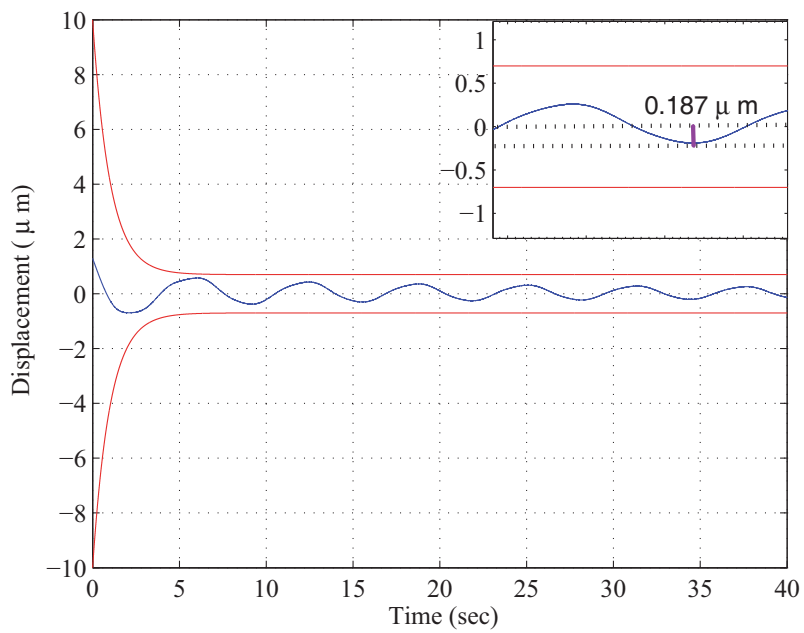
Figure 6.9: The tracking error

132
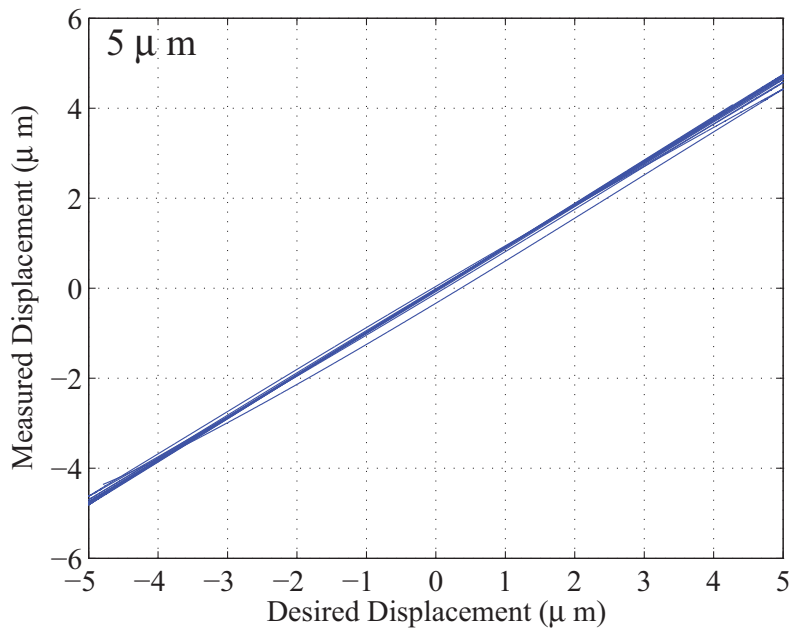
Figure 6.10: The input-output relation of the magnetostrictive actuator with prescribed adaptive controller
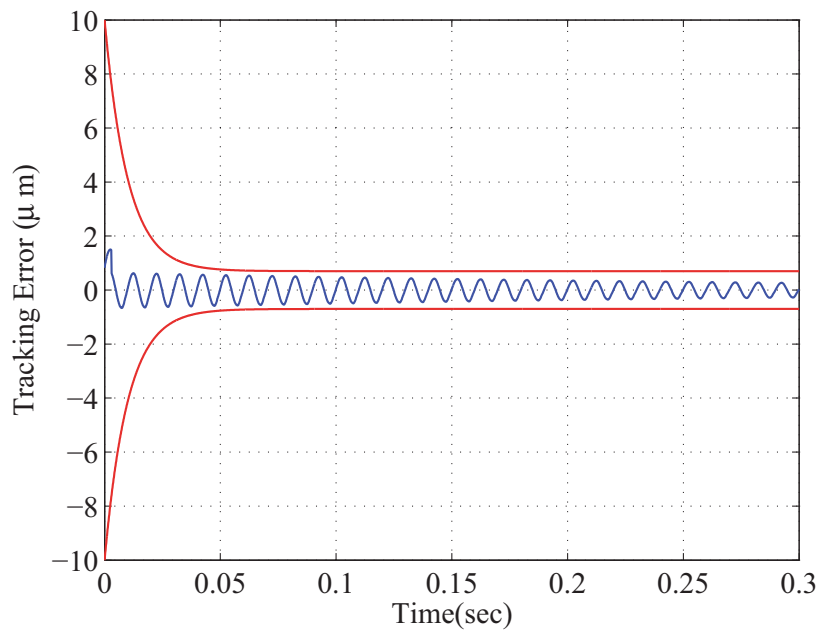
Figure 6.11: The tracking error with desired input $x_d = 5sin(100 \cdot 2\pi t)$
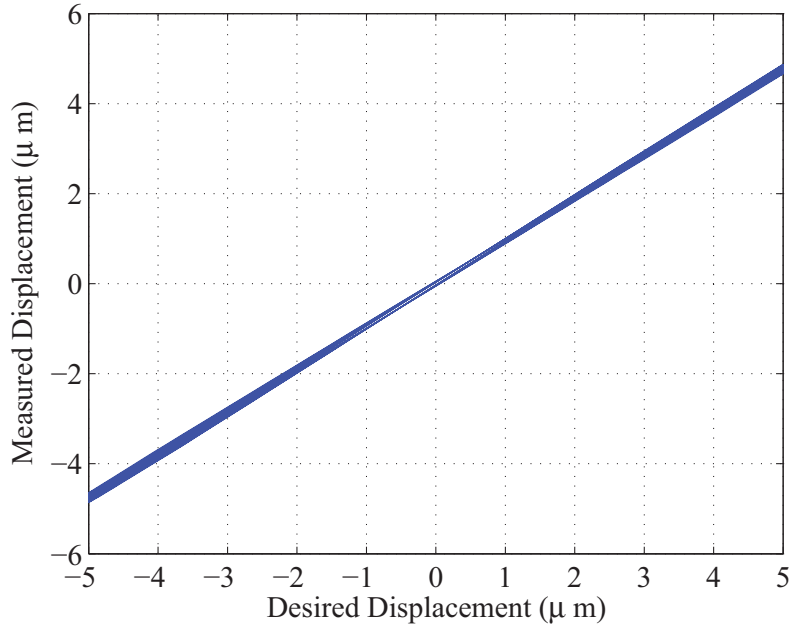
Figure 6.12: The input-output relation of the magnetostrictive actuator with prescribed adaptive controller under the desired input $x_d = 5sin(100 \cdot 2\pi t)$

$c_1 = 30$, $\eta_\zeta = 2$, $\Gamma_a = 2$, $\eta_D = 25$. The initial state is chosen as $x(0) = 1.3$. In addition, in the implementation the function $sgn(z_n)$ is replaced by $sat(z_n)$ to avoid the chattering effect. The experimental results are shown in Figures 6.8-6.12. Figure 6.8 shows the control signal. Figure 6.9 shows the tracking error. It can be seen that a fairly satisfactory tracking performance is achieved and the tracking error converges to a small neighborhood of zero. The input-output relation of the magnetostrictive actuator with prescribed adaptive controller is demonstrated in Figure 6.10. The input and output responses of the actuator gradually converges to a nearly linear relationship instead of nonlinear compensation error showing in Figure 6.6. To further illustrate the effectiveness of the adopted controller, a desired signal $x_d = 5sin(100 \cdot 2\pi t)$ with higher frequency is applied. The prescribed performance function is selected as $\rho = (1 - 0.07)e^{-100t} + 0.07$ with $\overline{M} = 10$, $\underline{M} = -10$. Figures 6.11 and 6.12 show the tracking error and the input-output relation of the magnetostrictive-actuated dynamic system with the prescribed adaptive controller. From above experimental results, it

can be seen that the developed prescribed adaptive controller shows an excellent tracking performance.

6.6 Concluding Remarks

This chapter deals with the entire controller design for the magnetostrictive-actuated dynamic system. The developed ASPI model was used to describe the asymmetric hysteresis effect, the direct inverse compensation approach was utilized to obtain the inverse compensator of the ASPI model. Due to the presence of the estimated error, the inverse compensation error is unavoidable. By means of the composition theorem, the analytical inverse compensation error was derived. To suppress such a compensation error, a prescribed adaptive control method was applied, in which the global stability of the closed loop system with a prescribed transient and steady-state performance of the tracking error can be guaranteed. The effectiveness of the proposed control scheme was validated via the experimental tests.

Chapter 7

Conclusions and Future Work

7.1 Concluding Remarks

Magnetostrictive actuators featuring high energy densities, large strokes and fast responses appear poised to play an increasingly important role in fields of requiring micro positioning. However, such actuators invariably exhibit hysteresis nonlinearities and dynamic behaviors that could cause oscillations and instability in the system which will severely deteriorate the micropositioning and tracking performance of the actuator. This dissertation research aims at developing an effective modeling and control methodology to overcome the hysteresis and dynamic effect and ensure the closed-loop stability and the micro-positioning performance for the magnetostrictive-actuated dynamic system.

At beginning, a series of the experimental tests have been conducted to present the input-output behaviors of the magnetostrictive-actuated dynamic system under different input amplitudes (1A-5A), frequencies (1Hz-200Hz) as well as mechanical loads ($m = 0$ Kg, 10.0 Kg, 21. 5Kg and 33 Kg). The experimental results were thoroughly investigated. It can be observed from the experimental tests that when the actuator works in the low frequency, the mechanical loads have little influence on the input-output relationship of the actuator; the input-output relationship of the actuator shows a static hysteretic phenomena. Howev-

er, when the actuator works in high frequencies, the mechanical loads greatly change the input-output behaviors of the system, which leads to a complex dynamic input and output behaviors.

In order to describe the complex dynamic behaviors, a dynamic model based on the principle of operation of the magnetostrictive actuator has been proposed, which comprehensively considers the electric, magnetic and mechanical domain as well as the interactions among them. The developed model includes two parts the hysteresis components and the dynamic components. To particularly describe the hysteresis effect, an asymmetric shifted Prandtl-Ishlinskii (ASPI) model has been proposed, which concludes three components: a Prandtl-Ishlinskii (PI) operator, a shift operator and an auxiliary function. The advantage for the proposed ASPI model are that it can describe the asymmetric hysteresis behavior and facilitates the construction of the analytical inverse of the ASPI model. The validity of the proposed model was demonstrated through experimental tests and the experimental results have verified the effectiveness of the proposed model.

In order to improve the positioning precision of the magnetostrictive actuator, the hysteresis effect shown in the actuator should be carefully treated. Therefore, the feedforward inverse compensation approaches have been adopted. At beginning, we chose the Preisach model to represent the hysteresis effect in the cascading model structure, and the inverse multiplicative structure compensator was then applied. However, inverse multiplicative structure needs the exact knowledge of the hysteresis model, which is very restrict for a practical actuator. Then, we utilized the ASPI model to describe the asymmetric hysteresis effect in the cascading model structure and applied the direct inverse compensation approach to find the inverse of the ASPI model. Both inverse compensation approaches have been examined on the magnetostrictive-actuated platform.

In the practical control systems, the use of an estimated hysteresis model in deriving the inverse compensator would be expected to yield some degree of hysteresis compensation error. This error causes tracking error in the closed-loop control system. To accommodate such a compensation error, the analytical expression of the inverse compensation error has

been derived first. Then, a prescribed adaptive control method was applied to suppress the compensation error and simultaneously guaranteeing global stability of the closed loop system with a prescribed transient and steady-state performance of the tracking error. The effectiveness of the proposed control scheme has been validated on the magnetostrictive-actuated experimental platform. The experimental results demonstrate an excellent tracking performance by using the proposed control scheme.

7.2 Recommendations for Future Works

As the continuation of the studies in this dissertation research, the following research topics in this area can be conducted in the future.

- In Chapter 4, for the identification of the dynamic system, we estimate the parameters of the hysteresis part and dynamic part separately. Although the estimations show the good agreement with the experiments, the challenge lies in how to come up with an identification method that can estimate the parameters of the hysteresis part and dynamic part together, which would be a very interesting topic for the further research.

- In Chapter 6, we implement the controller based on the reduced dynamic system, since some states in the dynamic system are not measurable. Therefore, it is desirable to develop an output feedback controller in the future work.

7.3 Publications

Several papers reporting results of this dissertation research have been published/submitted in journals and international conferences as listed below.

Journal Papers:

- Z. Li, C.-Y. Su, and T. Chai, "Nonlinear control of smart material based actuator

with Preisach hysteresis description: a prescribed adaptive control approach," *IEEE Transactions on Control System Technology*, 2014 (accepted).

- Z. Li, C.-Y. Su, and X. Chen, "Modeling and inverse adaptive control of asymmetric hysteresis systems with applications to magnetostrictive actuator," *Control Engineering Practice*, vol. 33, pp. 148-160, 2014.

- Z. Li, C.-Y. Su, and T. Chai, "Compensation of hysteresis nonlinearity in magnetostrictive actuators with inverse multiplicative structure for Preisach model," *IEEE Transactions on Automation Science and Engineering*, vol. 11, pp. 613-619, 2014.

- S. Liu, C.-Y. Su, and Z. Li "Robust Adaptive Inverse Control of a Class of Nonlinear Systems With Prandtl-Ishlinskii Hysteresis Model," *IEEE Transactions on Automatic Control*, vol. 59, pp. 2170-2175, 2014.

- Z. Li, C.-Y. Su, X. Chen, and S. Liu, "Prescribed adaptive control of unknown hysteresis in smart material actuated systems," *Production & Manufacturing Research*, vol. 1, pp. 712-724, 2014.

- G. Gu, Z. Li, L. Zhu, and C.-Y. Su, "A comprehensive dynamic modeling approach for giant magnetostrictive material actuators," *Smart Materials and Structures*, vol. 22, 125005, 2013.

- Z. Li, O. Aljanaideh, S. Rakheja, C-Y. Su, and M. Al Janaideh, "Compensation of play operator-based Prandtl-Ishlinskii hysteresis model using a stop operator with application to piezoelectric actuators," *International Journal of Advanced Mechatronic Systems*, vol. 4, pp.25-31, 2012.

Book Chapter:

- Z. Li, S. Liu, and C-Y. Su, "A novel analytical inverse compensation approach for Preisach model," *Intelligent Robotics and Applications*, Springer, 2013.

Conference Papers:

- Z. Li, C-Y. Su, and T.Y. Chai, "Dynamic modeling and identification of magnetostrictive actuators for control of micromanipulation," *in Proceeding of the 11th World Congress on Intelligent Control and Automation*, Shenyang, China, 2014 (T J Tarn's Best Paper Award on Control Applications).

- Z. Li, C-Y. Su, X. Chen, and T.Y. Chai, "Prescribed adaptive control of nonlinear system with unknown Bouc-Wen model," *in Proceeding of IEEE 52rd Annual Conference on Decision and Control*, Florence, Italy, 2013.

- Z. Li, Y. Feng, S. Liu, and C.-Y. Su, "Prescribed adaptive control of a class of nonlinear system preceded by actuators with hysteresis," *in Proceeding of Manufacturing Modeling, Management, and Control*, St. Petersburg, Russia, 2013, pp. 1849-1854.

- Z. Li, C-Y. Su, T.Y. Chai, and Y. Feng, "Prescribed adaptive control of a class of nonlinear system with asymmetric hysteresis," *in Proceeding of 6th IFAC Symposium on Mechatronic Systems*, Hangzhou, China, 2013, pp.325-331.

- S. Liu, X.J. Sheng, Z. Li and C-Y. Su, "Inverse control of a class of nonlinear systems with modified generalized Prandtl-Ishlinskii hysteresis," *in Proceeding of 38th Annual Conference on IEEE Industrial Electronics Society*, Montreal, Canada, 2012, pp. 2319-2324.

- S. Liu, Z. Li, and C-Y. Su, "Robust adaptive control of a class of nonlinear system with an Asymmetric Shifted Prandtl-Ishnlinskii hysteresis model," *in Proceeding of 2012 International Conference on Advanced Mechatronic Systems (ICAMechS)*, Tokyo, Japan, 2012, pp. 217-222.

- Z. Li, T.Y. Chai, Y. Feng, and C-Y. Su, "Modeling of rate-dependent asymmetric hysteresis nonlinearity for magnetostrictive actuators," *in Proceeding of 2012 International Conference on Information and Automation*, Shenyang, China, 2012, pp. 174-179.

- Z. Li, Y. Feng, T.Y. Chai, J. Fu, and C-Y. Su, "Modeling and compensation of asymmetric hysteresis nonlinearity for magnetostrictive actuators with an asymmetric shifted Prandtl-Ishlinskii model," *in Proceeding of 2012 American Control Conference*, Montreal, Canada, 2012, pp. 1658-1663.

- Z. Li, O. Aljanaideh, S. Rakheja, C-Y. Su, and M. Al Janaideh, "Compensation of hysteresis nonlinearity for a piezoelectric actuator using a stop operator-based Prandtl-Ishlinskii model," *in Proceeding of 2011 International Conference on Advanced Mechatronic Systems*, Zhengzhou, China, 2011, pp. 169-174.

Bibliography

[1] M. Rakotondrabe, "Bouc-wen modeling and inverse multiplicative structure to compensate hysteresis nonlinearity in piezoelectric actuators," *IEEE Transactions on Automation Science and Engineering*, vol. 8, no. 2, pp. 428–431, 2011.

[2] X. Tan and O. Bennani, "Fast inverse compensation of Preisach-type hysteresis operators using field-programmable gate arrays," in *American Control Conference, Seattle, USA*, pp. 2365–2370, 2008.

[3] S. Liu, C.-Y. Su, and Z. Li, "Robust adaptive inverse control of a class of nonlinear systems with prandtl-ishlinskii hysteresis model," *IEEE Transactions on Automatic Control*, vol. 59, no. 8, pp. 2170–2175, 2014.

[4] A. G. Olabi and A. Grunwald, "Design and application of magnetostrictive materials," *Materials and Design*, vol. 29, no. 2, pp. 469–483, 2008.

[5] H. Zhu, J. Liu, X. Wang, Y. Xing, and H. Zhang, "Applications of Terfenol-D in China," *Journal of Alloys and Compounds*, vol. 258, no. 1, pp. 49–52, 1997.

[6] F. Claeyssen, N. Lhermet, R. Le Letty, and P. Bouchilloux, "Actuators, transducers and motors based on giant magnetostrictive materials," *Journal of Alloys and Compounds*, vol. 258, no. 1, pp. 61–73, 1997.

[7] B.-T. Yang, D.-H. Yang, and P.-Y. Xu, "Large stroke and nanometer-resolution giant magnetostrictive assembled actuator for driving segmented mirrors in very large

astronomical telescopes," *Sensors and Actuators A: Physical*, vol. 179, pp. 193–203, 2012.

[8] R. Smith, *Smart Material Systems: Model Development.* Society for Industrial and Applied Mathematics, 2005.

[9] S. Karunanidhi and M. Singaperumal, "Design, analysis and simulation of magnetostrictive actuator and its application to high dynamic servo valve," *Sensors and Actuators A: Physical*, vol. 157, no. 2, pp. 185–197, 2010.

[10] C.-L. Wang, X. Cheng, and P. An, "Modeling and simulation of a high-frequency micropump based on giant magnetostrictive material (gmm)," *Journal of Coal Science and Engineering (China)*, vol. 16, no. 2, pp. 206–209, 2010.

[11] O. Aljanaideh, M. Al Janaideh, S. Rakheja, and C.-Y. Su, "Compensation of rate-dependent hysteresis nonlinearities in a magnetostrictive actuator using an inverse prandtl ishlinskii model," *Smart Materials and Structures*, vol. 22, no. 2, p. 025027, 2013.

[12] Z. Li, Y. Feng, T. Chai, J. Fu, and C.-Y. Su, "Modeling and compensation of asymmetric hysteresis nonlinearity for magnetostrictive actuators with an asymmetric shifted prandtl-ishlinskii model," in *American Control Conference (ACC), Montreal, Canada*, pp. 1658–1663, 2012.

[13] X. B. Tan and J. S. Baras, "Modeling and control of hysteresis in magnetostrictive actuators," *Automatica*, vol. 40, no. 9, pp. 1469–1480, 2004.

[14] L. Li, C. Zhang, B. Yan, L. Zhang, and X. Li, "Research of fast-response giant magnetostrictive actuator for space propulsion system," *IEEE Transactions on Plasma Science*, vol. 39, no. 2, pp. 744–748, 2011.

[15] W. S. Oates, P. G. Evans, R. C. Smith, and M. J. Dapino, "Experimental implementation of a hybrid nonlinear control design for magnetostrictive actuators," *Journal of Dynamic Systems, Measurement, and Control*, vol. 131, no. 4, p. 041004, 2009.

[16] D. Davino, A. Giustiniani, and C. Visone, "Experimental properties of an efficient stress-dependent magnetostriction model," *Journal of Applied Physics*, vol. 105, no. 7, pp. 105–107, 2009.

[17] Y.-H. Ma and J.-Q. Mao, "On modeling and tracking control for a smart structure with stress-dependent hysteresis nonlinearity," *Acta Automatica Sinica*, vol. 36, no. 11, pp. 1611–1619, 2010.

[18] Z. Li, C.-Y. Su, and T. Chai, "Compensation of hysteresis nonlinearity in magnetostrictive actuators with inverse multiplicative structure for preisach model," *IEEE Transactions on Automation Science and Engineering*, vol. 11, no. 2, pp. 613–619, 2014.

[19] Z. Li, C.-Y. Su, and X. Chen, "Modeling and inverse adaptive control of asymmetric hysteresis systems with applications to magnetostrictive actuator," *Control Engineering Practice*, vol. 33, pp. 148–160, 2014.

[20] C. Natale, F. Velardi, and C. Visone, "Identification and compensation of preisach hysteresis models for magnetostrictive actuators," *Physica B: Condensed Matter*, vol. 306, no. 1, pp. 161–165, 2001.

[21] I. D. Mayergoyz, "Dynamic preisach models of hysteresis," *IEEE Transactions on Magnetics*, vol. 24, no. 6, pp. 2925–2927, 1988.

[22] R. B. Mrad and H. Hu, "A model for voltage-to-displacement dynamics in piezoceramic actuators subject to dynamic-voltage excitations," *IEEE/ASME Transactions on Mechatronics*, vol. 7, no. 4, pp. 479–489, 2002.

[23] M. Al Janaideh and P. Krejci, "Inverse rate-dependent Prandtl-Ishlinskii model for feedforward compensation of hysteresis in a piezomicropositioning actuator," *IEEE/ASME Transactions on Mechatronics*, vol. 18, no. 5, pp. 1498–1507, 2013.

[24] M. Al Janaideh, C.-Y. Su, and S. Rakheja, "Development of the rate-dependent Prandtl-Ishlinskii model for smartă actuators," *Smart Materials and Structures*, vol. 17, no. 3, p. 035026, 2008.

[25] Y. Ma and J. Mao, "Modeling and control for giant magnetostrictive actuators with stress-dependent hysteresis," in *IEEE International Conference on Automation and Logistics, Qingdao, China*, pp. 1083–1088, 2008.

[26] O. Bottauscio, P. E. Roccato, and M. Zucca, "Modeling the dynamic behavior of magnetostrictive actuators," *IEEE Transactions on Magnetics*, vol. 46, no. 8, pp. 3022–3028, 2010.

[27] D. C. Jiles and D. L. Atherton, "Theory of ferromagnetic hysteresis," *Journal of Magnetism and Magnetic Materials*, vol. 61, no. 1-2, pp. 48–60, 1986.

[28] M. Goldfarb and N. Celanovic, "Modeling piezoelectric stack actuators for control of micromanipulation," *IEEE Control Systems*, vol. 17, no. 3, pp. 69–79, 1997.

[29] H. Adriaens, W. Koning, and R. Banning, "Modeling piezoelectric actuators," *IEEE/ASME Transactions on Mechatronics*, vol. 5, no. 4, pp. 331–341, 2000.

[30] M. Brokate and J. Sprekels, *Hysteresis and Phase Transitions.* New York: Springer-Verlag, 1996.

[31] T. Wu and A. Kareem, "Aerodynamics and aeroelasticity of cable-supported bridges: identification of nonlinear features," *Journal of Engineering Mechanics*, vol. 139, no. 12, pp. 1886–1893, 2013.

[32] J. Fuller, M. Best, N. Garret, and M. Passmore, "The importance of unsteady aerodynamics to road vehicle dynamics," *Journal of Wind Engineering and Industrial Aerodynamics*, vol. 117, pp. 1–10, 2013.

[33] R. I. Leine and H. Nijmeijer, *Dynamics and bifurcations of non-smooth mechanical systems*, vol. 18. Springer Science and Business, 2013.

[34] P. C. Krause, O. Wasynczuk, S. D. Sudhoff, and S. Pekarek, *Analysis of electric machinery and drive systems*, vol. 75. John Wiley and Sons, 2013.

[35] Y.-K. Wen, "Method for random vibration of hysteretic systems," *Journal of the Engineering Mechanics Division*, vol. 102, no. 2, pp. 249–263, 1976.

[36] R. Cross, "Mach, methodology, hysteresis and economics," in *Journal of Physics: Conference Series*, vol. 138, p. 012004, 2008.

[37] E. M. Izhikevich, *Dynamical systems in neuroscience.* MIT press, 2007.

[38] A. Kostyukov, "Muscle hysteresis and movement control: a theoretical study," *Neuroscience*, vol. 83, no. 1, pp. 303–320, 1998.

[39] A. Elwakil and M. Kennedy, "Systematic realization of a class of hysteresis chaotic oscillators," *International journal of circuit theory and applications*, vol. 28, no. 4, pp. 319–334, 2000.

[40] M. Parodi, M. Storace, and S. Cincotti, "Static and dynamic hysteretic features in a pwl circuit," *International journal of circuit theory and applications*, vol. 24, no. 2, pp. 183–199, 1996.

[41] F. Preisach, "Über die magnetische nachwirkung," *Zeitschrift für Physik*, vol. 94, pp. 277–302, 1935.

[42] I. D. Mayergoyz, "Mathematical-models of hysteresis," *IEEE Transactions on Magnetics*, vol. 22, no. 5, pp. 603–608, 1986.

[43] A. Visintin, "Mathematical models of hysteresis," *The science of hysteresis*, vol. 1, pp. 1–114, 2006.

[44] P. Krejci, *Hysteresis, convexity and dissipation in hyperbolic equation.* International series of Math Science and applications, 1986.

[45] A. Visintin, *Differential Models of Hysteresis.* New York: Springer-Verlag, 1994.

[46] M. Brokate and A. Visintin, "Properties of the preisach model for hysteresis," *Journal fur die reine und angewandte Mathematik*, vol. 28, no. 402, pp. 1–40, 1989.

[47] X. Tan and R. V. Iyer, "Modeling and control of hysteresis," *IEEE Control Systems Magazine*, vol. 29, no. 1, pp. 26–28, 2009.

[48] H. T. Banks and A. J. Kurdila, "Hysteretic control influence operators representing smart material actuators: identification and approximation," in *Proceedings of the 35th IEEE Conference on Decision and Control, Kobe, Japan*, pp. 3711–3716, 1996.

[49] I. D. Mayergoyz, *Mathematical models of hysteresis and their applications*. Academic Press, 2003.

[50] G. Bertotti, "Dynamic generalization of the scalar preisach model of hysteresis," *IEEE Transactions on Magnetics*, vol. 28, no. 5, pp. 2599–2601, 1992.

[51] X. B. Tan and J. S. Baras, "Modeling and control of hysteresis in magnetostrictive actuators," *Automatica*, vol. 40, no. 9, pp. 1469–1480, 2004.

[52] P. Ge and J. Musa, "Tracking control of a piezoceramic actuator," *IEEE Transactions on Control Systems Technology*, vol. 4, no. 3, pp. 209–216, 1996.

[53] D. Hughes and J. T. Wen, "Preisach modeling of piezoceramic and shape memory alloy hysteresis," in *Proceedings of the 4th IEEE Conference on Control Applications, New York, US*, pp. 1086–1091, 1995.

[54] D. N. C. Nam and K. K. Ahn, "Identification of an ionic polymer metal composite actuator employing Preisach type fuzzy NARX model and particle swarm optimization," *Sensors and Actuators A: Physical*, vol. 183, pp. 105–114, 2012.

[55] Y. M. Han, S. C. Lim, H. G. Lee, S. B. Choi, and H. J. Choi, "Hysteresis identification of polymethylaniline-based ER fluid using Preisach model," *Materials and Design*, vol. 24, no. 1, pp. 53–61, 2003.

[56] C.-Y. Su, Q. Wang, X. Chen, and S. Rakheja, "Adaptive variable structure control of a class of nonlinear systems with unknown prandtl-ishlinskii hysteresis," *IEEE Transactions on Automatic Control*, vol. 50, no. 12, pp. 2069–2074, 2005.

[57] K. Kuhnen, "Modeling,identification and compensation of complex hysteretic nonlinearities," *European Journal of Control*, vol. 9, no. 4, pp. 407–418, 2003.

[58] H. Jiang, H. Ji, J. Qiu, and Y. Chen, "A modified prandtl-ishlinskii model for modeling asymmetric hysteresis of piezoelectric actuators," *IEEE Transactions on Ultrasonics, Ferroelectrics and Frequency Control*, vol. 57, no. 5, pp. 1200–1210, 2010.

[59] C.-A. Jiang, M.-C. Deng, and A. Inoue, "Robust stability of nonlinear plants with a non-symmetric prandtl-ishlinskii hysteresis model," *International Journal of Automation and Computing*, vol. 7, no. 2, pp. 213–218, 2010.

[60] A. Janaideh, J. Mao, S. Rakheja, X. W.F., and C. Su, "Generalized prandtl-ishlinskii hysteresis model: Hysteresis modeling and its inverse for compensation in smart actuators," in *Proceedings of the 47th IEEE Conference on Decision and Control, Cancun, Mexico*, pp. 5182–5187, 2008.

[61] H. T. Banks, A. J. Kurdila, and G. Webb, "Identification of hysteretic control influence operators representing smart actuators part i: Formulation," *Mathematical Problems in Engineering*, vol. 3, no. 4, pp. 287–328, 1997.

[62] W. S. Galinaitis and R. C. Rogers, "Control of a hysteretic actuator using inverse hysteresis compensation," in *5th Annual International Symposium on Smart Structures and Materials*, pp. 267–277, 1998.

[63] M. Hodgdon, "Applications of a theory of ferromagnetic hysteresis," *IEEE Transactions on Magnetics*, vol. 24, no. 1, pp. 218–221, 1988.

[64] Y. Feng, C. A. Rabbath, and C.-Y. Su, "Inverse duhem model based robust adaptive control for flap positioning system with sma actuators," in *18th IFAC World Congress, Milano, Italy*, pp. 8126–8131, 2011.

[65] J. Song and A. Der Kiureghian, "Generalized boucŨwen model for highly asymmetric hysteresis," *Journal of Engineering Mechanics*, vol. 132, no. 6, pp. 610–618, 2006.

[66] B. F. Spencer Jr, S. J. Dyke, M. K. Sain, and J. D. Carlson, "Phenomenological model for magnetorheological dampers," *Journal of Engineering Mechanics*, vol. 123, no. 3, pp. 230–238, 1997.

[67] P. Krejci and K. Kuhnen, "Inverse control of systems with hysteresis and creep," *IEE Proceedings Control Theory and Applications*, vol. 148, no. 3, pp. 185–192, 2001.

[68] F. Ding, X. Liu, and J. Chu, "Gradient-based and least-squares-based iterative algorithms for hammerstein systems using the hierarchical identification principle," *IET Control Theory and Applications*, vol. 7, no. 2, pp. 176–184, 2013.

[69] F. Giri and E.-W. Bai, *Block-oriented nonlinear system identification*. Springer, 2010.

[70] E. Reynders, "System identification methods for (operational) modal analysis: review and comparison," *Archives of Computational Methods in Engineering*, vol. 19, no. 1, pp. 51–124, 2012.

[71] J. Zhou, C. Wen, and T. Li, "Adaptive output feedback control of uncertain nonlinear systems with hysteresis nonlinearity," *IEEE Transactions on Automatic Control*, vol. 57, no. 10, pp. 2627–2633, 2012.

[72] M. Rakotondrabe, C. Clevy, and P. Lutz, "Complete open loop control of hysteretic, creeped, and oscillating piezoelectric cantilevers," *IEEE Transactions on Automation Science and Engineering*, vol. 7, no. 3, pp. 440–450, 2010.

[73] B. Mokaberi and A. A. G. Requicha, "Compensation of scanner creep and hysteresis for afm nanomanipulation," *IEEE Transactions on Automation Science and Engineering*, vol. 5, no. 2, pp. 197–206, 2008.

[74] Z. Li, O. Aljanaideh, S. Rakheja, C. Su, and M. Al Janaideh, "Compensation of play operator-based Prandtl Ishlinskii hysteresis model using a stop operator with applica-

149

tion to piezoelectric actuators," *International Journal of Advanced Mechatronic Systems*, vol. 4, no. 1, pp. 25–31, 2012.

[75] C. Visone, "Hysteresis modelling and compensation for smart sensors and actuators," *Journal of Physics: Conference Series*, vol. 138, no. 1, p. 012028, 2008.

[76] S. Mittal and C. H. Menq, "Hysteresis compensation in electromagnetic actuators through Preisach model inversion," *IEEE/ASME Transactions on Mechatronics*, vol. 5, no. 4, pp. 394–409, 2000.

[77] X. B. Tan and J. S. Baras, "Adaptive identification and control of hysteresis in smart materials," *IEEE Transactions on Automatic Control*, vol. 50, no. 6, pp. 827–839, 2005.

[78] C. Su, Y. Tan, and Y. Stepanenko, "Adaptive control of a class of nonlinear systems preceded by an unknown backlash-like hysteresis," in *Proceedings of the 39th IEEE Conference on Decision and Control, Sydney, Australia*, vol. 2, pp. 1459–1464, 2000.

[79] J. Zhou, C. Wen, and Y. Zhang, "Adaptive backstepping control of a class of uncertain nonlinear systems with unknown backlash-like hysteresis," *IEEE Transactions on Automatic Control*, vol. 49, no. 10, pp. 1751–1759, 2004.

[80] C. Wen and J. Zhou, "Decentralized adaptive stabilization in the presence of unknown backlash-like hysteresis," *Automatica*, vol. 43, no. 3, pp. 426–440, 2007.

[81] C.-Y. S. qingqing Wang, "Robust adaptive control of a class of nonlinear systems including actuator hysteresis with prandtlŰishlinskii presentations," *Automatica*, 2006.

[82] S. Bashash and N. Jalili, "Robust adaptive control of coupled parallel piezo-flexural nanopositioning stages," *IEEE/ASME Transactions on Mechatronics*, vol. 14, no. 1, pp. 11–20, 2009.

[83] X. Zhang, Y. Lin, and J. Mao, "A robust adaptive dynamic surface control for a class of nonlinear systems with unknown prandtlŰishilinskii hysteresis," *International Journal of Robust and Nonlinear Control*, vol. 21, no. 13, pp. 1541–1561, 2011.

[84] W.-F. Xie, J. Fu, H. Yao, and C. Y. Su, "Neural network-based adaptive control of piezoelectric actuators with unknown hysteresis," *International Journal of Adaptive Control and Signal Processing*, vol. 23, no. 1, pp. 30–54, 2009.

[85] B. Ren, S. S. Ge, C.-Y. Su, and T. H. Lee, "Adaptive neural control for a class of uncertain nonlinear systems in pure-feedback form with hysteresis input," *IEEE Transactions on Systems, Man, and Cybernetics, Part B: Cybernetics*, vol. 39, no. 2, pp. 431–443, 2009.

[86] Q. Shen, T. Zhang, and C. Zhou, "Decentralized adaptive fuzzy control of time-delayed interconnected systems with unknown backlash-like hysteresis," *Journal of Systems Engineering and Electronics*, vol. 19, no. 6, pp. 1235–1242, 2008.

[87] Y. Li, S. Tong, and T. Li, "Adaptive fuzzy output feedback control of uncertain nonlinear systems with unknown backlash-like hysteresis," *Information Sciences*, vol. 198, no. 0, pp. 130–146, 2012.

[88] J. Zhou, C. Wen, and T. Li, "Adaptive output feedback control of uncertain nonlinear systems with hysteresis nonlinearity," *IEEE Transactions on Automatic Control*, vol. 57, no. 10, pp. 2627–2633, 2012.

[89] G. Tao and P. V. Kokotovic, "Adaptive control of systems with backlash," *Automatica*, vol. 29, no. 2, pp. 323–335, 1993.

[90] G. Tao and P. V. Kokotovic, "Adaptive control of plants with unknown hystereses," *IEEE Transactions on Automatic Control*, vol. 40, no. 2, pp. 200–212, 1995.

[91] A. M. Janaideh, C.-Y. Su, and S. Rakheja, "Inverse compensation error of the prandtl-ishlinskii model," *IEEE Conference on Decision and Control, Maui, Hawaii, USA*, pp. 1597–1602, 2012.

[92] F. Ikhouane, V. Mañosa, and J. Rodellar, "Dynamic properties of the hysteretic bouc-wen model," *Systems and Control Letters*, vol. 56, no. 3, pp. 197–205, 2007.

[93] X. Y. Zhang and Y. Lin, "Adaptive tracking control for a class of pure-feedback nonlinear systems including actuator hysteresis and dynamic uncertainties," *IET, Control Theory and Applications*, vol. 5, no. 16, pp. 1868–1880, 2011.

[94] C. P. Bechlioulis and G. A. Rovithakis, "Adaptive control with guaranteed transient and steady state tracking error bounds for strict feedback systems," *Automatica*, vol. 45, no. 2, pp. 532–538, 2009.

[95] C. P. Bechlioulis and G. A. Rovithakis, "Robust adaptive control of feedback linearizable mimo nonlinear systems with prescribed performance," *IEEE Transactions on Automatic Control*, vol. 53, no. 9, pp. 2090–2099, 2008.

[96] J. Na, "Adaptive prescribed performance control of nonlinear systems with unknown dead zone," *International Journal of Adaptive Control and Signal Processing*, 2012.

[97] I. K. M. Kristic and P. V. Kokotovic, *Nonlinear and Adaptive Control Design.* New York: Wiley, 1995.

[98] L. Riccardi, D. Naso, B. Turchiano, and H. Janocha, "Adaptive control of positioning systems with hysteresis based on magnetic shape memory alloys," *IEEE Transactions on Control Systems Technology*, vol. 21, no. 6, pp. 2011–2023, 2013.

[99] J.-C. Shen, W.-Y. Jywe, H.-K. Chiang, and Y.-L. Shu, "Precision tracking control of a piezoelectric-actuated system," *Precision Engineering*, vol. 32, no. 2, pp. 71–78, 2008.

[100] J. Zhong and B. Yao, "Adaptive robust precision motion control of a piezoelectric positioning stage," *IEEE Transactions on Control Systems Technology*, vol. 16, no. 5, pp. 1039–1046, 2008.